AD_____

Award Number: W81XWH-13-1-0133

TITLE: Regulation of Breast Cancer Stem Cells by Tissue Rigidity

PRINCIPAL INVESTIGATOR: Adam J. Engler

CONTRACTING ORGANIZATION: University of California, San Diego
La Jolla, CA 92093

REPORT DATE: June 2015

TYPE OF REPORT: Annual report

PREPARED FOR: U.S. Army Medical Research and Materiel Command
                          Fort Detrick, Maryland 21702-5012

REPORT DOCUMENTATION PAGE

Form Approved
OMB No. 0704-0188

1. REPORT DATE	2. REPORT TYPE	3. DATES COVERED
June 2015	Annual	06/01/2014– 05/31/2015

4. TITLE AND SUBTITLE
Regulation of Breast Cancer Stem Cell by Tissue Rigidity

5a. CONTRACT NUMBER
W81XWH-13-1-0133

5b. GRANT NUMBER

5c. PROGRAM ELEMENT NUMBER

6. AUTHOR(S)
Jing Yang, Adam Engler, Laurent Fattet, and Matthew Ondeck.

5d. PROJECT NUMBER

5e. TASK NUMBER

5f. WORK UNIT NUMBER

E-Mail: jingyang@ucsd.edu; aengler@ucsd.edu

7. PERFORMING ORGANIZATION NAME(S) AND ADDRESS(ES) AND ADDRESS(ES)

University of California, San Diego
9500 Gilman Drive, MC0636
La Jolla, CA 92093

8. PERFORMING ORGANIZATION REPORT NUMBER

9. SPONSORING / MONITORING AGENCY NAME(S) AND ADDRESS(ES)
U.S. Army Medical Research and Materiel Command
Fort Detrick, Maryland 21702-5012

10. SPONSOR/MONITOR'S ACRONYM(S)

11. SPONSOR/MONITOR'S REPORT NUMBER(S)

12. DISTRIBUTION / AVAILABILITY STATEMENT
Approved for Public Release; Distribution Unlimited

13. SUPPLEMENTARY NOTES

14. ABSTRACT
The presence of a fibrotic focus in breast tumors is associated with a 10-50-fold increase in tissue stiffness and correlates with distant metastasis and poor outcome. Recent studies indicate that increasing tissue rigidity promotes breast cancer progression, however the underlying molecular mechanism is largely unknown. Breast cancer stem cells have both long-term self-renewal capacity and the ability to initiate tumors. In this proposal, we hypothesize that tissue rigidity regulates breast cancer stem cell properties and function, therefore assisting breast tumor development and promoting chemoresistance.

Our major findings are the following.
1. We developed two hydrogel systems and determined their mechanic properties.
2. We found that increasing tissue rigidities promoted breast cancer stem cell properties.
3. We uncovered that a mechanistic link between tissue rigidity and breast cancer stem cells was via the activation of the EMT program.
4. We found that the EMT-inducing transcription factor Twist1 was essential for high tissue-rigidity-induced EMT.
5. We identified a novel Twist1/G3BP2 mechanotransduction pathway that responds to increasing matrix stiffness in the tumor microenvironment to drive EMT, cancer stem cell properties, invasion, and metastasis.

Together, these results indicate that increasing matrix stiffness promotes EMT via an integrin and Twist1-dependent pathway to regulate breast cancer stem cell function, thus impacting breast cancer progression.

15. SUBJECT TERMS
Matrix stiffness, breast cancer stem cell, Epithelial-Mesenchymal Transition (EMT).

16. SECURITY CLASSIFICATION OF:			17. LIMITATION OF ABSTRACT	18. NUMBER OF PAGES	19a. NAME OF RESPONSIBLE PERSON USAMRMC
a. REPORT	b. ABSTRACT	c. THIS PAGE			19b. TELEPHONE NUMBER *(include area code)*
U	U	U	UU	47	

Table of Contents

1. INTRODUCTION

Breast tumors are frequently detected through physical palpation as a rigid mass residing within the soft normal mammary tissue. The presence of a fibrotic focus in breast tumors is associated with a 10-50-fold increase in tissue stiffness and correlates with distant metastasis and poor outcome. Recent studies indicate that increasing tissue rigidity promotes breast cancer progression, however the underlying molecular mechanism is largely unknown. Breast cancer stem cells have both long-term self-renewal capacity and the ability to initiate tumors. In this proposal, we hypothesize that tissue rigidity regulates breast cancer stem cell properties and function, therefore assisting breast tumor development and promoting chemoresistance. Therefore, the proposed research aims to determine the impact of matrix stiffness on breast cancer stem cell function and to understand the molecular mechanism underlying this regulation. Given the critical role of breast cancer stem cells in breast tumor progression and chemoresistance, our research could lead to novel therapeutics targeting the mechanotransduction pathway to eradicate breast cancer stem cells and overcome chemoresistance.

2. KEYWORDS
breast cancer stem cell, matrix stiffness, Epithelial-Mesenchymal Transition, Invasion, metastasis

3. ACCOMPLISHMENTS

- **What were the major goals of the project?**

- **What was accomplished under these goals?**
Task 1. Determine the impact of matrix stiffness on breast cancer stem cell function, Months 1-18:

1. Determine the role of matrix stiffness on regulating breast cancer stem cell properties in 3D mammary culture.

a. Establish the 3D hydrogel culture systems for harvesting large numbers of cells for FACS analysis(Dr. Engler's group).

As reported in the 2014 annual report, Dr. Engler's group has successfully developed the methods to produce two types of hydrogels on which to culture mammary epithelial cells, one with static properties as proposed (polyacrlyamide) and also one with dynamic properties that could remodel with time (hyaluronic acid); the dynamically stiffening material better mirrors the temporal nature of tumor stiffening. Both systems can fully mimic the physiological ranges of tissue rigidities from normal mammary gland (~150Pa) to human breast cancer (~5000Pa). In both systems, matrix stiffness can be accurately defined independently of biochemical factors, such as concentration of ECM proteins and growth factors.

The first system is the 3D PA-Matrigel overlay culture system, where matrix stiffness (or substrate elasticity) is defined by a polyacrylamide (PA) base with calibrated elastic moduli ranging between the ~150 Pascal (Pa) of normal mammary glands and the ~5700 Pa of breast

tumor tissues (1, 2). We found that this 3D PA-Matrigel culture system allows the formation of polarized mammary ductal acini in the compliant "soft" matrix, while rigid matrix stiffness induced an EMT-like phenotype including loss of epithelial polarity, and degradation of basement membrane, and loosening of cell-cell adhesion (Fig. 6D), consistent with previous publications (1).

One significant problem with model systems that rely on polyacrylamide and/or matrigel to recapitulate the mammary niche is that they present constant niche properties to mammary cells, which is not the case with cancer. Mammary acini do not develop in a niche with tumor-like stiffness, e.g. 500–5000 Pa. Rather this stiffening occurs after tissue maturation and mammary acini formation. Thus in parallel with the grant activities, the Yang and Engler labs have also pursued creating dynamic hydrogels that stiffen on demand to pose the similar question as Paszek et al but in a more biomimetic niche: "Does the mature

Figure 1. (A) Stiffness shown before and after additional UV crosslinking step of the indicated amount of time. (B) Images of acini pre- and post-stiffening to the indicated stiffness value and after 3 additional days in culture. Numbers indicate the percentage of acini having normal aspect ratios, as determined in panel (C). ***P<0.001.

mammary acinar structure desensitize mammary epithelial cells to changes in matrix stiffness?" As described in the 2014 progress report, to accomplish this, we substituted a previously developed hyaluronic acid (HA) hydrogel that was modified with a UV-sensitive methacrylate to permit "on demand" free radical polymerization (3). When MCF10A cells were allowed to mature in HA hydrogels with a single round of crosslinking, cells on stiffer matrices (3000, and 5000 Pa) underwent EMT whereas those on soft (100 Pa) did not (Figure 1).

In the past year, we have also continued to develop an understanding of how dynamic matrix changes influence EMT. Previously we showed that a subset of MECs (~25-35%), when grown into acini, were resistant to matrix stiffening, which would occur during tumorigenesis. This is unlike what one observes with static and stiff matrices, where few cells fail to undergo stiffness-mediated EMT. In this most recent year, we have asked two additional questions: (1) what is the sensitivity of cells to the range of dynamic stiffening from no change to a 30-fold stiffening, and (2) is this response cell autonomous?

When single cells are plated on substrates, previous work from Paszek et al (1) identified changes in cells between 400 to 600 Pascals (Pa) of stiffness. As shown in Figure X, when we stiffen the matrix to 1000 Pa, we still see the majority of cells remaining as acini. Only after
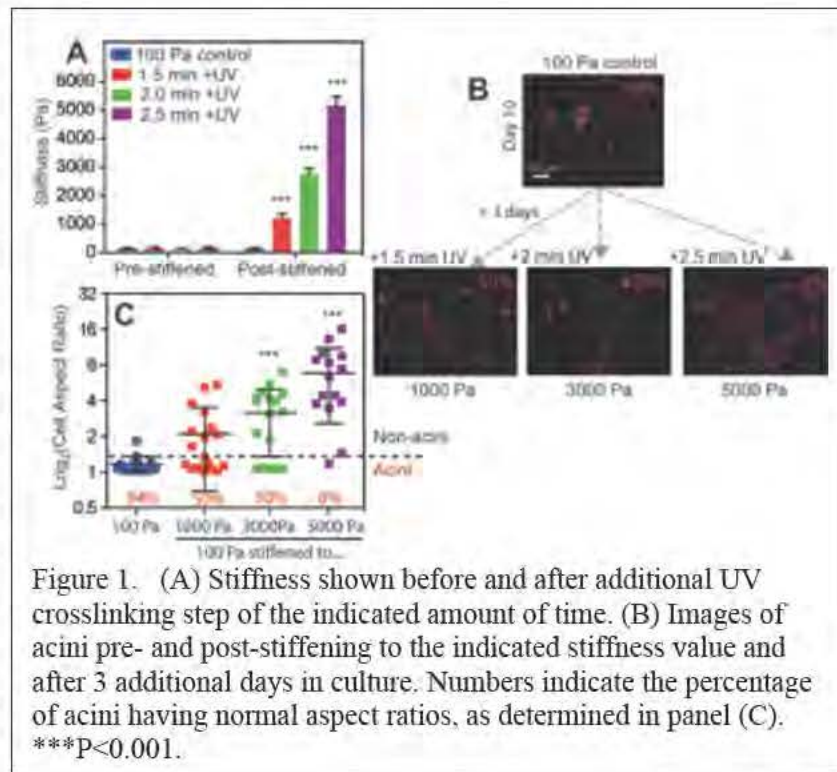
3000 Pa do we see most cells respond. Important with our observations in year 1, we still see 25-35% of acini not responding to stiffness. That begged the second question: is this response cell autonomous? To answer this question, we replated acini and EMT cells from stiffened matrices onto a second matrix that was either soft, stiff, or stiffened from soft to stiff. When replating acini if sensing was intrinsic to a cell, it would no longer care about stiffness and remain as an acinus. Conversely EMT cells would undergo EMT independent of stiffness after it was first induced. However, we did not observe this behavior and the majority of cells appeared to follow the signaling of their local environment (Figure 2). These results suggest

Figure 2. (A) Schematic of replating experiment, indicating the initial percentages of cells remaining as acini or undergoing EMT. Images of cells from the (B) acini and (D) EMT fractions of the primary culture that were separated and replated into the indicated conditions are shown. The percent of cells maintaining aciniar morphology for each condition are also shown for cells originating from (C) acinar and (E) EMT cells.

that mechanosensing is very transient. It also suggests that the population of non-responding cells changes based on local signaling.

b. Use Anchorage-independent mammosphere assay to determine the impact of matrix stiffness on breast CSC mammosphere forming ability (Dr. Yang's group).

   As described in the 2014 report, we have completed this subaim and found that increasing matrix stiffness significantly increases the mammosphere formation ability in breast cancer cells.

c. Use FACS analysis of ALDEFLUOR and CSC cell surface markers to test the impact of matrix stiffness on breast CSC properties (Dr. Yang's group).

As reported in the 2014 report, we found that CSC cell surface markers CD44 and CD24 and ALDEFLUOR assay were not sufficient to identify cancer stem cell markers in MCF10A cells cultured in vitro. Published literatures show that different cancer stem cells can be enriched with very diverse members of molecular markers and it is unclear whether any of these markers play a biological role in regulating cancer stem cell function. Therefore, we decided to focus more on using functional assays (including mammosphere formation described in Task 1b above and tumor initiation assay in vivo described below) to characterize cancer stem cells, instead of relying on molecular markers.

2. Determine whether rigid matrix stiffness promotes tumor initiation efficiency in vivo.
For unknown reasons, the USAMRMC Animal Care and Use Review Office (ACURO) did not review our animal protocol submitted in Jan. 2013 until Sept. 2014. After we resubmitted the updated protocol in Sept. 2014 with two follow-up reminders, we finally received animal protocol approval on Dec. 8, 2014. Therefore, we started performing the proposed animal experiments only in the past 6 months. Due to our fast progress in Aim 2, we spent more efforts and resources in Aim 2 to perform in vitro experiments in the past year.

a. Establish mammary implantation models and determine the proper dose of BAPN treatment on matrix stiffness in vivo, (Dr. Yang's group).
Towards this goal, we have implanted EPH4Ras cells in the mammary fat pads and treated half of the mice daily with β-aminopropionitrile (BAPN), a non-reversible LOX inhibitor (4, 5), to inhibit collagen crosslinking. We tested various dose used and the delivery routes (orally through drinking water vs. intraperitoneal injection). In collaboration with Dr. Robert Sah at UCSD Bioengineering, Dr. Albert Chen in his group has adapted the equipment and analysis software to measure and analyze the elastic modulus of tumor samples by unconfined compression testing (6). Our preliminary data showed that the equilibrium elastic modulus of the EPH4Ras tumor samples was in average 800Pa and that BAPN treatment reduced the elastic modulus of EPH4Ras tumor samples by 40% without obvious toxicity (Fig.3A). To further evaluate whether BAPN reduces fibrillar collagen in tumors, we used two-photon-excited Second-Harmonic Generation (SHG) microscopy to image and quantify fibrillar collagen curvature ratio (7) in unstained tumor sections and confirmed the effect of BAPN (Fig. 3B). Furthermore, BAPN treatment resulted in more epithelial tumors with higher E-cadherin expression (Fig. 3C). We found that intraperitoneal injection at a dose of 100 mg/kg in 100 μl PBS resulted in the best LOX inhibition
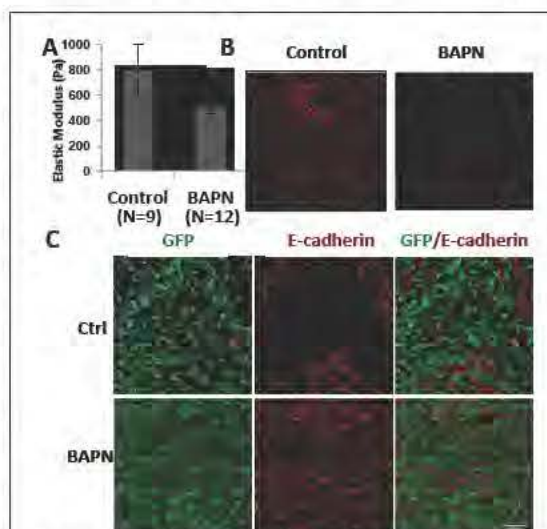
Figure 3. BAPN treatment reduces matrix stiffness, fibrillar collagen and EMT phenotypes in breast tumor xenografts. A) BAPN treatment reduced equilibrium modulus calculated between 5% and 15% strain in primary tumors. B) SHG imaging confirmed reduced straight fibrillar collagen in primary tumors upon BAPN treatment. C) BAPN treatment resulted in more epithelial tumors with higher E-cadherin expression. Tumor cells were labeled with GFP.

4

with less side effects. Therefore, we have successfully established the condition for BAPN treatment in vivo.

Task 2. Determine the mechanotransduction pathways that regulate cancer stem cell in response to matrix stiffness.

Although we initially planned to pursue this aim in the 2nd and 3rd year of the funding cycle, we have made very interesting observations on the role of matrix stiffness in regulating epithelial-mesenchymal transition (EMT) via activating the EMT-inducing transcription factor Twist1 soon after starting this project. Given that the EMT program has been tightly linked to giving rise to breast cancer stem cell properties (8, 9), we have pursued this mechanistic aim immediately ahead of schedule and with much more emphasis given the critical role of EMT in breast cancer progression.

1. Determine the role of known mechanosensing pathways in regulating cancer stem cell function.
a. Test whether β1 integrin and its downstream kinases are requried for transmitting matrix stiffness to CSC regulation in the 3D PA-Matrigel assays (Dr. Engler and Dr. Yang's group).

As described in our 2014 report, we have completed this subaim last year and found that induction of EMT is regulated by mechanical force in a β1 integrin-dependent manner.

2. Test the involvement of Epithelial-Mesenchymal Transition in regulating breast cancer stem cell in response to matrix stiffness (Dr. Yang's group and Dr. Adam's group).
a. Use shRNA lentivirus to knock down individual genes in human breast cancer cell lines and test their effects on CSC properties in response to rigid matrix stiffness, Months 24-28 (Dr. Yang's group). We have completed this aim and published the results ahead of schedule.

To understand whether EMT-inducing transcription factors plays functional roles in the mechanosensing response, we have tested whether knocking down individual
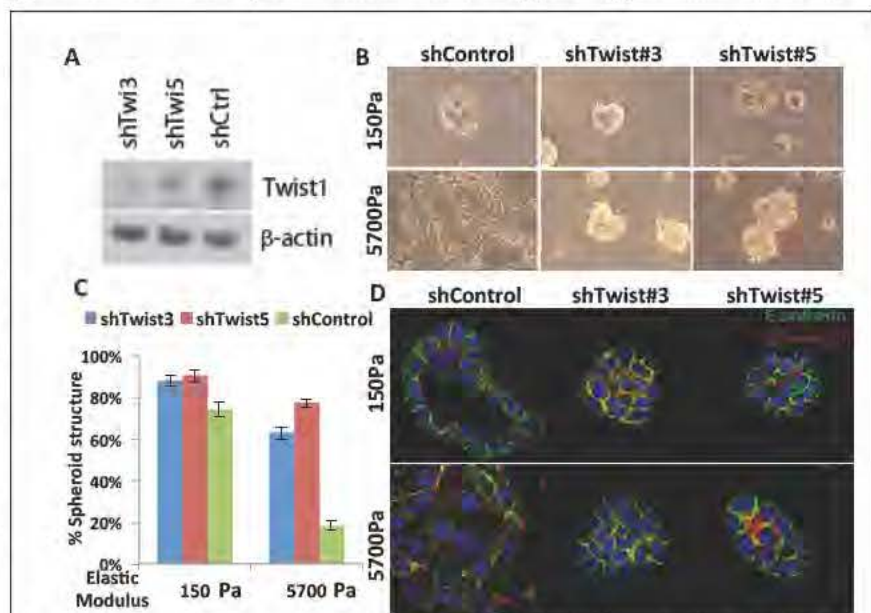
Figure 4. Twist1 is required for rigid matrix stiffness-induced EMT phenotype. A) Western blot analysis shows the knockdown level of Twist1 by two independent shRNAs in EPH4Ras cells. B-C) Knocking down Twist1 blocked EMT-like invasion and recued spheroids formation in rigid matrix in EPH4Ras cells. D) Immunostaining of EPH4Ras cells shows that knocking down Twist1 prevented loosing of adherent junctions as evident by E-cadherin (green) membrane localization.

EMT-inducing transcription factors blocks the EMT-like phenotype induced by rigid matrix stiffness. There are three major families of EMT-inducing transcription factors, Twist1/2, Snail1/2, and Zeb1/2. Based on the availability of shRNAs against these factors, we have tested shRNAs again Twist1 and Snail2 to date. We used two independent shRNAs to knock down endogenous Twist1 (Fig. 4A) or Snail2 expression in MCF10A and EPH4Ras cells and applied the resulting cells to the 3D mammary acini cultures with matrix stiffness arranging from 150 Pa to 5700 Pa. Significantly, in both cell types, knockdown of Twist1, but not Snail2, prevented the EMT-like invasive phenotype induced by the stiff matrix stiffness of 5700Pa; instead these mammary cells formed spheroid mammary ductal acini similar to that in the compliant matrix stiffness of 150Pa (Fig.4B-4D). Since high stiffness alone was not sufficient to induce a complete EMT, we further investigated whether Twist1 is also required for the induction of a full EMT by mechanical signals in concert with the EMT-inducing biochemical signal TGF-beta(10). Indeed, knockdown of Twist1 also completely blocked induction of EMT by TGF-beta at high matrix stiffness and rescued acinar development (data not shown). Together, these results indicate that Twist1 is a key player in a cellular mechanosensing pathway and plays an essential role in mediating EMT in response to matrix stiffness.

We next aimed to understand how Twist1 is regulated by matrix stiffness to mediate EMT and invasion. Since Drosophila Twist1 mRNA expression is induced by mechanical forces(11), we examined Twist1 mRNA and protein expression under various matrix rigidities and found no differences (Fig. 5A and 5B). Surprisingly, immunostaining showed that Twist1 was largely cytoplasmic on the compliant matrix of 150Pa and translocated into the nucleus on the rigid matrix of 5700Pa. High stiffness-induced
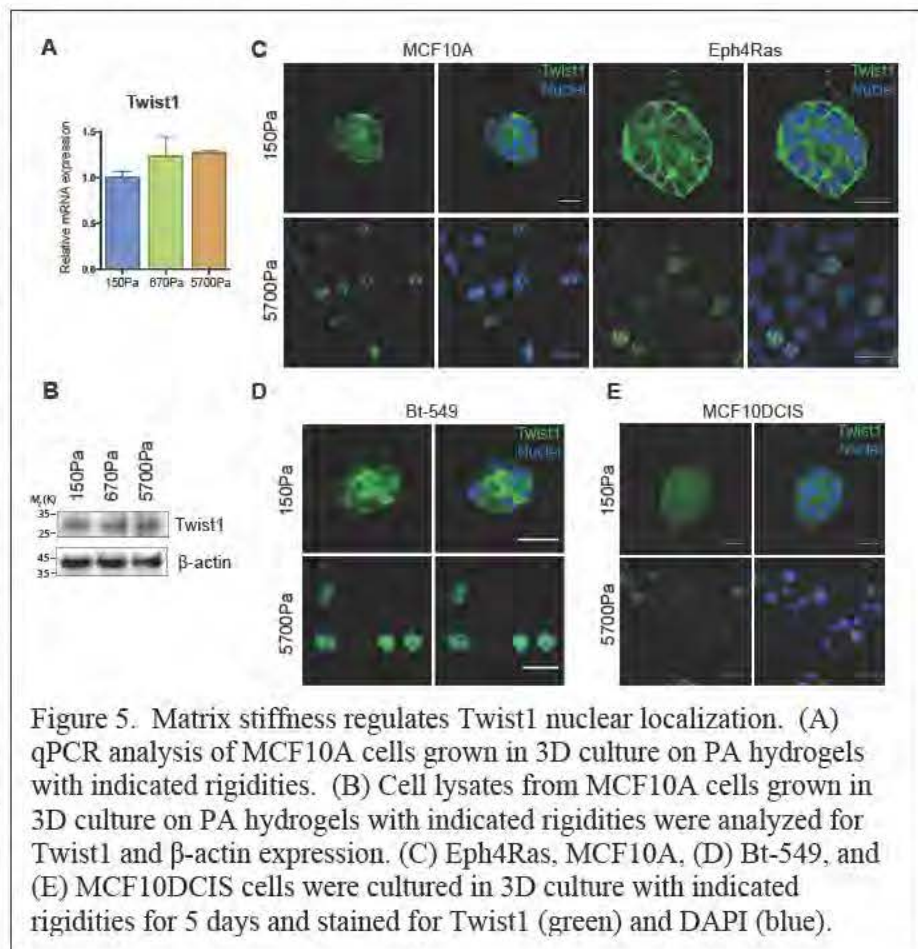
Figure 5. Matrix stiffness regulates Twist1 nuclear localization. (A) qPCR analysis of MCF10A cells grown in 3D culture on PA hydrogels with indicated rigidities. (B) Cell lysates from MCF10A cells grown in 3D culture on PA hydrogels with indicated rigidities were analyzed for Twist1 and β-actin expression. (C) Eph4Ras, MCF10A, (D) Bt-549, and (E) MCF10DCIS cells were cultured in 3D culture with indicated rigidities for 5 days and stained for Twist1 (green) and DAPI (blue).

nuclear translocation of Twist1 was observed in human MCF10A and mouse Eph4Ras cells (Fig. 5C), and in MCF10DCIS and Bt-549 human breast cancer cells (Fig. 5D and 5E), suggesting that nuclear translocation of Twist1 is a conserved response to increasing matrix stiffness. These

results suggest that matrix stiffness could directly impinge upon the EMT program by controlling Twist1 nuclear translocation.

To understand the molecular mechanism underlying Twist1 cytoplasmic retention, we used mass spectrometry analysis to identify Twist1-binding proteins that anchor Twist1 in the cytoplasm. Ras GTPase-activating protein-binding protein 2 (G3BP2) stood out as a promising candidate based on previous studies showing that G3BP2 regulates cytoplasmic retention of MDM2 and IκBα(12, 13). We confirmed that both endogenously expressed Twist1 co-immunoprecipitated with endogenous G3BP2 (Fig. 6A). Previous studies identified a region of IκBα responsible for binding to G3BP2(13). Sequence alignment of this G3BP2-interacting region of IκBα with Twist1 and MDM2 revealed a consensus G3BP2-binding motif, Q-X-X-X-E-L-Q-[ET]-X-[KR]-[LPV] (Fig. 6B). Interestingly, this G3BP2-binding motif is highly conserved among vertebrate Twist1 proteins, but to a significantly lesser degree in *Drosophila* in which Twist expression, rather than localization, is regulated by mechanical cues(11) (Fig. 6C). Deletion of this motif (ΔQT mutant) in Twist1 abolished its interaction with G3BP2 (Fig. 6D). Together, these data show that G3BP2 binds to Twist1 through the conserved G3BP2-binding motif on vertebrate Twist1 proteins.
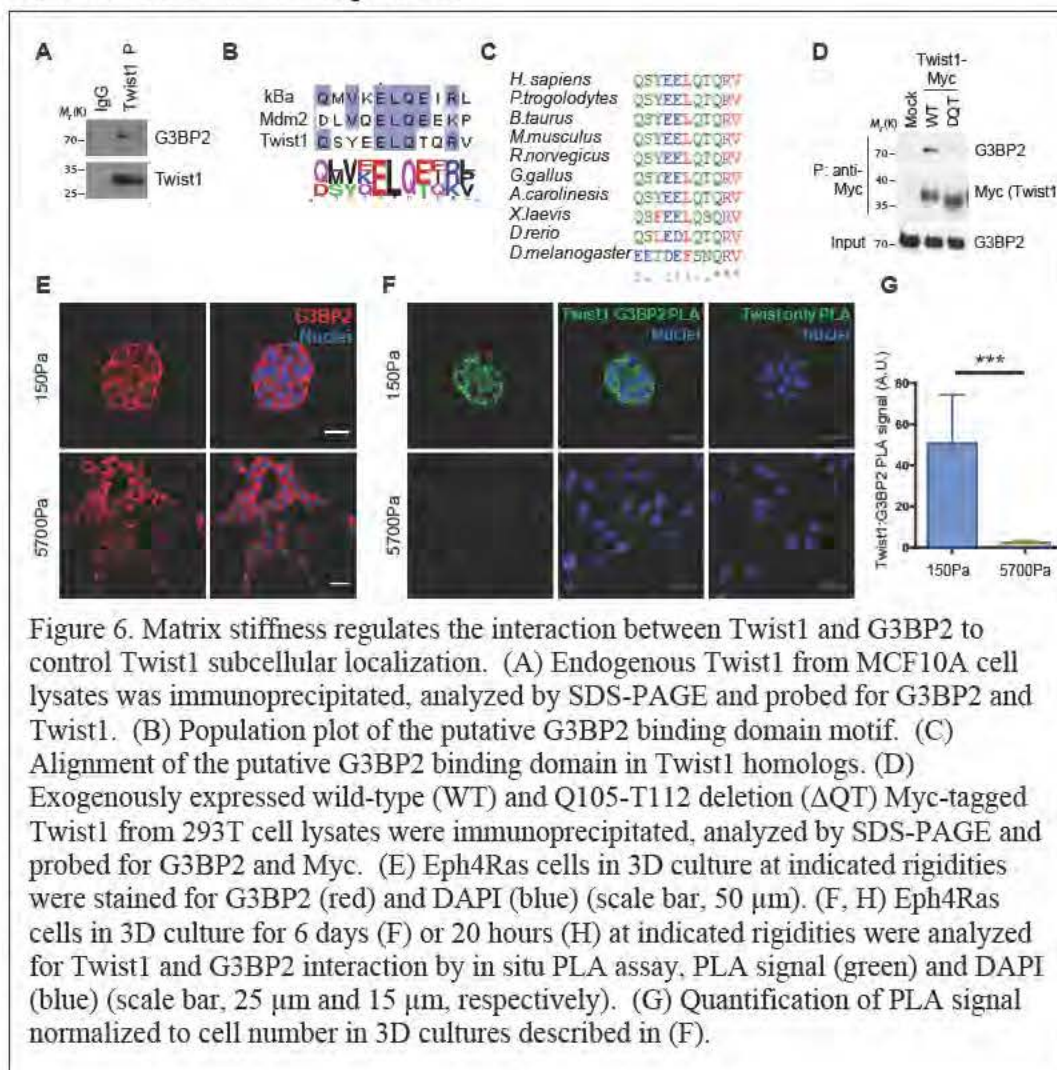
Figure 6. Matrix stiffness regulates the interaction between Twist1 and G3BP2 to control Twist1 subcellular localization. (A) Endogenous Twist1 from MCF10A cell lysates was immunoprecipitated, analyzed by SDS-PAGE and probed for G3BP2 and Twist1. (B) Population plot of the putative G3BP2 binding domain motif. (C) Alignment of the putative G3BP2 binding domain in Twist1 homologs. (D) Exogenously expressed wild-type (WT) and Q105-T112 deletion (ΔQT) Myc-tagged Twist1 from 293T cell lysates were immunoprecipitated, analyzed by SDS-PAGE and probed for G3BP2 and Myc. (E) Eph4Ras cells in 3D culture at indicated rigidities were stained for G3BP2 (red) and DAPI (blue) (scale bar, 50 μm). (F, H) Eph4Ras cells in 3D culture for 6 days (F) or 20 hours (H) at indicated rigidities were analyzed for Twist1 and G3BP2 interaction by in situ PLA assay, PLA signal (green) and DAPI (blue) (scale bar, 25 μm and 15 μm, respectively). (G) Quantification of PLA signal normalized to cell number in 3D cultures described in (F).

To directly test whether matrix stiffness regulates Twist1-G3BP2 interaction, we utilized *in situ* proximity ligation assay (PLA) to examine the interaction of endogenous Twist1 and G3BP2 proteins in 3D acinar cultures of Eph4Ras cells. PLA technology

directly detects endogenous Twist1/G3BP2 interactions with high specificity and sensitivity in intact acini using antibodies against Twist1 and G3BP2. Indeed, at 150Pa a strong PLA signal, indicating Twist1/G3BP2 interaction, was specifically enriched in the cytoplasm. In contrast, very little PLA signal was detected at 5700Pa, indicating that Twist1 is released from G3BP2 and translocates into the nucleus at high matrix rigidity (Fig. 6F and 6G). These experiments demonstrate that matrix stiffness directly regulates the interaction between Twist1 and G3BP2 to control Twist1 subcellular localization.

We next asked whether G3BP2 is functionally required for Twist1
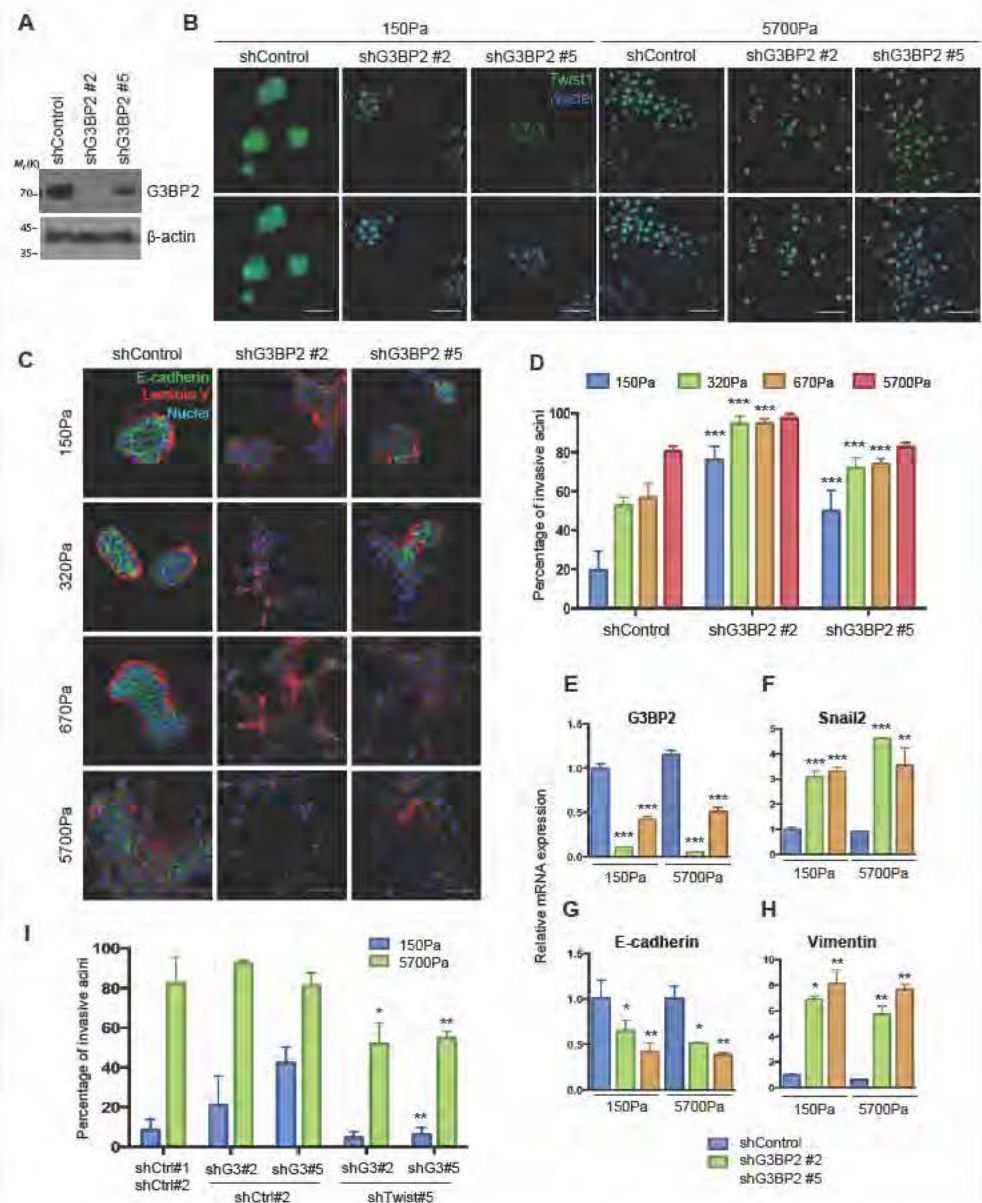
Figure 7. Loss of G3BP2 cooperates with increasing matrix stiffness to promote Twist1 nuclear localization and EMT. (A) Cell lysates from Eph4Ras cells expressing control or G3BP2 shRNAs were analyzed by SDS-PAGE and probed for G3BP2 and β-actin. (B) Eph4Ras cells expressing control or G3BP2 shRNAs were cultured in 3D culture with indicated rigidities for 5 days and stained for Twist1 (green) and DAPI (blue). (C) Eph4Ras cells expressing control or G3BP2 shRNAs were cultured in 3D culture with varying rigidities for 5 days and stained for E-cadherin (green), Laminin V (red) and DAPI (blue). (D) Quantification of invasive acini in 3D culture described in (C) from 3 independent experiments (P<0.001). qPCR analysis of (E) G3BP2, (F) Snail2, (G) E-cadherin and (H) Vimentin in Eph4Ras cells expressing control or G3BP2 shRNAs 3D cultured under indicated matrix rigidities for 5 days (**, P<0.01; ***, P<0.001). (I) Quantification of invasive acini of Eph4Ras cells expressing control (shCtrl#1) or G3BP2 shRNAs, together with control (shCtrl#2) or Twist1 shRNA (shTwist1#5), 3D cultured under indicated matrix rigidities for 5 days (*, P<0.05; **, P<0.01).

cytoplasmic retention in compliant matrices. We used shRNAs to knock down G3BP2 expression and determined the impact on Twist1 localization (Fig. 7A, 7E). For both MCF10A and Eph4Ras cells on compliant matrices, knockdown of G3BP2 resulted in nuclear accumulation of Twist1, suggesting that G3BP2 is necessary for cytoplasmic sequestration of Twist1 in response to low matrix stiffness (Fig. 7B). These data strongly support a critical role of G3BP2 in regulating Twist1 subcellular localization in response to matrix stiffness.

To test the impact of G3BP2 loss on EMT and invasion, we cultured Eph4Ras and MCF10A cells on a gradient of PA hydrogels with elasticities ranging from 150Pa to 5700Pa in 3D culture. G3BP2 knockdown and the resulting constitutive Twist1 nuclear localization significantly increased the percentage of invasive acini at matrix rigidities ranging from 150Pa to 670Pa (Fig. 7C and 7D). Importantly, loss of G3BP2 and increasing matrix stiffness synergistically resulted in destabilization of basement membrane, an EMT phenotype, and invasion of cells into the surrounding ECM (Fig. 7C and 7D). The EMT phenotype was characterized by down-regulation of E-cadherin and disruption of basement membrane as shown by Laminin V staining (Fig. 7C). Furthermore, G3BP2 knockdown repressed expression of E-cadherin and induced expression of Vimentin (Fig. 7G and 7H). To determine whether the EMT phenotype resulting from G3BP2 knockdown is dependent on Twist1, we knocked down both Twist1 and G3BP2 and found that the EMT and invasive phenotype were significantly suppressed compared to cells that were only depleted of G3BP2 (Fig. 7I). Snail2, a direct transcription target of Twist1(14), was induced upon G3BP2 knockdown, while double knockdown of G3BP2 and Twist1 blocked Snail2 induction, suggesting that the effects of G3BP2 knockdown are dependent on Twist1(Fig. 7F). These data indicate that G3BP2 directly impacts EMT and invasion in response to matrix stiffness and provide a mechanism by which the Twist1-G3BP2 mechanotransduction pathway can facilitate tumor invasion. Furthermore, it suggests that down-regulation of G3BP2 expression in tumor cells could cooperate with increasing matrix stiffness in the tumor microenvironment to facilitate tumor invasion and metastasis.

b. Test whether the EMT program plays a key role in tumor progression in mammary xenografts in response to rigid v.s. compliant matrix stiffness (Dr. Yang's group). We have conducted this subaim ahead of schedule in the past year.

To test the role of G3BP2 in tumor progression *in vivo*, we employed a human xenograft tumor model of comedo ductal carcinoma *in situ*, the MCF10DCIS cell line(15), which is a derivative of MCF10A cells expressing oncogenic Ras. This xenograft model recapitulates the development of ductal carcinoma in situ (DCIS) in human breast cancer. Concordant with our results in Eph4Ras and MCF10A mammary epithelial cells, knockdown of G3BP2 in conjunction with increasing matrix stiffness promoted Twist1 nuclear localization and an invasive phenotype in MCF10DCIS cells in 3D culture, indicating that the Twist1-G3BP2 mechanotransduction pathway is intact in this model (Fig. 8A, 8B). We injected these cells into the mammary fat pads of NOD/SCID mice and allowed tumor formation for 7 weeks. There was no significant difference in the weight of control and shG3BP2 primary mammary tumors (Fig. 8C). Immunostaining confirmed significantly lower levels of G3BP2 in tumors with G3BP2 knockdown (Fig. 8D). Interestingly, in control tumors, αSMA-positive mesenchymal cells were largely present at the edge of the tumor; in contrast, these cells often infiltrated into the

intratumoral region in shG3BP2 tumors, a phenotype associated with DCIS to invasive ductal carcinoma progression (Fig. 8D).

We next examined whether knockdown of G3BP2 affects tumor invasion and metastasis. Tumors expressing G3BP2 shRNAs presented not only local invasion into the surrounding mammary tissue, but also regional invasion into the nearby peritoneal wall, visualized as GFP
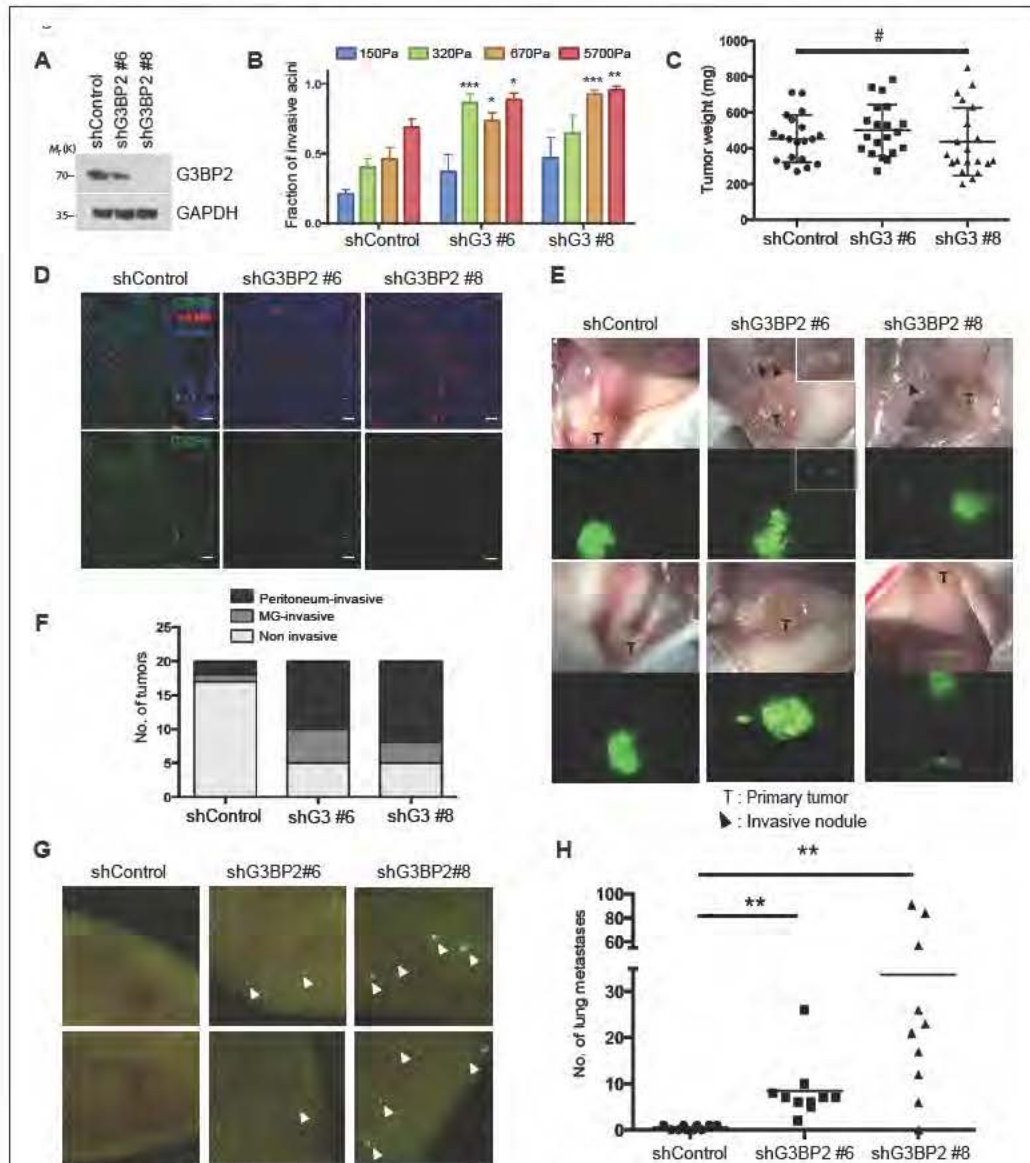
Figure 8. Loss of G3BP2 induces tumor invasion *in vivo*. (A) Cell lysates from MCF10DCIS cells expressing control or G3BP2 shRNAs were analyzed by SDS-PAGE and probed for G3BP2 and GAPDH. (B) Quantification of invasive acini formed by MCF10DCIS cells expressing control or G3BP2 shRNAs cultured in 3D culture with varying rigidities for 5 days (*, P<0.05; **, P<0.01; ***, P<0.001). (C) Tumor weight of MCF10DCIS xenograft tumors expressing control or G3BP2 shRNAs (#, not statistically significant, T-test, n=20 tumors), (D) Tissue sections of control and shG3BP2 MCF10DCIS xenografts stained with G3BP2 (green), αSMA (red), and DAPI (blue) and imaged by confocal microscopy. (E) Fluorescent and brightfield images of GFP (green) labeled MCF10DCIS xenograft tumors *in situ*. (F) Quantification of local (MG-invasive) and regional (Peritoneum-invasive) invasion of MCF10DCIS xenograft tumors. (**G**) Fluorescent images and (**H**) quantification of lung metastases (green, indicated by arrows) from MCF10DCIS xenograft tumors (**, P<0.01, T-test, n=10 mice).

10

positive tumor cells in these regions (Fig. 8E and 8F). More importantly, tumors expressing G3BP2 shRNAs consistently presented with a striking increase in the number of distant metastases in the lungs compared to tumors expressing a control shRNA (mean increase: 15 and 65-fold for shG3BP2#6 and #8 versus control, respectively) (Fig. 8G, 8H). Together, these results strongly support a key role for G3BP2 in suppressing invasion and metastasis *in vivo*.

SUMMARY of RESEARCH ACCOMPLISHMENTS

- We developed two hydrogel systems and determined their mechanic properties.
- We found that increasing tissue rigidities promoted breast cancer stem cell properties.
- We uncovered that a mechanistic link between tissue rigidity and breast cancer stem cells was via the activation of the EMT program.
- We found that the EMT-inducing transcription factor Twist1 was essential for high tissue-rigidity-induced EMT.
- We identified a novel Twist1/G3BP2 mechanotransduction pathway that responds to increasing matrix stiffness in the tumor microenvironment to drive EMT, cancer stem cell properties, invasion, and metastasis.

• **What opportunities for training and professional development has the project provided?**
Nothing to report.

• **How were the results disseminated to communities of interest?**
Dr. Yang has presented this research to three-times breast cancer survivor and donor Vivian Hadge in May 2015.

• **What do you plan to do during the next reporting period to accomplish the goals?**
Plan for the coming year: We plan to continue the study as described in the SOW submitted in the original application. We will specifically focus on the following subaims.

Task 1
   2. Determine whether rigid matrix stiffness promotes tumor initiation efficiency in vivo.
      c. Perform mammary implantation experiments to determine whether BAPN treatment reduces enrichment of CSC subpopulation by FACS in vivo.
   3. Determine whether rigid matrix stiffness promotes CSC-mediated chemoresistance in vivo, Month 8-18.
      a. Establish the Epirubicin chemotherapy treatment condition to enrich CSCs in mice.
      b. Perform chemotherapy-induced CSC enrichment in vivo experiments to test the role of matrix stiffness in mediating CSC-mediated chemoresistence in mice.

Task 2. Determine the mechanotransduction pathways that regulate cancer stem cell in response to matrix stiffness.
   1. Determine the role of known mechanosensing pathways in regulating cancer stem cell function.

a. Test whether Rho-generated cytoskeletal tension is requried for transmitting matrix stiffness to CSC regulation in the 3D PA-Matrigel assays.
b. Determine whether any of the inhibitors that are tested positive in a) and b) inhibit CSC-mediated tumor initation in mammary tumor xenografts in vivo.
c. Determine whether any of the inhibitors that are tested positive in a) and b) inhibit CSC-mediated chemoresistence in mammary tumor xenografts in vivo.

REFERENCES

1.   Paszek MJ, Zahir N, Johnson KR, Lakins JN, Rozenberg GI, Gefen A, Reinhart-King CA, Margulies SS, Dembo M, Boettiger D, Hammer DA, Weaver VM. Tensional homeostasis and the malignant phenotype. Cancer Cell. 2005;8(3):241-54.
2.   Johnson KR, Leight JL, Weaver VM. Demystifying the effects of a three-dimensional microenvironment in tissue morphogenesis. Methods Cell Biol. 2007;83:547-83. PMCID: 2658721.
3.   Guvendiren M, Burdick JA. Stiffening hydrogels to probe short- and long-term cellular responses to dynamic mechanics. Nat Commun. 2012;3:792.
4.   Lucero HA, Kagan HM. Lysyl oxidase: an oxidative enzyme and effector of cell function. Cell Mol Life Sci. 2006;63(19-20):2304-16.
5.   Levental KR, Yu H, Kass L, Lakins JN, Egeblad M, Erler JT, Fong SF, Csiszar K, Giaccia A, Weninger W, Yamauchi M, Gasser DL, Weaver VM. Matrix crosslinking forces tumor progression by enhancing integrin signaling. Cell. 2009;139(5):891-906. PMCID: 2788004.
6.   Chen AC, Bae WC, Schinagl RM, Sah RL. Depth- and strain-dependent mechanical and electromechanical properties of full-thickness bovine articular cartilage in confined compression. J Biomech. 2001;34:1-12.
7.   Wolf K, Alexander S, Schacht V, Coussens LM, von Andrian UH, van Rheenen J, Deryugina E, Friedl P. Collagen-based cell migration models in vitro and in vivo. Seminars in cell & developmental biology. 2009;20(8):931-41.
8.   Mani SA, Guo W, Liao MJ, Eaton EN, Ayyanan A, Zhou AY, Brooks M, Reinhard F, Zhang CC, Shipitsin M, Campbell LL, Polyak K, Brisken C, Yang J, Weinberg RA. The epithelial-mesenchymal transition generates cells with properties of stem cells. Cell. 2008;133(4):704-15. PMCID: 2728032.
9.   Morel AP, Lievre M, Thomas C, Hinkal G, Ansieau S, Puisieux A. Generation of breast cancer stem cells through epithelial-mesenchymal transition. PLoS One. 2008;3(8):e2888. PMCID: 2492808.
10.   Leight JL, Wozniak MA, Chen S, Lynch ML, Chen CS. Matrix rigidity regulates a switch between TGF-beta1-induced apoptosis and epithelial-mesenchymal transition. Molecular biology of the cell. 2012;23(5):781-91. PMCID: 3290638.
11.   Desprat N, Supatto W, Pouille PA, Beaurepaire E, Farge E. Tissue deformation modulates twist expression to determine anterior midgut differentiation in Drosophila embryos. Dev Cell. 2008;15(3):470-7.
12.   Kim MM, Wiederschain D, Kennedy D, Hansen E, Yuan ZM. Modulation of p53 and MDM2 activity by novel interaction with Ras-GAP binding proteins (G3BP). Oncogene. 2007;26(29):4209-15.

13.   Prigent M, Barlat I, Langen H, Dargemont C. IkappaBalpha and IkappaBalpha /NF-kappa B complexes are retained in the cytoplasm through interaction with a novel partner, RasGAP SH3-binding protein 2. The Journal of biological chemistry. 2000;275(46):36441-9.
14.   Casas E, Kim J, Bendesky A, Ohno-Machado L, Wolfe CJ, Yang J. Snail2 is an essential mediator of Twist1-induced epithelial mesenchymal transition and metastasis. Cancer Research. 2011;71(1):245-54. PMCID: 3025803.
15.   Miller FR, Santner SJ, Tait L, Dawson PJ. MCF10DCIS.com xenograft model of human comedo ductal carcinoma in situ. J Natl Cancer Inst. 2000;92(14):1185-6.

4. IMPACT

•   **What was the impact on the development of the principal discipline(s) of the project?**

Results from our two years of proposed research have identified a mechanotransduction pathway that transmits the mechanical cues from the breast tumor microenvironment to influence breast cancer stem cell properties via activation of Twist1 and the EMT program.   Breast tumors are often detected through physical palpation due to their apparent "hardness" compared to their normal compliant tissues. The presence of a fibrotic focus in breast tumors is a prognostic marker of distant metastasis and correlates with poor survival. Besides the biochemical factors from tumor stroma, fibrotic tumor lesions are associated with a 20-50 fold increase in tissue rigidity. Combining cell and molecular biology techniques with new bioengineering research tools, we have begun to uncover a novel mechanotransduction pathway that link tissue rigidity to breast cancer stem cell function.

•   **What was the impact on other disciplines?** Nothing to report.

•   **What was the impact on technology transfer?** Nothing to report.

•   **What was the impact on society beyond science and technology?**

Not only does understanding the impact of tissue rigidity on breast cancer stem cells enhance our knowledge of the molecular regulation of cancer stem cell, it also has direct impact on breast tumor prognosis and cancer treatment. Since cancer stem cells are thought to be responsible for breast tumor initiation and progression, genes and pathways involved in mechanoregulation of cancer stem cells holds promise to be useful prognostic markers for breast cancer. Given the critical role of breast cancer stem cells in breast tumor progression and chemoresistance, our research could lead to novel therapeutics targeting the mechanotransduction pathway to eradicate breast cancer stem cells and overcome chemoresistance.

5. CHANGES/PROBLEMS

We have published one paper in Nature Cell Biology early this year to report part of the findings of the proposed research. No significant changes in the research proposal, budget, vertebrate animals, and biohazards were made from the original application.

6. PRODUCTS

• **Publications, conference papers, and presentations**
   ▪ **Journal publications:** One research article that reports the main funding of the proposed research by both PI and the partnering PI were published in 2015.

Spencer C. Wei, Laurent Fattet, Jeff H. Tsai, Yurong Guo, Vincent H. Pai, Hannah E. Majecki, Albert C. Chen, Robert L. Sah, Susan S. Taylor, **Adam J. Engler**, **Jing Yang.** (2015) Matrix stiffness drives Epithelial-Mesenchymal Transition and tumor metastasis via a Twist1-G3BP2 mechanotransduction pathway. *Nature Cell Biology.* 17(5): 678-88. Acknowledgement of federal support: Yes.

One review article was also published in the past year with partial support from this grant. Haeyun Jung, Laurent Fattet, and **Jing Yang**. (2014) Molecular Pathways: Linking Tumor Microenvironment to Epithelial-Mesenchymal Transition in Metastasis. *Clinical Cancer research* 21(5); 1-7. Acknowledgement of federal support: Yes.

- ▪ **Presentations:**

2014	Gordon Conference on Rare Cells in Circulation: CTCs and metastasis, Mount Holyoke College, MA
2014	University of California, San Diego, Dept. of Bioengineering, La Jolla, CA
2014	Roswell Park Cancer Center, Buffalo, NY
2014	Stanford University Cancer Biology Program, Stanford, CA
2014	University of Kentucky, Lexington, KY
2015	"Pathways in Development and Cancer" conference, Freiburg, Germany
2015	Karmanos Cancer Institute, Detroit, MI
2015	University of California, Irvine Stem Cell Institute, Irvine, CA

7. PARTICIPANTS & OTHER COLLABORATING ORGANIZATIONS
- • **What individuals have worked on the project?**

Name:	Jing Yang
Project Role:	PI
Nearest person month worked	0.6 month
Contribution to Project	Dr. Yang is responsible for conceiving and overseeing the project, guiding her postdoctoral fellow Dr. Laurent Fattet to perform the proposed experiments. She will also coordinate all collaborations with Dr. Adam Engler for the project.
Funding Support	

Name:	Adam Engler
Project Role:	Partnering PI
Nearest person month worked	0.2 month
Contribution to Project	Dr. Engler is responsible for guiding his graduate student Matthew Ondeck to perform the proposed experiments. He will also coordinate all collaborations with Dr. Yang for the project.
Funding Support	

Name:	Laurent Fattet
Project Role:	Postdoctoral researcher

Nearest person month worked	12 months
Contribution to Project	Dr. Fattet is a postdoctoral fellow in the Yang lab and devoted 100% efforts on this project. He has made major contribution to the proposed research and published co-first author paper on this project in 2015.
Funding Support	

Name:	Matthew Ondeck
Project Role:	Graduate student
Nearest person month worked	3 months
Contribution to Project	Mr. Ondeck is a graduate student in the Engler lab and devoted 25% efforts on this project. He has developed tunable HA hydrogel described in Task 1 and continue to study how EMC stiffening can dynamically regulate breast cancer stem cells.
Funding Support	

- **Has there been a change in the active other support of the PD/PI(s) or senior/key personnel since the last reporting period?** No.
- **What other organizations were involved as partners?** No.

8. SPECIAL REPORTING REQUIREMENTS
Both PI and the partnering PI will submit the duplicate report. For individual tasks, the contribution from each PI groups is marked. Both groups are located at Univ. of California, San Diego, La Jolla, CA.

9. APPENDICES:
Two journal publications with the support of this grant are attached.

nature
cell biology

Matrix stiffness drives epithelial–mesenchymal transition and tumour metastasis through a TWIST1–G3BP2 mechanotransduction pathway

Spencer C. Wei[1,2,7,8], Laurent Fattet[1,8], Jeff H. Tsai[1], Yurong Guo[3], Vincent H. Pai[1,2], Hannah E. Majeski[1,2], Albert C. Chen[4], Robert L. Sah[4], Susan S. Taylor[1,3,5], Adam J. Engler[4] and Jing Yang[1,6,9]

Matrix stiffness potently regulates cellular behaviour in various biological contexts. In breast tumours, the presence of dense clusters of collagen fibrils indicates increased matrix stiffness and correlates with poor survival. It is unclear how mechanical inputs are transduced into transcriptional outputs to drive tumour progression. Here we report that TWIST1 is an essential mechanomediator that promotes epithelial–mesenchymal transition (EMT) in response to increasing matrix stiffness. High matrix stiffness promotes nuclear translocation of TWIST1 by releasing TWIST1 from its cytoplasmic binding partner G3BP2. Loss of G3BP2 leads to constitutive TWIST1 nuclear localization and synergizes with increasing matrix stiffness to induce EMT and promote tumour invasion and metastasis. In human breast tumours, collagen fibre alignment, a marker of increasing matrix stiffness, and reduced expression of G3BP2 together predict poor survival. Our findings reveal a TWIST1–G3BP2 mechanotransduction pathway that responds to biomechanical signals from the tumour microenvironment to drive EMT, invasion and metastasis.

Breast tumours are often detected by manual palpation, as they are more rigid than their surrounding normal tissue. This increase in tissue rigidity, or matrix stiffness, plays a significant role during tumour progression[1–5]. Organized collagen fibre alignment, which is a surrogate marker for increasing matrix stiffness in the tumour microenvironment, is associated with breast tumour progression[6–8]. The importance of mechanical forces in regulating cellular behaviours is also evident during embryogenesis[9–11]. For example, mesenchymal stem cells undergo lineage selection into either neurons or muscle and bone in response to distinct matrix elasticities[12]. The transcription co-activator YAP accumulates in the nucleus in stiffer matrices to allow osteogenic differentiation of mesenchymal stem cells[13]. How changes in the mechanical properties of extracellular matrix are converted into biochemical and transcriptional responses to direct tumour cell behaviour remains unknown.

Studies have shown that human mammary epithelial cells form normal ductal acini on compliant matrices that recapitulate the stiffness of normal mammary glands. On matrices with increased rigidity similar to breast tumours, however, cells lose apical–basal polarity, form weaker junctions and invade through the basement membrane[1,2]. These cellular changes in response to increasing stiffness resemble many morphological features associated with EMT, a developmental program also critical for tumour cell dissemination and metastasis[14,15]. During EMT, cells lose their epithelial characteristics, including cell junctions and polarity, and acquire a mesenchymal morphology and the ability to invade. The EMT program is orchestrated through a network of transcription factors, including TWIST1, TWIST2 (refs 16,17), SNAI1, SNAI2 (refs 18–20), ZEB1 and ZEB2 (refs 21,22). Therefore, we set out to understand how matrix stiffness regulates the EMT molecular pathway to promote tumour invasion and metastasis.

RESULTS

TWIST1 is essential for matrix-stiffness-induced EMT and invasion

The basic helix–loop–helix (bHLH) transcription factor, TWIST1, is essential for the ability of tumour cells to metastasize through activation of EMT and extracellular matrix degradation[16,23]. Mechanical
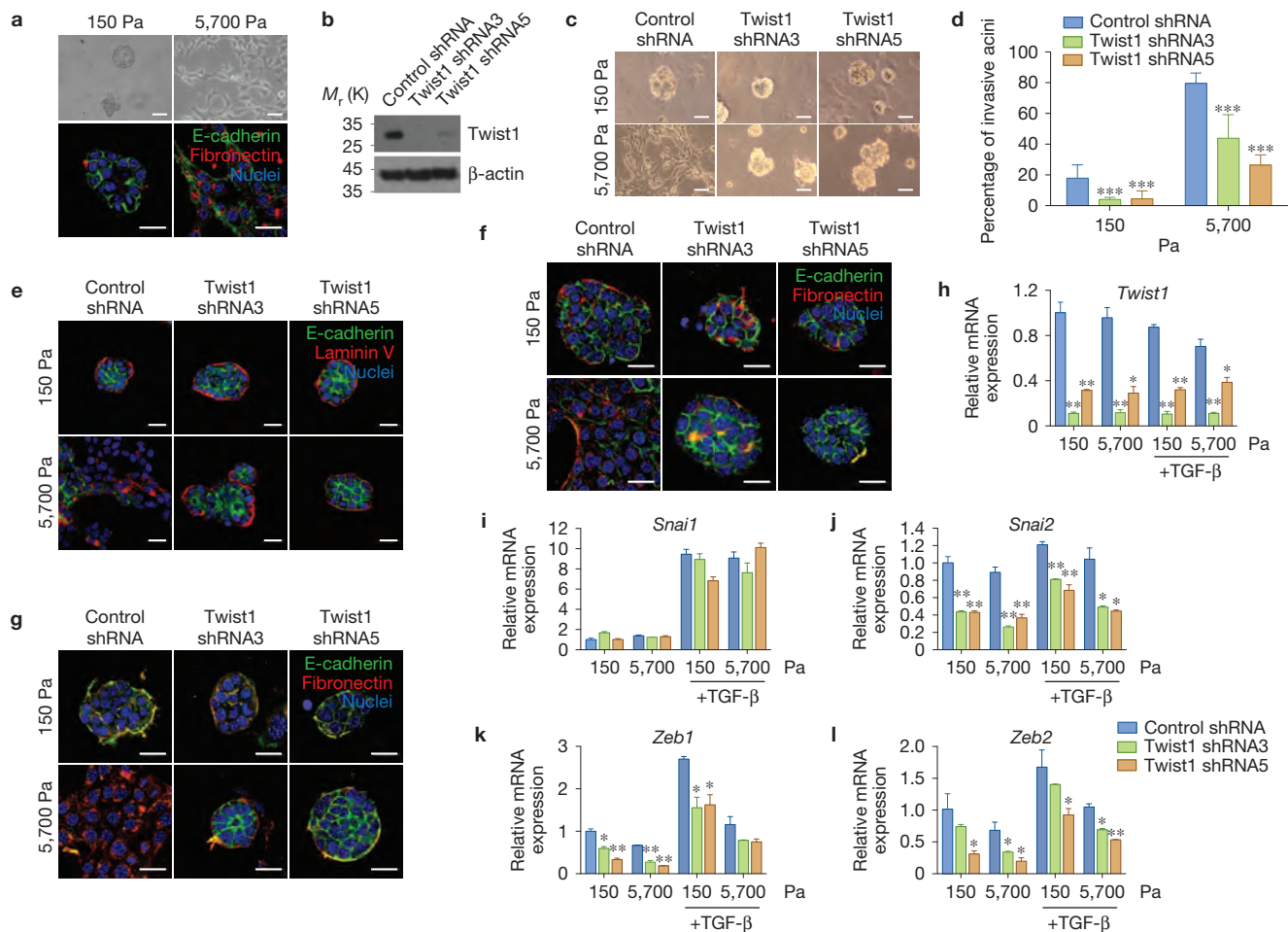
Figure 1 TWIST1 is essential for matrix-stiffness-induced EMT and invasion. (**a**) Eph4Ras cells after 5 days of growth in 3D culture on polyacrylamide hydrogels with the indicated rigidities imaged by bright-field (top) or stained (bottom) for E-cadherin (green), fibronectin (red) and nuclei (blue; scale bars, 25 μm). (**b**) Cell lysates from Eph4Ras cells expressing control and *Twist1* shRNAs were analysed by SDS–PAGE and probed for Twist1 and β-actin. Unprocessed original scans of the blots are shown in Supplementary Fig. 7. (**c**) Bright-field images of Eph4Ras cells expressing control or *Twist1* knockdown shRNAs after 5 days growth in 3D culture on polyacrylamide hydrogels with the indicated rigidities (scale bars, 50 μm). (**d**) Quantification of invasive acini in 3D culture described in **c** from 3 independent experiments (***, $P < 0.001$, unpaired two-tailed *t*-test with Welch's correction, $n = 50$ acini per experiment, 3 independent experiments, error bars represent s.d.).

(**e**) Eph4Ras cells expressing control or *Twist1* knockdown shRNAs after 5 days growth in 3D culture on polyacrylamide hydrogels with the indicated rigidities stained for laminin V (red), E-cadherin (green) and nuclei (blue; scale bars, 25 μm). (**f**,**g**) Eph4Ras cells expressing control or *Twist1* shRNAs were cultured in 3D culture with the indicated rigidities in the absence (**f**) or presence of 5 ng ml^{-1} TGF-β (**g**) for 8 days and stained for E-cadherin (green), fibronectin (red) and nuclei (blue; scale bars, 25 μm). (**h–l**) qPCR analysis of *Twist1* (**h**), *Snai1* (**i**), *Snai2* (**j**), *Zeb1* (**k**) and *Zeb2* (**l**) mRNA expression in Eph4Ras cells expressing control or *Twist1* shRNAs cultured under the indicated matrix rigidities in the absence or presence of 5 ng ml^{-1} TGF-β (*, $P < 0.05$; **, $P < 0.01$; unpaired two-tailed *t*-test with Welch's correction, $n = 3$ independent experiments, statistics source data can be found in Supplementary Table 1; error bars represent s.d.).

forces induce Twist expression during *Drosophila* larval development[24]; therefore, we investigated whether increasing matrix stiffness regulates mammalian TWIST1 to promote EMT and tumour invasion. We employed a collagen-coated polyacrylamide hydrogel system with calibrated elastic moduli ranging from the ~150 pascals (Pa) of normal mammary glands to the ~5,700 Pa of breast tumour tissues[1,25] in a three-dimensional (3D) Matrigel overlay culture system[26–28]. Non-transformed human MCF10A and tumorigenic mouse Eph4Ras mammary epithelial cells were used because unlike normal mammary epithelial cells *in vivo*[29], both cell lines endogenously express TWIST1, suggesting that genetic or epigenetic alterations predispose them to tumour progression[23,30,31]. Both cells developed polarized ductal acini surrounded by intact basement membrane on compliant

150 Pa matrices. In contrast, at a high matrix stiffness of 5,700 Pa, cells presented a partial EMT phenotype (Fig. 1a), similar to the matrix-stiffness-induced malignant phenotype described previously[1]. Notably, the intact basement membrane observed at low stiffness was destabilized at high matrix stiffness, consistent with previous observations that increasing matrix stiffness induces cellular invasion[1,2,32] (Supplementary Fig. 1A). As loss of basement membrane integrity is a critical event during the metastatic cascade, we used this pronounced response as a functional readout of cellular invasion in conjunction with changes in EMT markers.

Using this system, we investigated whether TWIST1 is required for induction of EMT and invasion in response to high matrix stiffness. We generated Eph4Ras and MCF10A cells expressing short hairpin
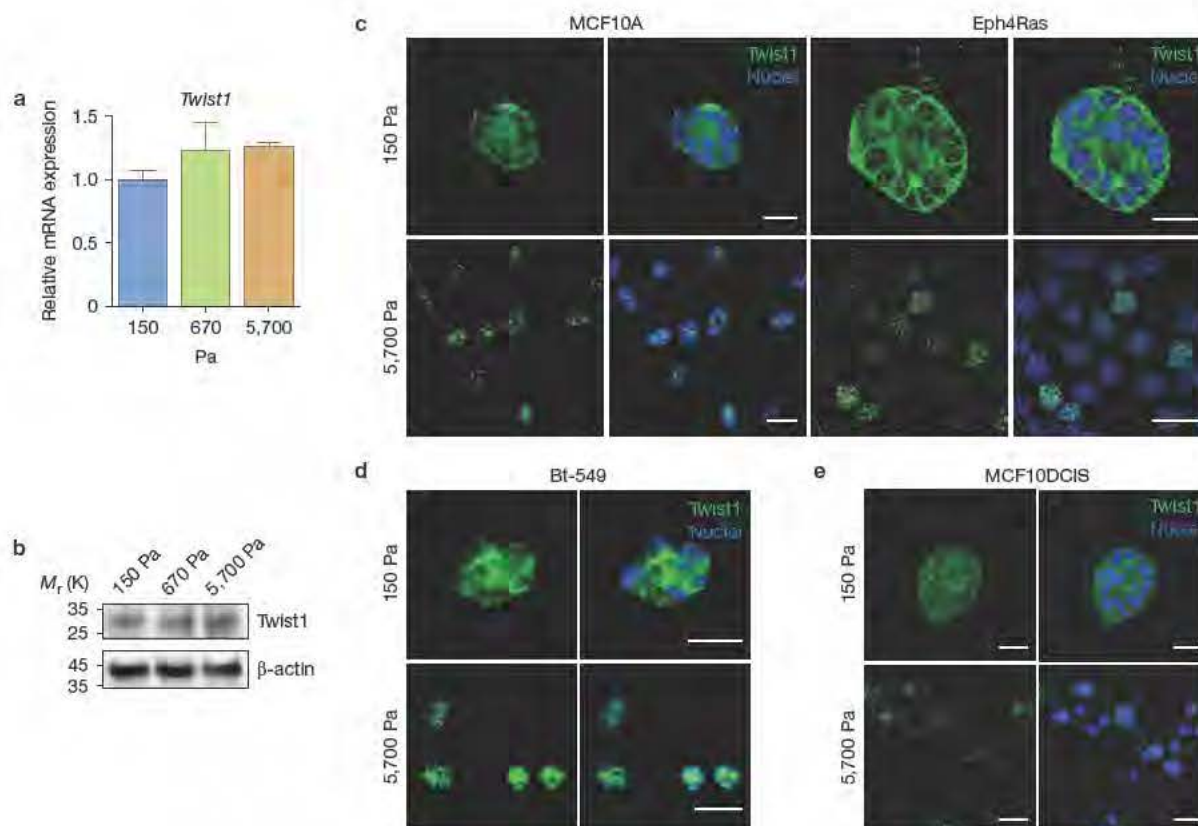
Figure 2 Matrix stiffness regulates TWIST1 nuclear localization. (a) qPCR analysis of MCF10A cells grown in 3D culture on polyacrylamide hydrogels with the indicated rigidities (not significant, unpaired two-tailed t-test with Welch's correction, $n = 3$ independent experiments, statistics source data can be found in Supplementary Table 1; error bars represent s.d.). (b) Cell lysates from MCF10A cells grown in 3D culture on polyacrylamide hydrogels with the indicated rigidities were analysed by SDS–PAGE and probed for TWIST1 and β-actin. Unprocessed original scans of the blots are shown in Supplementary Fig. 7. (c–e) Eph4Ras, MCF10A (c), Bt-549 (d) and MCF10DCIS (e) cells were cultured in 3D culture with the indicated rigidities for 5 days and stained for TWIST1 (green) and nuclei (blue; scale bars, 25 μm).

RNAs (shRNAs) against *TWIST1* and tested their mechanosensing competence (Fig. 1b and Supplementary Fig. 1B–D). Knockdown of *TWIST1* prevented the invasive phenotype at 5,700 Pa; instead, these cells formed basally polarized acini with strong junctional E-cadherin on rigid matrices (Fig. 1c–f and Supplementary Fig. 1E). Importantly, knockdown of *Twist1* prevented stiffness-induced basement membrane destabilization, as shown by basal laminin V staining (Fig. 1e), demonstrating that matrix-stiffness-induced invasion is *Twist1*-dependent. As high stiffness alone was not sufficient to induce a complete EMT (Fig. 1f), we investigated whether TWIST1 is also required for the induction of a full EMT by mechanical signals in concert with the EMT-inducing biochemical signal TGF-β (ref. 33). Consistent with published data[34], although TGF-β was not sufficient to induce EMT on soft matrix, rigid matrix together with TGF-β triggered a complete EMT, evidenced by both immunostaining and quantitative PCR (qPCR) analysis of EMT markers (Fig. 1g and Supplementary Fig. 1F,G). Importantly, knockdown of *Twist1* completely blocked induction of EMT by TGF-β at high matrix stiffness and rescued acinar development (Fig. 1g). Together, these data indicate an essential role for TWIST1 in mediating matrix-stiffness-induced EMT and invasion.

As the EMT program is orchestrated synergistically by a number of EMT-inducing transcription factors, we next aimed to understand how the EMT transcription program is regulated by matrix stiffness and TGF-β. The messenger RNA levels of EMT-inducing transcription factors, *Twist1*, *Snai1*, *Snai2*, *Zeb1* and *Zeb2* did not change significantly in response to changes in matrix stiffness alone (Fig. 1h–l). On TGF-β treatment, only *Snai1* mRNA is markedly induced in a Twist1-independent manner (Fig. 1i), as reported previously[31]. However, without Twist1, TGF-β-induced *Snai1* expression alone could not induce even a partial EMT or any invasive phenotype on soft or hard matrices (Fig. 1g). The mRNA expression levels of *Snai2*, *Zeb1* and *Zeb2* were significantly dampened on *Twist1* knockdown (Fig. 1j–l), further supporting a key role of TWIST1 in regulating EMT gene response. These data suggest that TWIST1-dependent mechanotransduction, together with induction of *Snai1* by TGF-β, is required to induce a complete EMT at high matrix stiffness.

Matrix stiffness regulates TWIST1 nuclear localization

We next aimed to understand how TWIST1 is regulated by matrix stiffness to mediate EMT and invasion. As Drosophila *Twist* mRNA expression is induced by mechanical forces[24], we examined TWIST1 mRNA and protein expression under various matrix rigidities and found no differences (Fig. 2a,b). Surprisingly, immunostaining showed that TWIST1 was largely cytoplasmic on the compliant matrix of 150 Pa and translocated into the nucleus on the rigid matrix of
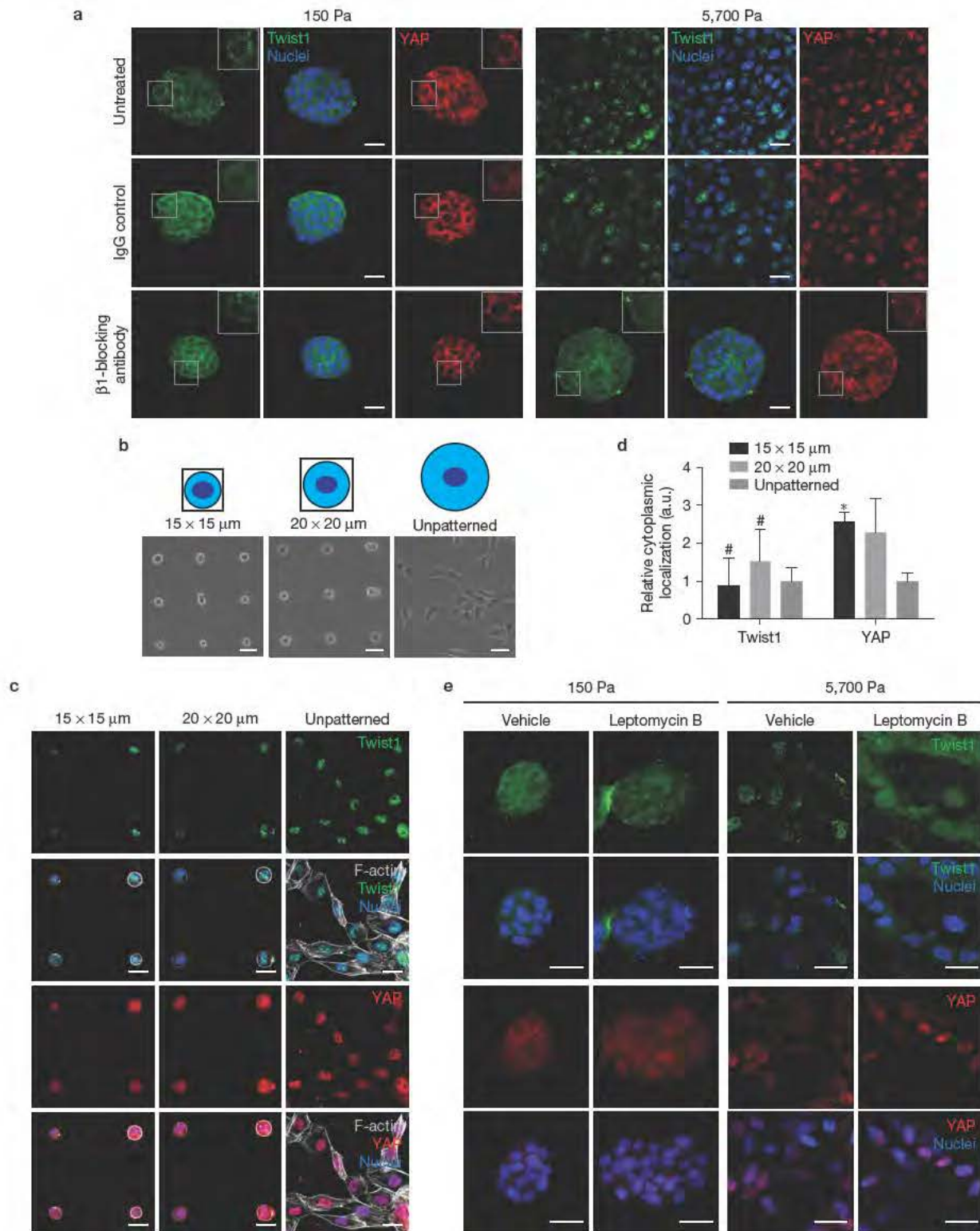
Figure 3 TWIST1 and YAP nuclear localization are regulated by distinct mechanotransduction pathways. (**a**) MCF10A cells were cultured in 3D culture on polyacrylamide hydrogels with the indicated rigidities in the presence of a control IgG or a β1-integrin-blocking antibody (AIIB2) for 5 days and stained for TWIST1 (green), YAP (red) and nuclei (blue; scale bars, 25 μm). (**b,c**) Bright-field images (scale bars, 50 μm; **b**) and confocal images of MCF10A cells cultured on micropatterned glass coverslips for 6 h stained for TWIST1 (green), YAP (red), F-actin (greyscale) and nuclei (blue; scale bars, 25 μm; **c**). (**d**) Quantification of relative cytoplasmic localized TWIST1 and YAP. (#, not significant; *, $P < 0.01$, unpaired two-tailed t-test with Welch's correction, $n = 25$ cells per experiment, 3 independent experiments, error bars represent s.d.). (**e**) MCF10A cells were cultured in 3D culture on polyacrylamide hydrogels with the indicated rigidities in the absence or presence of leptomycin B and stained for TWIST1 (green), YAP (red) and nuclei (blue; scale bars, 25 μm).

Figure 4 Matrix stiffness regulates the interaction between TWIST1 and G3BP2 to control TWIST1 subcellular localization. (**a**) Endogenous TWIST1 from MCF10A cell lysates was immunoprecipitated, analysed by SDS–PAGE and probed for G3BP2 and TWIST1. (**b**) Population plot of the putative G3BP2-binding domain motif. (**c**) Alignment of the putative G3BP2-binding domain in TWIST1 homologues. (**d**) Exogenously expressed wild-type (WT) and Gln105-Thr112 deletion (ΔQT) Myc-tagged Twist1 from 293T cell lysates were immunoprecipitated, analysed by SDS–PAGE and probed for G3BP2 and Myc. (**e**) Eph4Ras cells in 3D culture at the indicated rigidities were stained for G3BP2 (red) and nuclei (blue; scale bars, 50 μm). (**f**) Eph4Ras cells in 3D culture for 6 days at the indicated rigidities were analysed for Twist1 and G3bp2 interaction by *in situ* PLA assay, PLA signal (green) and DAPI (blue; scale bars, 25 μm. (**g**) Quantification of PLA signal normalized to cell number in 3D cultures described in **f** (***, $P < 0.001$, unpaired two-tailed *t*-test with Welch's correction, $n = 50$ acini, 3 independent experiments, error bars represent s.d.). (**h**) Eph4Ras cells in 3D culture for 20 h at the indicated rigidities were analysed for Twist1 and G3bp2 interaction by *in situ* PLA assay, PLA signal (green) and DAPI (blue; scale bars, 15 μm). (**i**) Quantification of PLA signal normalized to cell number in 3D cultures described in **h** (***, $P < 0.001$, unpaired two-tailed *t*-test with Welch's correction, $n = 25$ acini, 3 independent experiments, error bars represent s.d.). (**j**) Exogenously expressed wild-type (WT), Y107F and Y107E Myc-tagged Twist1 from 293T cell lysates were immunoprecipitated and analysed by SDS–PAGE, and probed for G3BP2 and Myc. Unprocessed original scans of the blots are shown in Supplementary Fig. 7.

5,700 Pa. High-stiffness-induced nuclear translocation of TWIST1 was observed in human MCF10A and mouse Eph4Ras cells (Fig. 2c), and in MCF10DCIS and Bt-549 human breast cancer cells (Fig. 2d,e), suggesting that nuclear translocation of TWIST1 is a conserved response to increasing matrix stiffness. These results suggest that matrix stiffness could directly impinge on the EMT program by controlling TWIST1 nuclear translocation.

TWIST1 subcellular localization is regulated by a distinct mechanotransduction pathway independent of YAP

We next investigated whether integrin activation is necessary for TWIST1 nuclear localization at high matrix stiffness because

mechanosensing responses to matrix stiffness are mediated in part through clustering and activation of integrins[1,35]. Treatment with a β1-integrin-blocking antibody (AIIB2) prevented nuclear translocation of TWIST1 and blocked the invasive phenotype induced by high matrix stiffness[1,2] (Fig. 3a), further supporting a critical role for TWIST1 in mediating matrix-stiffness-induced EMT and invasion. Notably, blockade of β1-integrin activation also prevented nuclear localization of YAP, which was recently identified as one of the few known mechanoresponsive transcription regulators[13]. Therefore, integrin activation is critical to the mechanoregulation of both Twist1 and YAP.

Next we examined whether TWIST1 and YAP are regulated by similar mechanoregulatory machineries. As matrix stiffness also affects
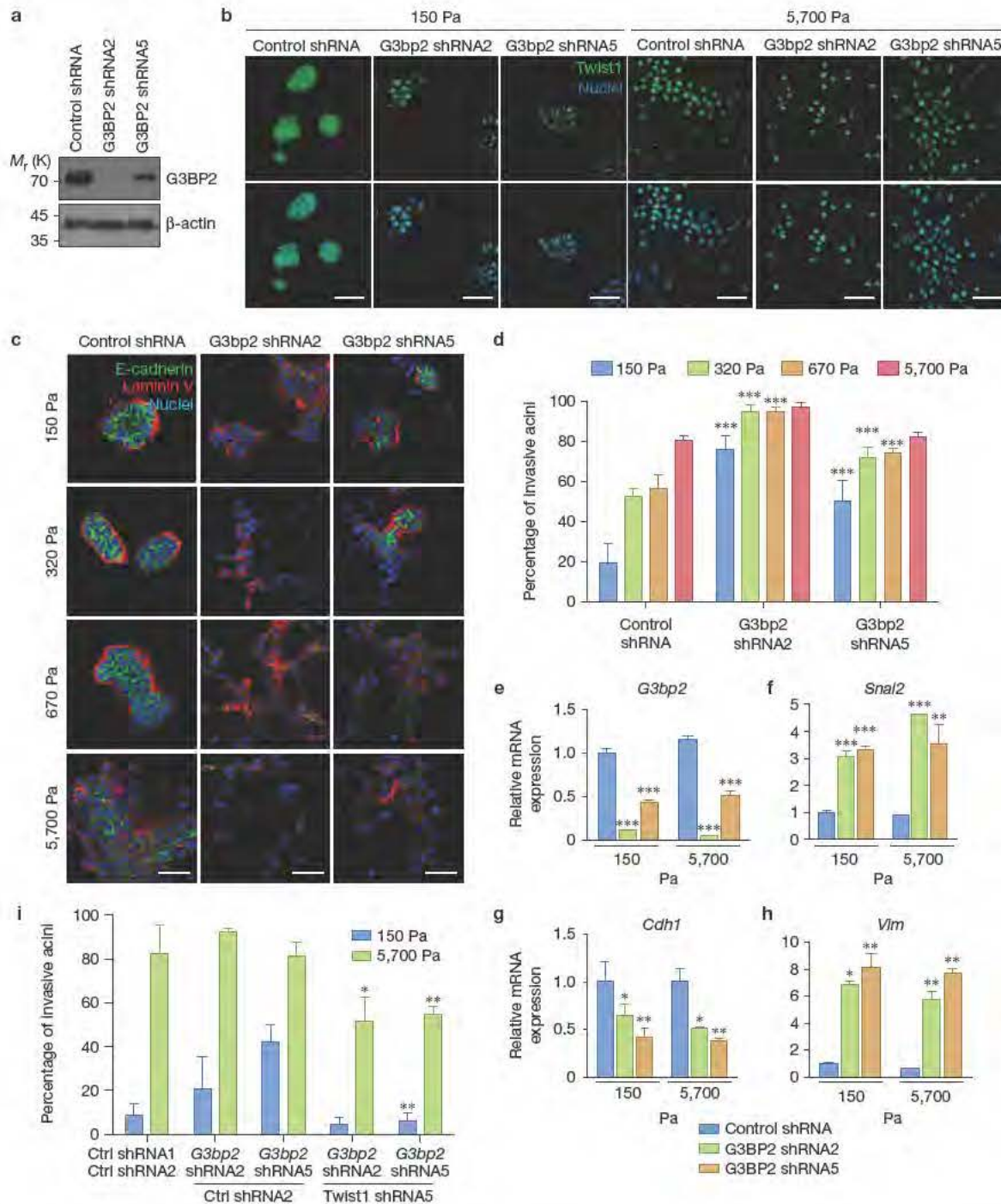
Figure 5 Loss of G3BP2 cooperates with increasing matrix stiffness to promote TWIST1 nuclear localization and EMT. (**a**) Cell lysates from Eph4Ras cells expressing control or *G3bp2* shRNAs were analysed by SDS–PAGE and probed for G3BP2 and β-actin. Unprocessed original scans of the blots are shown in Supplementary Fig. 7. (**b**) Eph4Ras cells expressing control or *G3bp2* shRNAs were cultured in 3D culture with the indicated rigidities for 5 days and stained for Twist1 (green) and nuclei (blue; scale bars, 50 μm). (**c**) Eph4Ras cells expressing control or *G3bp2* shRNAs were cultured in 3D culture with varying rigidities for 5 days and stained for E-cadherin (green), laminin V (red) and nuclei (blue; scale bars, 50 μm). (**d**) Quantification of invasive acini in 3D culture described in **c** from 3 independent experiments (***, $P < 0.001$, unpaired two-tailed *t*-test with Welch's correction, $n=50$ acini per experiment, 3 independent experiments,

error bars represent s.d.). (**e–h**) qPCR analysis of *G3bp2* (**e**), *Snai2* (**f**), *Cdh1* (**g**) and *Vim* (**h**) in Eph4Ras cells expressing control or *G3bp2* shRNAs 3D cultured under the indicated matrix rigidities for 5 days (*, $P < 0.05$; **, $P < 0.01$; ***, $P < 0.001$, unpaired two-tailed *t*-test with Welch's correction, $n=4$ independent experiments, Supplementary Table 1, error bars represent s.d.). (**i**) Quantification of invasive acini of Eph4Ras cells expressing control (Ctrl shRNA1) or *G3bp2* shRNAs, together with control (Ctrl shRNA2) or *Twist1* shRNA (Twist1 shRNA5), 3D cultured under the indicated matrix rigidities for 5 days, from 3 independent experiments (*, $P < 0.05$; **, $P < 0.01$, unpaired two-tailed *t*-test with Welch's correction, $n=50$ acini per experiment, 3 independent experiments; double knockdown compared with the respective single knockdown, error bars represent s.d.).
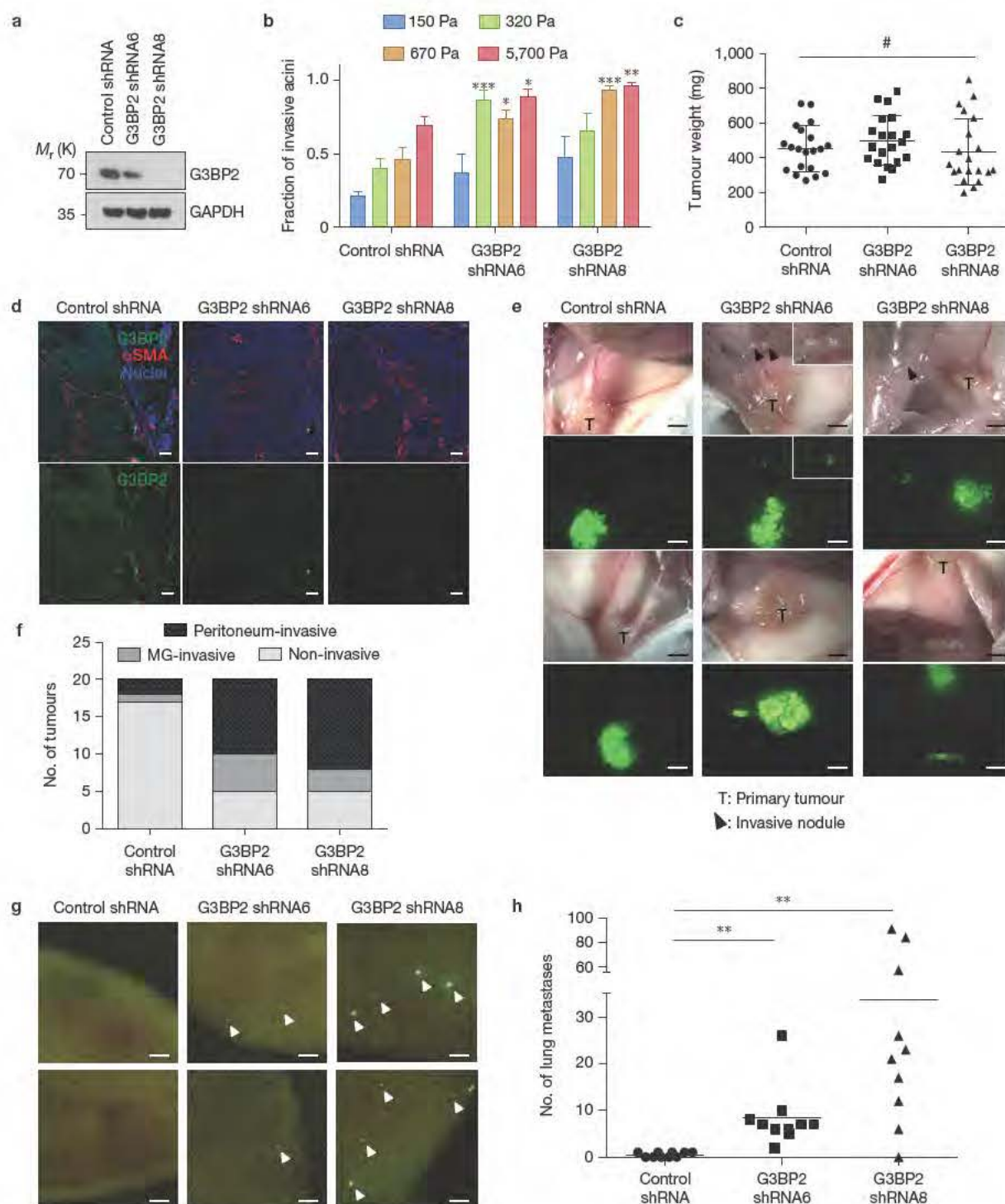
Figure 6 Loss of G3BP2 induces tumour invasion *in vivo*. (a) Cell lysates from MCF10DCIS cells expressing control or *G3BP2* shRNAs were analysed by SDS–PAGE and probed for G3BP2 and GAPDH. Unprocessed original scans of the blots are shown in Supplementary Fig. 7. (b) Quantification of invasive acini formed by MCF10DCIS cells expressing control or *G3BP2* shRNAs cultured in 3D culture with varying rigidities for 5 days (*, $P < 0.05$; **, $P < 0.01$; ***, $P < 0.001$, unpaired two-tailed t-test with Welch's correction, $n = 50$ acini per experiment, 3 independent experiments; error bars denote s.e.m.). (c) Tumour weight of MCF10DCIS xenograft tumours expressing control or *G3BP2* shRNAs (#, not statistically significant, unpaired two-tailed t-test with Welch's correction, $n = 20$ tumours from 10 mice per group,

3 independent experiments, error bars represent s.d.). (d) Tissue sections of control and G3BP2 shRNA MCF10DCIS xenografts stained for G3BP2 (green), αSMA (red) and nuclei (blue) and imaged by confocal microscopy (scale bars, 50 μm). (e) Fluorescent and bright-field images of GFP (green)-labelled MCF10DCIS xenograft tumours *in situ* (scale bars, 5 mm). (f) Quantification of local (MG-invasive) and regional (Peritoneum-invasive) invasion of MCF10DCIS xenograft tumours. (g,h) Fluorescent images (scale bars, 100 μm; g) and quantification (h) of lung metastases (green, indicated by arrows) from MCF10DCIS xenograft tumours (**, $P < 0.01$, unpaired two-tailed t-test with Welch's correction, $n = 10$ mice per experiment, 3 independent experiments).
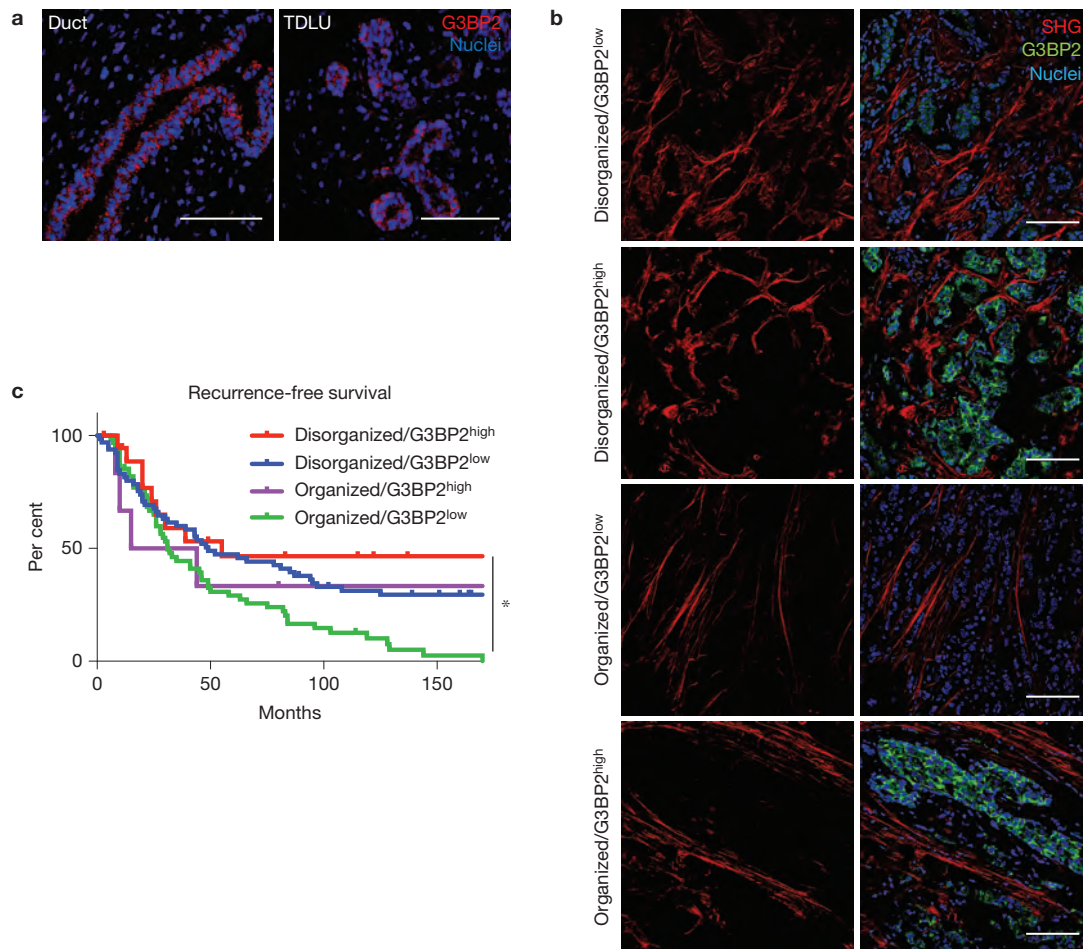
Figure 7 Downregulation of G3BP2 and increasing collagen organization synergistically predict poor outcome in breast cancer patients. (**a**) Confocal microscopy of normal human breast terminal ductal lobular units (TDLU) and ducts stained for G3BP2 (red) and nuclei (blue; scale bars, 100 μm). (**b**) Representative images of stage-3 human breast tumours analysed for collagen organization by SHG (red), and stained for G3BP2 (green) and TO-PRO-3 for nuclei (blue) respectively (scale bars, 100 μm). (**c**) Kaplan–Meier curve of recurrence-free survival for stage-3 breast cancer patients, stratified by collagen organization (SHG) and G3BP2 expression (∗, Disorganized collagen/G3BP2high tumours versus Organized collagen/G3BP2low, log-rank P value = 0.0135, $n = 152$ breast tumours; Disorganized collagen/G3BP2high $n = 19$ breast tumours; Disorganized collagen/G3BP2low $n = 65$ breast tumours; Organized collagen/G3BP2high $n = 6$ breast tumours; Disorganized collagen/G3BP2low $n = 62$ breast tumours).

cell shape, we sought to distinguish their impacts on TWIST1 nuclear localization. First, we used micropatterning to selectively alter cell shapes without changing underlying matrix rigidity. Restrictive patterns with areas of 225 μm² and 400 μm² prevented any cell spreading; in contrast, MCF10A cells on unpatterned regions were able to spread effectively (Fig. 3b). TWIST1 nuclear localization was not affected by changes in cell shape in either MCF10A or Eph4Ras cells (Fig. 3b–d and Supplementary Fig. 2). To confirm that micropatterning-restriction of cell spreading was effective, we also examined the localization of YAP. In contrast to TWIST1, YAP subcellular localization was responsive to changes in cell shape (Fig. 3c,d), consistent with previous reports that YAP localization is sensitive to any changes in actin cytoskeleton[13,36]. This difference suggests the existence of distinct mechanoregulatory mechanisms for TWIST1 and YAP. These data also suggest that matrix stiffness directly regulates TWIST1 subcellular localization independently of changes in cell shape.

As TWIST1 protein subcellular localization could be regulated by nuclear transport, we explored whether TWIST1 nuclear import

and export might be regulated by matrix stiffness. Treatment of MCF10A cells with leptomycin B, a nuclear export inhibitor[37], did not promote nuclear accumulation of TWIST1 on compliant matrices (Fig. 3e, upper panel). In contrast, YAP accumulated into the nucleus on inhibition of nuclear export (Fig. 3e, lower panel). Therefore, similar to the micropatterning experiment, inhibition of nuclear export differentially affected matrix stiffness regulation of TWIST1 and YAP, supporting the existence of distinct Twist1 and YAP mechanotransduction pathways. Furthermore, as TWIST1 contains two functional nuclear localization sequences[38], these results suggest that TWIST1 is likely to be actively anchored in the cytoplasm on compliant matrices, therefore preventing nuclear translocation.

Matrix stiffness regulates the interaction between TWIST1 and G3BP2 to control TWIST1 subcellular localization

To understand the molecular mechanism underlying TWIST1 cytoplasmic retention, we used mass spectrometry analysis to identify TWIST1-binding proteins that anchor TWIST1 in the cytoplasm

(Supplementary Fig. 3A). Ras GTPase-activating protein-binding protein 2 (G3BP2) stood out as a promising candidate on the basis of previous studies showing that G3BP2 regulates cytoplasmic retention of MDM2 and NFKBIA (refs 39,40). We confirmed that both endogenously and exogenously expressed TWIST1 co-immunoprecipitated with endogenous G3BP2 (Fig. 4a and Supplementary Fig. 3C). Previous studies identified a region of NFKBIA responsible for binding to G3BP2 (ref. 40). Sequence alignment of this G3BP2-interacting region of NFKBIA with TWIST1 and MDM2 revealed a consensus G3BP2-binding motif, Q-X-X-X-E-L-Q-[ET]-X-[KR]-[LPV] (Fig. 4b). Interestingly, this G3BP2-binding motif is highly conserved among vertebrate Twist1 proteins, but to a significantly lesser degree in *Drosophila* in which Twist expression, rather than localization, is regulated by mechanical cues[24] (Fig. 4c). Deletion of this motif (ΔQT mutant) in Twist1 abolished its interaction with G3BP2 (Fig. 4d). Consistent with its putative role as a cytoplasmic anchoring protein, G3BP2 was observed only in the cytoplasm in Eph4Ras, MCF10A and Bt-549 cells at all matrix rigidities (Fig. 4e and Supplementary Fig. 3B). Together, these data show that G3BP2 binds to TWIST1 through the conserved G3BP2-binding motif on vertebrate TWIST1 proteins.

To directly investigate whether matrix stiffness regulates Twist1–G3BP2 interaction, we used an *in situ* proximity ligation assay (PLA) to examine the interaction of endogenous Twist1 and G3bp2 proteins in 3D acinar cultures of Eph4Ras cells. PLA technology directly detects endogenous Twist1/G3bp2 interactions with high specificity and sensitivity in intact acini using antibodies against Twist1 and G3bp2. Indeed, at 150 Pa a strong PLA signal, indicating Twist1/G3bp2 interaction, was specifically enriched in the cytoplasm. In contrast, very little PLA signal was detected at 5,700 Pa, indicating that Twist1 is released from G3bp2 and translocates into the nucleus at high matrix rigidity (Fig. 4f,g). To understand whether Twist1–G3bp2 interaction is specifically regulated by matrix stiffness, and not by secondary changes in cell polarity or adherens junctions due to matrix-stiffness-induced EMT, we examined Twist1–G3bp2 interaction in single cells devoid of apical–basal polarity and mature adherens junctions. PLA analysis in single cells detected strong interaction between G3bp2 and Twist1 in the cytoplasm at low stiffness, but not at high stiffness (Fig. 4h,i), identical to what we observed in mammary organoids with mature adherens junctions and polarity. These experiments demonstrate that matrix stiffness directly regulates the interaction between Twist1 and G3bp2 to control Twist1 subcellular localization.

Next, we investigated how the interaction between TWIST1 and G3BP2 could be regulated in response to changes in matrix stiffness. Interestingly, the tyrosine residue Tyr 103 (Tyr 107 in murine Twist1), which lies within the identified G3BP2-binding motif of human TWIST1, is predicted as a potential phosphorylation site. This provided a very attractive potential mechanism by which increased matrix stiffness activates integrins and then signals through tyrosine kinases to release TWIST1 from G3BP2. Supportive of this possibility, mass spectrometry analysis of a human lung adenocarcinoma cell line reveals phosphorylation of Tyr 103 on endogenous TWIST1 (ref. 41), albeit with no known functional consequence. Interestingly, the phospho-deficient Y107F Twist1 mutant co-immunoprecipitated with G3BP2 with similar efficiency as wild-type Twist1 but the interaction between the phospho-mimetic Y107E Twist1 mutant and G3BP2 was markedly attenuated (Fig. 4j). These data strongly suggest that increasing matrix stiffness could disrupt Twist1–G3BP2 binding through phosphorylation of Tyr 107 within the G3BP2-binding motif of Twist1.

Loss of G3BP2 cooperates with increasing matrix stiffness to promote TWIST1 nuclear localization and EMT

We next investigated whether G3BP2 is functionally required for TWIST1 cytoplasmic retention in compliant matrices. We used shRNAs to knock down *G3BP2* expression and determined the impact on TWIST1 localization (Fig. 5a,e, and Supplementary Fig. 4A). For both MCF10A and Eph4Ras cells on compliant matrices, knockdown of *G3BP2* resulted in nuclear accumulation of TWIST1, suggesting that G3BP2 is necessary for cytoplasmic sequestration of TWIST1 in response to low matrix stiffness (Fig. 5b and Supplementary Fig. 4B). TWIST1 nuclear localization at high matrix stiffness was not affected by knockdown of *G3BP2*, consistent with our model in which G3BP2 and TWIST1 dissociate at high matrix stiffness. In further support of distinct mechanoregulation of TWIST1 and YAP, knockdown of *G3BP2* did not affect YAP localization (Supplementary Fig. 4D). These data strongly support a critical role for G3BP2 in regulating TWIST1 subcellular localization in response to matrix stiffness.

To determine the impact of G3BP2 loss on EMT and invasion, we cultured Eph4Ras cells on a gradient of polyacrylamide hydrogels with elasticities ranging from 150 Pa to 5,700 Pa in 3D culture. *G3bp2* knockdown and the resulting constitutive Twist1 nuclear localization significantly increased the percentage of invasive acini at matrix rigidities ranging from 150 Pa to 670 Pa. Importantly, loss of *G3bp2* and increasing matrix stiffness synergistically resulted in destabilization of basement membrane, an EMT phenotype and invasion of cells into the surrounding ECM (Fig. 5c,d). The EMT phenotype was characterized by downregulation of E-cadherin and disruption of basement membrane as shown by laminin V staining (Fig. 5c). Furthermore, *G3bp2* knockdown repressed expression of E-cadherin and induced expression of vimentin (Fig. 5g,h). To determine whether the EMT phenotype resulting from *G3bp2* knockdown is dependent on Twist1, we knocked down both *Twist1* and *G3bp2* and found that the EMT and invasive phenotype were significantly suppressed compared with cells that were depleted of only G3bp2 (Fig. 5i). *Snai2*, a direct transcription target of TWIST1 (ref. 42), was induced following *G3bp2* knockdown; in contrast, double knockdown of *G3bp2* and *Twist1* blocked *Snai2* induction, suggesting that the effects of *G3bp2* knockdown are dependent on *Twist1* (Fig. 5f and Supplementary Fig. 4C). These data indicate that G3BP2 directly impacts EMT and invasion in response to matrix stiffness and provide a mechanism by which the TWIST1–G3BP2 mechanotransduction pathway can facilitate tumour invasion. Furthermore, they suggest that downregulation of G3BP2 expression in tumour cells could cooperate with increasing matrix stiffness in the tumour microenvironment to facilitate tumour invasion and metastasis.

Loss of G3BP2 promotes tumour invasion and metastasis *in vivo*

To investigate the role of G3BP2 in tumour progression *in vivo*, we employed a human xenograft tumour model of comedo ductal carcinoma *in situ*, the MCF10DCIS cell line[43], which is a derivative of MCF10A cells expressing oncogenic Ras. This xenograft model reca-

pitulates the development of ductal carcinoma *in situ* (DCIS) in human breast cancer. Concordant with our results in Eph4Ras and MCF10A mammary epithelial cells, knockdown of *G3BP2* in conjunction with increasing matrix stiffness promoted TWIST1 nuclear localization and an invasive phenotype in MCF10DCIS cells in 3D culture, indicating that the TWIST1–G3BP2 mechanotransduction pathway is intact in this model (Fig. 6a,b, and Supplementary Fig. 5). We injected these cells into the mammary fat pads of NOD/SCID mice and allowed tumour formation for 7 weeks. There was no significant difference in the weight of control and *G3BP2* shRNA primary mammary tumours (Fig. 6c). Immunostaining confirmed significantly lower levels of G3BP2 in tumours with *G3BP2* knockdown (Fig. 6d). Interestingly, in control tumours, αSMA-positive mesenchymal cells were largely present at the edge of the tumour; in contrast, these cells often infiltrated into the intratumoral region in *G3BP2* shRNA tumours, a phenotype associated with the progression of DCIS to invasive ductal carcinoma (Fig. 6d).

We next examined whether knockdown of G3BP2 affects tumour invasion and metastasis. Tumours expressing *G3BP2* shRNAs presented not only local invasion into the surrounding mammary tissue, but also regional invasion into the nearby peritoneal wall, visualized as GFP-positive tumour cells in these regions (Fig. 6e,f). More importantly, tumours expressing *G3BP2* shRNAs consistently presented with a striking increase in the number of distant metastases in the lungs compared with tumours expressing a control shRNA (mean increase: 15- and 65-fold for *G3BP2* shRNA6 and shRNA8 versus control, respectively; Fig. 6g,h). Together, these results strongly support a key role for G3BP2 in suppressing tumour invasion and metastasis *in vivo*.

Downregulation of G3BP2 and increasing collagen organization synergistically predict poor outcome in breast cancer patients

We next investigated whether the TWIST1–G3BP2 mechanotransduction pathway has a significant role in human cancer progression. We first analysed The Cancer Genome Atlas (TCGA) breast cancer (TCGA_BRCA_G4502A_07_3) data set and observed a decrease in overall survival in patients with tumours with low *G3BP2* expression (Supplementary Fig. 6A,B). Furthermore, consistent with a role in preventing EMT and invasion, we observed that G3BP2 protein expression was restricted to the luminal epithelial cells in normal human breast and colon tissues (Fig. 7a and Supplementary Fig. 6D). We next analysed G3BP2 expression and collagen organization in a cohort of 152 stage-3 breast tumours from the NCI Cancer Diagnosis Program (Fig. 7b). We analysed collagen fibre alignment by second harmonic generation imaging (SHG) and used it as a surrogate marker for tissue rigidity. In agreement with previous publications[6–8,44,45], stage-3 patients presenting stiffer tumours (organized collagen structures) had a median recurrence-free survival time of 31 months compared with 49 months in patients with more compliant tumours (disorganized collagen; $P = 0.0014$; Supplementary Fig. 6C). Importantly, the level of G3BP2 expression, together with matrix stiffness, could further stratify these patients to predict outcome (Fig. 7c). Patients with disorganized collagen/G3BP2[high] tumours had markedly improved outcomes with a 10-year recurrence-free survival rate of 46.4% compared with 10.1% of patients with organized collagen/G3BP2[low] tumours. Patients whose tumours presented either low G3BP2 or

organized collagen fibres had intermediate survival outcomes (31.18% and 33.33% 10-year recurrence-free survival, $P = 0.0284$), reflective of the cooperative effect of G3BP2 loss and increasing matrix stiffness on tumour progression. The association between downregulation of G3BP2 and poor prognosis was independent of tumour grade or oestrogen receptor status (Supplementary Fig. 6E,F). Concordant with data from 3D culture and animal tumour models, these results demonstrate that increasing rigidity in the tumour microenvironment, in concert with downregulation of G3BP2, promotes human breast tumour progression.

DISCUSSION

In summary, we demonstrate that increasing matrix stiffness in the tumour microenvironment directly activates EMT, tumour invasion, and metastasis through the EMT-inducing transcription factor TWIST1. This mechanotransduction pathway may have important implications in breast tumours, as G3BP2 loss and tissue rigidity act synergistically to promote tumour progression. Given that matrix stiffening and ECM reorganization has been observed in many human tumour types[10], the Twist1–G3BP2 mechanotransduction pathway warrants further investigation as a key mode of EMT activation as well as for therapeutic applications.

Mechanistically, our study reveals a molecular pathway directly linking mechanical forces with transcriptional regulation of the EMT program. Our findings suggest a model in which increasing matrix stiffness induces integrin-dependent phosphorylation events and release of TWIST1 from its cytoplasmic anchor G3BP2 to enter the nucleus and drive transcriptional events of EMT and invasion. Notably, to our knowledge, low stiffness and integrin disengagement are the only conditions in which cytoplasmic retention of TWIST1 are observed, thus providing a unique mode of EMT regulation[46]. Interestingly, our analyses showed that matrix stiffness regulates TWIST1 and YAP/TAZ through distinct molecular mechanisms, suggesting that multiple mechanotransduction pathways exist. We found that the TWIST1–G3BP2 signalling axis is responsive only to matrix stiffness and is independent of cell shape, cell polarity and adherens junction; in contrast, YAP/TAZ are sensitive to all of these factors. At present, the complete molecular pathways that transmit the mechanical signals from extracellular matrix to either the YAP/TAZ or TWIST1 signalling axis remain to be elucidated. Understanding the similarities and differences between the YAP/TAZ versus TWIST1 mechanotransduction pathways will provide further insight into how different mechanical cues are interpreted into unique biological responses. Given the importance of mechanoregulation in embryonic morphogenesis, such information would have broad implications not only in tumour progression, but also in development. □

METHODS

Methods and any associated references are available in the online version of the paper.

Note: Supplementary Information is available in the online version of the paper

AUTHOR CONTRIBUTIONS

S.C.W. and J.Y. conceived the project and wrote the manuscript. S.C.W. and L.F. performed most of the experiments and prepared the figures. J.H.T., Y.G., V.H.P., H.E.M. and A.C.C. contributed to the experimental work. R.L.S., S.S.T. and A.J.E. advised on experimental design. L.F., J.H.T. and A.J.E. revised the manuscript.

COMPETING FINANCIAL INTERESTS

The authors declare no competing financial interests.

1. Paszek, M. J. *et al.* Tensional homeostasis and the malignant phenotype. *Cancer Cell* **8,** 241–254 (2005).
2. Levental, K. R. *et al.* Matrix crosslinking forces tumor progression by enhancing integrin signaling. *Cell* **139,** 891–906 (2009).
3. Jaalouk, D. E. & Lammerding, J. Mechanotransduction gone awry. *Nat. Rev. Mol. Cell Biol.* **10,** 63–73 (2009).
4. Calvo, F. *et al.* Mechanotransduction and YAP-dependent matrix remodelling is required for the generation and maintenance of cancer-associated fibroblasts. *Nat. Cell Biol.* **15,** 637–646 (2013).
5. Butcher, D. T., Alliston, T. & Weaver, V. M. A tense situation: forcing tumour progression. *Nat. Rev. Cancer* **9,** 108–122 (2009).
6. Colpaert, C., Vermeulen, P., Van Marck, E. & Dirix, L. The presence of a fibrotic focus is an independent predictor of early metastasis in lymph node-negative breast cancer patients. *Am. J. Surg. Pathol.* **25,** 1557–1558 (2001).
7. Hasebe, T. *et al.* Prognostic significance of fibrotic focus in invasive ductal carcinoma of the breast: a prospective observational study. *Mod. Pathol.* **15,** 502–516 (2002).
8. Conklin, M. W. *et al.* Aligned collagen is a prognostic signature for survival in human breast carcinoma. *Am. J. Pathol.* **178,** 1221–1232 (2011).
9. Engler, A. J., Humbert, P. O., Wehrle-Haller, B. & Weaver, V. M. Multiscale modeling of form and function. *Science* **324,** 208–212 (2009).
10. DuFort, C. C., Paszek, M. J. & Weaver, V. M. Balancing forces: architectural control of mechanotransduction. *Nat. Rev. Mol. Cell Biol.* **12,** 308–319 (2011).
11. Hoffman, B. D., Grashoff, C. & Schwartz, M. A. Dynamic molecular processes mediate cellular mechanotransduction. *Nature* **475,** 316–323 (2011).
12. Engler, A. J., Sen, S., Sweeney, H. L. & Discher, D. E. Matrix elasticity directs stem cell lineage specification. *Cell* **126,** 677–689 (2006).
13. Dupont, S. *et al.* Role of YAP/TAZ in mechanotransduction. *Nature* **474,** 179–183 (2011).
14. Yang, J. & Weinberg, R. A. Epithelial-mesenchymal transition: at the crossroads of development and tumor metastasis. *Dev. Cell* **14,** 818–829 (2008).
15. Thiery, J. P., Acloque, H., Huang, R. Y. & Nieto, M. A. Epithelial-mesenchymal transitions in development and disease. *Cell* **139,** 871–890 (2009).
16. Yang, J. *et al.* Twist, a master regulator of morphogenesis, plays an essential role in tumor metastasis. *Cell* **117,** 927–939 (2004).
17. Fang, X. *et al.* Twist2 contributes to breast cancer progression by promoting an epithelial–mesenchymal transition and cancer stem-like cell self-renewal. *Oncogene* **30,** 4707–4720 (2011).
18. Batlle, E. *et al.* The transcription factor snail is a repressor of E-cadherin gene expression in epithelial tumour cells. *Nat. Cell Biol.* **2,** 84–89 (2000).
19. Cano, A. *et al.* The transcription factor snail controls epithelial–mesenchymal transitions by repressing E-cadherin expression. *Nat. Cell Biol.* **2,** 76–83 (2000).
20. Hajra, K. M., Chen, D. Y. & Fearon, E. R. The SLUG zinc-finger protein represses E-cadherin in breast cancer. *Cancer Res.* **62,** 1613–1618 (2002).
21. Comijn, J. *et al.* The two-handed E box binding zinc finger protein SIP1 downregulates E-cadherin and induces invasion. *Mol. Cell* **7,** 1267–1278 (2001).
22. Eger, A. *et al.* ΔEF1 is a transcriptional repressor of E-cadherin and regulates epithelial plasticity in breast cancer cells. *Oncogene* **24,** 2375–2385 (2005).
23. Eckert, M. A. *et al.* Twist1-induced invadopodia formation promotes tumor metastasis. *Cancer Cell* **19,** 372–386 (2011).
24. Desprat, N., Supatto, W., Pouille, P. A., Beaurepaire, E. & Farge, E. Tissue deformation modulates twist expression to determine anterior midgut differentiation in Drosophila embryos. *Dev. Cell* **15,** 470–477 (2008).
25. Johnson, K. R., Leight, J. L. & Weaver, V. M. Demystifying the effects of a three-dimensional microenvironment in tissue morphogenesis. *Methods Cell Biol.* **83,** 547–583 (2007).
26. Bissell, M. J., Radisky, D. C., Rizki, A., Weaver, V. M. & Petersen, O. W. The organizing principle: microenvironmental influences in the normal and malignant breast. *Differentiation* **70,** 537–546 (2002).
27. Lee, G. Y., Kenny, P. A., Lee, E. H. & Bissell, M. J. Three-dimensional culture models of normal and malignant breast epithelial cells. *Nat. Methods* **4,** 359–365 (2007).
28. Debnath, J., Muthuswamy, S. K. & Brugge, J. S. Morphogenesis and oncogenesis of MCF-10A mammary epithelial acini grown in three-dimensional basement membrane cultures. *Methods* **30,** 256–268 (2003).
29. Xu, Y. *et al.* Inducible knockout of Twist1 in young and adult mice prolongs hair growth cycle and has mild effects on general health, supporting Twist1 as a preferential cancer target. *Am. J. Pathol.* **183,** 1281–1292 (2013).
30. Blick, T. *et al.* Epithelial mesenchymal transition traits in human breast cancer cell lines. *Clin. Exp. Metastasis* **25,** 629–642 (2008).
31. Tran, D. D., Corsa, C. A., Biswas, H., Aft, R. L. & Longmore, G. D. Temporal and spatial cooperation of Snail1 and Twist1 during epithelial–mesenchymal transition predicts for human breast cancer recurrence. *Mol. Cancer Res.* **9,** 1644–1657 (2011).
32. Provenzano, P. P. *et al.* Collagen reorganization at the tumor-stromal interface facilitates local invasion. *BMC Med.* **4,** 38 (2006).
33. Xu, J., Lamouille, S. & Derynck, R. TGF-β-induced epithelial to mesenchymal transition. *Cell Res.* **19,** 156–172 (2009).
34. Leight, J. L., Wozniak, M. A., Chen, S., Lynch, M. L. & Chen, C. S. Matrix rigidity regulates a switch between TGF-β1-induced apoptosis and epithelial-mesenchymal transition. *Mol. Biol. Cell* **23,** 781–791 (2012).
35. Friedland, J. C., Lee, M. H. & Boettiger, D. Mechanically activated integrin switch controls α5β1 function. *Science* **323,** 642–644 (2009).
36. Zhao, B. *et al.* Inactivation of YAP oncoprotein by the Hippo pathway is involved in cell contact inhibition and tissue growth control. *Genes Dev.* **21,** 2747–2761 (2007).
37. Kudo, N. *et al.* Leptomycin B inactivates CRM1/exportin 1 by covalent modification at a cysteine residue in the central conserved region. *Proc. Natl Acad. Sci. USA* **96,** 9112–9117 (1999).
38. Singh, S. & Gramolini, A. O. Characterization of sequences in human TWIST required for nuclear localization. *BMC Cell Biol.* **10,** 47 (2009).
39. Kim, M. M., Wiederschain, D., Kennedy, D., Hansen, E. & Yuan, Z. M. Modulation of p53 and MDM2 activity by novel interaction with Ras-GAP binding proteins (G3BP). *Oncogene* **26,** 4209–4215 (2007).
40. Prigent, M., Barlat, I., Langen, H. & Dargemont, C. IκBα and IκBα /NF-κ B complexes are retained in the cytoplasm through interaction with a novel partner, RasGAP SH3-binding protein 2. *J. Biol. Chem.* **275,** 36441–36449 (2000).
41. Wu, H. Y. *et al.* Combining alkaline phosphatase treatment and hybrid linear ion trap/Orbitrap high mass accuracy liquid chromatography-mass spectrometry data for the efficient and confident identification of protein phosphorylation. *Anal. Chem.* **81,** 7778–7787 (2009).
42. Casas, E. *et al.* Snail2 is an essential mediator of Twist1-induced epithelial mesenchymal transition and metastasis. *Cancer Res.* **71,** 245–254 (2011).
43. Miller, F. R., Santner, S. J., Tait, L. & Dawson, P. J. MCF10DCIS.com xenograft model of human comedo ductal carcinoma *in situ*. *J. Natl Cancer Inst.* **92,** 1185–1186 (2000).
44. Kakkad, S. M. *et al.* Collagen I fiber density increases in lymph node positive breast cancers: pilot study. *J. Biomed. Opt.* **17,** 116017 (2012).
45. Provenzano, P. P. *et al.* Collagen density promotes mammary tumor initiation and progression. *BMC Med.* **6,** 11 (2008).
46. Alexander, N. R. *et al.* N-cadherin gene expression in prostate carcinoma is modulated by integrin-dependent nuclear translocation of Twist1. *Cancer Res.* **66,** 3365–3369 (2006).

METHODS

Cell culture. MCF10A cells were grown in DMEM/F12 media supplemented with 5% horse serum, 20 ng ml^{-1} human EGF, 10 µg ml^{-1} insulin, 0.5 µg ml^{-1} hydrocortisone, penicillin, streptomycin and 100 ng ml^{-1} cholera toxin (Sigma-Aldrich). Eph4Ras cells were cultured as previously described in MEGM (Lonza) mixed 1:1 with DMEM/F12 media supplemented with 10 ng ml^{-1} human EGF, 10 µg ml^{-1} insulin, 0.5 µg ml^{-1} hydrocortisone, penicillin and streptomycin[23]. Bt-549 cells were grown in RPMI 1640 supplemented with L-glutamine, penicillin, streptomycin, 10% fetal bovine serum and 1 µg ml^{-1} insulin. All cell lines were tested for mycoplasma contamination.

Generation of stable knockdown cell lines. Stable gene knockdown cell lines were generated using lentiviral plasmid vectors. Briefly, shRNA target constructs were introduced by infection with lentiviruses. Concentrated viral supernatants were applied to target cells with 6 µg ml^{-1} protamine sulphate. Infected cells were then selected for with 2 µg ml^{-1} puromycin or blasticidin.

Polyacrylamide hydrogel preparation. Hydrogels were prepared as previously described on No. 1 12 mm and 25 mm coverslips[47]. Briefly, No. 1 glass coverslips were etched using 0.1 N NaOH, functionalized using 3-aminopropyltriethoxysilane (Sigma-Aldrich), rinsed with dH$_2$O, incubated in 0.5% glutaraldehyde in PBS, dried, and then acrylamide/bis-acrylamide mixtures polymerized between the functionalized coverslip and a glass slide coated with dichlorodimethylsiloxane (Sigma-Aldrich). Polyacrylamide-coated coverslips were then washed twice with dH$_2$O, incubated with 1 mM Sulpho-SANPAH (Thermo Scientific Pierce) in HEPES buffer under 365 nm ultraviolet light for 10 min, rinsed twice with 50 mM HEPES pH 8.5 buffer, incubated at 37 °C overnight with rat tail Collagen I (Millipore) in 50 mM HEPES pH 8.5 buffer, rinsed twice in 50 mM HEPES pH 8.5 buffer, and sterilized.

Three-dimensional (3D) cell culture. MCF10A and Eph4Ras cells were grown in 3D cell culture as previously described[28]. Briefly, Eph4Ras cells were seeded on hydrogels in 2% Matrigel (BD Biosciences) MEGM mixed 1:1 with DMEM/F12 and MCF10A cells seeded similarly in 2% Matrigel DMEM/F12 media supplemented with 2% horse serum, 5 ng ml^{-1} human EGF, 10 µg ml^{-1} insulin, 0.5 µg ml^{-1} hydrocortisone, penicillin, streptomycin and 100 ng ml^{-1} cholera toxin.

3D confocal microscopy. We used a protocol adapted from the method described in ref. 28. In brief, cells were fixed with 2% paraformaldehyde (PFA) for 20 min at room temperature, permeabilized with PBS-0.5% Triton X-100, quenched with 100 mM PBS–glycine, and then blocked with 20% goat serum-immunofluorescence (IF) buffer (130 mM NaCl, 7.7 mM NaN$_3$, 0.1% BSA, 0.2% Triton X-100, 0.05% Tween-20, PBS). Samples were incubated with primary antibodies overnight in 20% goat serum-IF buffer, washed 3 times with IF buffer, incubated with secondary antibodies for 1 h, washed 3 times with IF buffer, counterstained for nuclear for 15 min (5 ng ml^{-1} DAPI or TO-PRO-3), washed once with PBS, and mounted with Slow Fade Gold (Invitrogen). Confocal images were acquired using an Olympus FV1000 with 405, 488, 555 and 647 laser lines. Images were linearly analysed and pseudo-coloured using ImageJ analysis software.

Invasive acini quantification. Invasive acini were quantified using bright-field images with a minimum of 5 random low-magnification fields being analysed per condition per experiment. Acini were scored as either normally developed acini or acini that adopted a spread and invasive phenotype.

Second harmonic generation microscopy. Formalin-fixed paraffin embedded sections (5 µm) were re-hydrated and imaged using a multi-photon Leica SP5 confocal microscope using a Ti:sapphire light source and a ×20 water-immersion objective at 880 nm. Fields were acquired using resonant scanning mode, line averaging, and frame accrual. IF staining was sequentially imaged using scanning laser confocal microscopy. The scoring rubric (which was defined before blinded scoring) for SHG analysis was defined as 'organized collagen' in tumours having prominent linearized collagen fibres (with a circularity close to 0) or as 'disorganized collagen' in tumours having either collagen fibres with a high degree of circularity (that is, curved) or low/no SHG signal.

Tumour tissue microarrays. National Cancer Institute Cancer Diagnosis Program stage-3 breast cancer progression tumour tissue microarrays (TMA) were stained for G3BP2 by immunofluorescence for retrospective analysis. TMAs were concurrently imaged by confocal microscopy and SHG. Cores that were missing, damaged, or without detectable tumour cells were omitted from analyses. G3BP2 was scored blindly according to the following rubrics. G3BP2 expression was scored 0 for no detectable expression, 1 for very weak expression, 2 for moderate expression in greater than 75% of tumour cells, and 3+ for strong expression in greater than 75%

of tumour cells. Data for ER status and tumour grade were included in the annotated data set provided by the NCI CDP.

Antibodies. Primary antibodies include anti-β-actin (Abcam, ab13822, 1:3,000), anti-E-cadherin (BD, 610182, 1:200 for immunostaining, 1:1,000 for western blotting), anti-E-cadherin (Abcam, ab11512, Decma-1, 1:200), anti-G3BP2 (Sigma-Aldrich, HPA018425, 1:200, 1:1,000), anti-fibronectin (Sigma-Aldrich, F3648, 1:200), anti-integrin α6 (Millipore, MAB1378, NKI-GoH3, 1:200), anti-human laminin V (Chemicon, D4B5, 1:200), anti-mouse laminin V (kind gift from M. Aumailley, University of Cologne, Germany, 1:1,000), anti-Twist1 (Santa Cruz, ab50887, Twist2C1a, 1:100, 1:1,000), rabbit anti-Twist1 (Sigma-Aldrich, T6451, 1:1,000), 5b7 mouse anti-Twist1 hybridoma cell line (1:1,000), anti-YAP1 (Santa Cruz, H-125, 1:100). AIIB2 hybridoma supernatant was used for β1-integrin -blocking experiments (Developmental Studies Hybridoma Bank, 1:1,000). Secondary fluorescent antibodies used include anti-mouse, anti-rat and anti-rabbit conjugated with Alexa Fluor 488, 546 and 647 (Life Technologies). Secondary horseradish peroxidase (HRP)-conjugated antibodies used include anti-mouse, anti-rabbit and anti-chicken (Jackson Immunoresearch).

Immunoprecipitation. Cells were lysed using a 2-step protocol adapted from ref. 48. Cells were directly lysed with lysis buffer (20 mM Tris-HCl, 1% Triton X-100, 10 mM MgCl$_2$, 10 mM KCl, 2 mM EDTA, 1 mM NaF, 1 mM sodium orthovanadate, 2.5 mM β-glycerophosphate, 10% glycerol, pH 7.5), scraped off the culture dish, sonicated, supplemented to 400 mM NaCl, sonicated and diluted to 200 mM NaCl. Antibodies were conjugated to protein G beads (Invitrogen), crosslinked using disuccinimidyl suberate (Thermo Scientific Pierce) as per the manufacturer's protocol, incubated with lysates overnight at 4 °C, washed eight times with IP lysis buffer supplemented with 200 mM NaCl, and eluted using 50 mM DTT LDS sample buffer at 95 °C for 15 min. 5B7 mouse hybridoma concentrated supernatant was used. For immunoprecipitation of exogenously transfected Myc–Twist1, 293T cell lysates were collected 48 h after transfection and subjected to the 2-step lysis protocol. Immunoprecipitation was performed using anti-Myc antibody (9E10) crosslinked to protein A agarose beads (Invitrogen).

Mass spectrometry. The gel bands were excised and cut into 1 × 1-mm pieces. In gel digestion and extraction were done as previously described[49]. The peptides were separated on a reversed-phase HPLC analytical column (360 µm O.D. × 50 µm I.D., ODS-AQ 5 µm, 10 cm) with an integrated tip (1–2 µm) with a gradient of 0–40%B for 30 min, 40–100%B for 5 min, 100%–0%B for 2 min, and 0%B for 15 min using an Agilent 1100 quaternary pump and eluted into an LTQ Orbitrap. The LTQ Orbitrap was operated in a data-dependent mode. MS spectra were acquired in the Orbitrap with a resolution of 15,000 and MS/MS spectra were acquired in the LTQ. Tandem mass spectra were searched against the IPI mouse database using Bioworks with the following modification: differential Methionine 15.9949. For peptides an xcorr cutoff filter of 1.5 for +1, 2.0 for +2 and 2.5 for +3 was applied, and identified peptides were confirmed by manually inspecting the MS/MS spectra.

Micropatterning. Micropatterned coverslips were designed with and produced by CYTOO (http://www.cytoo.com). Square micropatterns were produced in blocks with a 90 µm pitch between each pattern with a block period of 1,300 µm. Each pattern block was produced in duplicate on each coverslip. Activated coverslips were coated with 20 µg ml^{-1} rat tail collagen I for 2 h at room temperature. Cells were then seeded for 6 h and then fixed for analysis by confocal microscopy. At least 25 random single cells from 5 random fields were analysed per condition.

Motif sequence alignment. Sequences were aligned using ExPASy SIB bioinformatics portal[50].

Proximity ligation assay. Cells were 3D cultured on polyacrylamide gels for 20 h or 6 days and fixed and processed as described for immunofluorescence before performing Duolink PLA (Sigma-Aldrich) as per the manufacturer's protocol. Briefly, mouse anti-Twist1 (Abcam, ab50887, Twist2C1a, 1:150) and rabbit anti-G3BP2 (Sigma-Aldrich, HPA018425, 1:600) primary antibodies were used to detect endogenous proteins and subsequently recognized by species-specific plus and minus PLA oligonucleotide-conjugated probes at 37 °C for 60 min. Interacting probes were then ligated at 37 °C for 30 min and detected by polymerase-mediated amplification at 37 °C for 100 min and subsequently analysed by fluorescent confocal microscopy. For analysis of formed day 6 acini a minimum of 50 cells from 5 random fields were quantified per condition. For analysis of single cells seeded for 20 h a minimum of 25 cells from 5 random fields were quantified per condition. To quantify the PLA signal, confocal images were thresholded using ImageJ analysis software. The area with positive PLA signals was then quantified and divided by the number of cells examined.

Xenograft tumour assay. All animal care and experiments were approved by the Institutional Animal Care and Use Committee of the University of California, San Diego. MCF10DCIS cells (1.0×10^6) suspended in 15 µl Matrigel (BD Biosciences) were injected bilaterally into the inguinal mammary fat pads of 8-week-old female SCID-beige mice. No statistical method was used to predetermine sample size and the experiments were not randomized. Mice were euthanized and tumour burden was analysed at 7 weeks post tumour implantation. Mice were dissected and tumour invasion was assessed *in situ* using a fluorescent dissection scope (Leica Microsystems). The investigators were not blinded to allocation during experiments and outcome assessment. All work with animals was performed in accordance with UC San Diego IACUC and AAALAC guidelines.

TCGA data set analysis. The TCGA breast cancer gene expression data set (TCGA BRCA G4502A_07_3) was downloaded from the UCSC Cancer Genome Browser (https://genome-cancer.ucsc.edu). Samples were stratified by *G3BP2* expression, with *G3BP2*^high and *G3BP2*^low samples with expression above and below mean G3BP2 expression, respectively. Overall patient survival in each group was then analysed.

Statistical analysis. All P values were derived from Student's t-test using unpaired two-tailed analysis with Welch's correction, unless otherwise noted. Error bars denote standard deviation unless otherwise noted. Kaplan–Meier survival curves were analysed by Cox–Mantel Log-rank analysis. Contingency tables were analysed using Fisher's exact analysis. Statistical significance was defined as $P < 0.05$, with regard to the null hypothesis. All qualitative data shown using representative data were repeated in at least 3 independent experiments.

Real-time PCR. RNA was extracted from cells using the RNeasy Mini and Micro Kit (Qiagen). cDNA was generated using random hexamer primers and a cDNA Reverse Transcription Kit (Applied Biosystems). Expression values were generated using ddCt values normalized to GAPDH. Experiments were performed in biological and technical triplicate using 7500 Fast (Applied Biosystems) and CFX Connect (Bio-Rad) real-time PCR detection systems. For data analysis in each comparison (one shRNA versus the control shRNA), unpaired two-tailed Student's t-tests with Welch's correction were used to determine statistical significance.

Murine primer sequences: Twist1 (5′-CAGCGGGTCATGGCTAAC-3′, 5′-CAGCTTGCCATCTTGGAGTC-3′), G3bp2 (5′-CCCGAGTATTTGCACAG GTT-3′, 5′-TCACTCAAGGTTGCATGAGC-3′), Snai1 (5′-AAGATGCACAT CCGAAGCC-3′, 5′-CGCAGGTTGGAGCGGTCAGC-3′), Snai2 (5′-ATGCCC AGTCTAGGAAATCG-3′, 5′-CAGTGAGGGCAAGAGAAAGG-3′), Zeb1 (5′-TGATGAAAACGGAACACCAGATG-3′, 5′-GTTGTCCTCGTTCTTCTCAT GG-3′), Zeb2 (5′-TGAAGAGAACTTTTCCTGCCCT-3′, 5′-ATTTGGTGCTGA TCTGTCCCT-3′), E-cadherin (5′-GGGTGAATTCCCAAAGAACC-3′, 5′-TGGCA ATGGCTTCTCTATCC-3′), vimentin (5′-CGGCTGCGAGAGAAATTGC-3′, 5′-C CACTTTCCGTTCAAGGTCAAG-3′).

Human primer sequences: E-cadherin (5′-TGCCCAGAAAATGAAAAAGG-3′, 5′-GTGTATGTGGCAATGCGTTC-3′), vimentin (5′-GAGAACTTTGCCGTTGA AGC-3′, 5′-GCTTCCTGTAGGTGGCAATC-3′), fibronectin (5′-CAGTGGGAGA CCTCGAGAAG-3′, 5′-TCCCTCGGAACATCAGAAAC-3′).

Shared murine and human primer sequences: GAPDH (5′-GACCCCTTCATT GACCTCAAC-3′, 5′-CTTCTCCATGGTGGTGAAGA-3′).

shRNA sequences. pSP108 lentiviral target sequences: Twist1 shRNA3, 5′-AAGC TGAGCAAGATTCAGACC-3′. Twist1 shRNA5, 5′-AGGTACATCGACTTCCTG TAC-3′. ControlshRNA (GFPshRNA), 5′-GCAAGCTGACCCTGAAG-3′.

pLKO.1 (Sigma-Aldrich) lentiviral target sequences: G3BP2shRNA2, 5′-AGT TAAATTGAGGTGGACATT-3′. G3BP2shRNA5, 5′-TTCGAGGAGAAGTAC GTTTAA-3′. G3BP2shRNA6, 5′-CGGGAGTTTGTGAGGCAATAT-3′. G3BP2 shRNA8, 5′-CCACAAAGTATTATCTCTGAA-3′.

47. Chaudhuri, T., Rehfeldt, F., Sweeney, H. L. & Discher, D. E. Preparation of collagen-coated gels that maximize *in vitro* myogenesis of stem cells by matching the lateral elasticity of *in vivo* muscle. *Methods Mol. Biol.* **621,** 185–202 (2010).
48. Klenova, E., Chernukhin, I., Inoue, T., Shamsuddin, S. & Norton, J. Immunoprecipitation techniques for the analysis of transcription factor complexes. *Methods* **26,** 254–259 (2002).
49. Guo, Y., Ma, S. F., Grigoryev, D., Van Eyk, J. & Garcia, J. G. 1-DE MS and 2-D LC-MS analysis of the mouse bronchoalveolar lavage proteome. *Proteomics* **5,** 4608–4624 (2005).
50. Artimo, P. *et al.* ExPASy: SIB bioinformatics resource portal. *Nucleic Acids Res.* **40,** W597–W603 (2012).
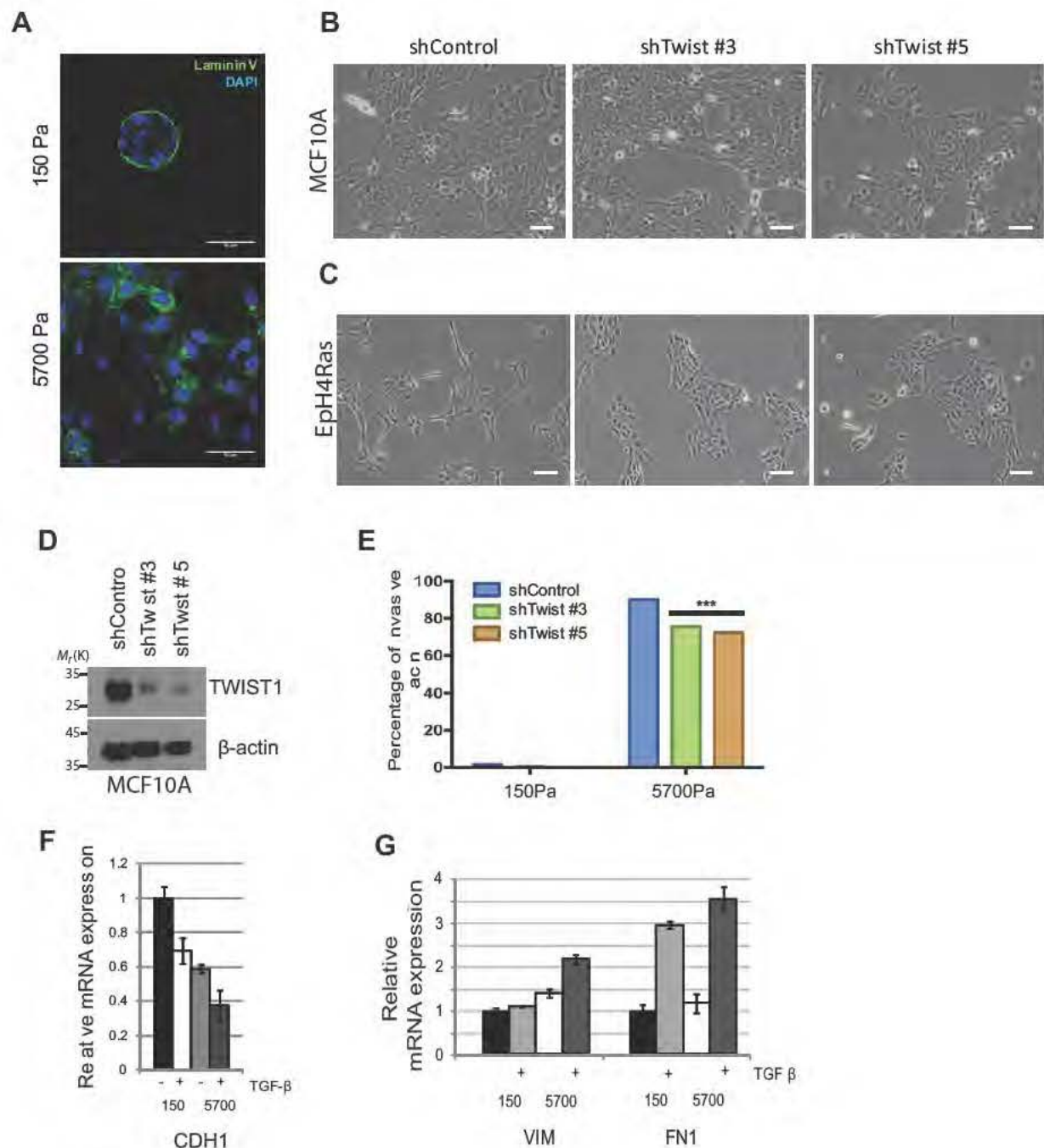
Supplementary Figure 1 TWIST1 is required for matrix stiffness-induced EMT. (**A**) Confocal microscopy of MCF10A cells grown in 3D culture for 5 days on varying matrix rigidities stained for Laminin V (green) and DAPI (blue) (scale bar, 50 µm). (**B-C**) Brightfield images of MCF10A (B) and Eph4Ras (C) cells expressing control and shTwist1 shRNAs (scale bar, 75 µm). (**D**) Lysates of control and shTwist expressing MCF10A cells analyzed by SDS-PAGE and probed for TWIST1 and β-Actin. (**E**) Quantification of invasive acini of MCF10A shTwist1 cells in 3D culture (***, P<0.001, unpaired two-tailed T-test with Welch's correction, n=50 acini/experiment, 3 independent experiments, error bars represent s.d.). (**F**) qPCR analysis of E-cadherin (CDH1) mRNA expression in MCF10A cells in 3D culture on PA hydrogels treated or not with 5 ng/ml TGF-β for 5 days (P<0.05, unpaired two-tailed T-test with Welch's correction, n=4 independent experiments, statistics source data can be found in Supplementary Table 1, error bars represent s.d.). (**G**) qPCR analysis of the mRNA expression of mesenchymal markers, Fibronectin (FN1) and Vimentin (VIM), in MCF10A cells in 3D culture on PA hydrogels treated or not with 5 ng/ml TGF-β for 5 days (P<0.05, unpaired two-tailed T-test with Welch's correction, n=4 independent experiments, statistics source data can be found in Supplementary Table 1, error bars represent s.d.).

A

Eph4Ras Micropatterned Cells
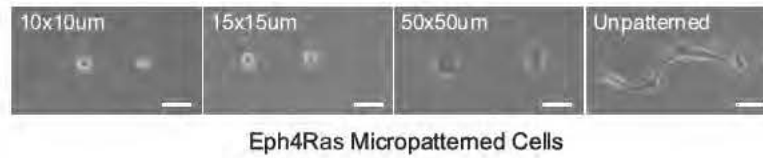
B
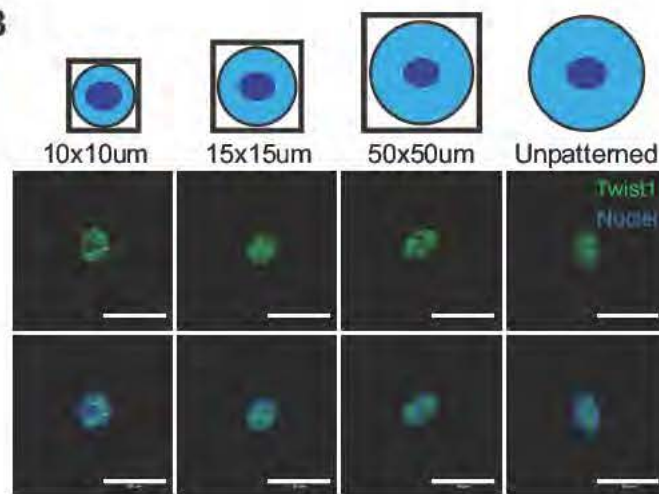
C
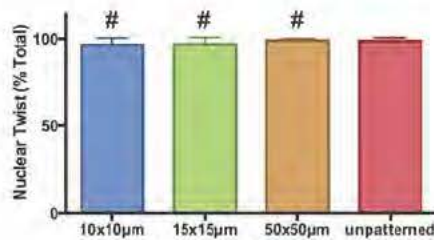
Supplementary Figure 2 Mechanoregulation of Twist1 nuclear localization in Eph4Ras cells. Brightfield images (**A**) and confocal images (scale bar, 50 μm) (**B**) of Eph4Ras cells cultured on micropatterned glass coverslips for 6 hours stained for Twist1 (green) and DAPI (blue) (scale bar, 20 μm).

(**C**) Quantification of nuclear localized Twist1 in percentage of the total cell number (#, not significant, unpaired two-tailed T-test with Welch's correction, n=25 cells/experiment, 3 independent experiments, error bars represent s.d.).
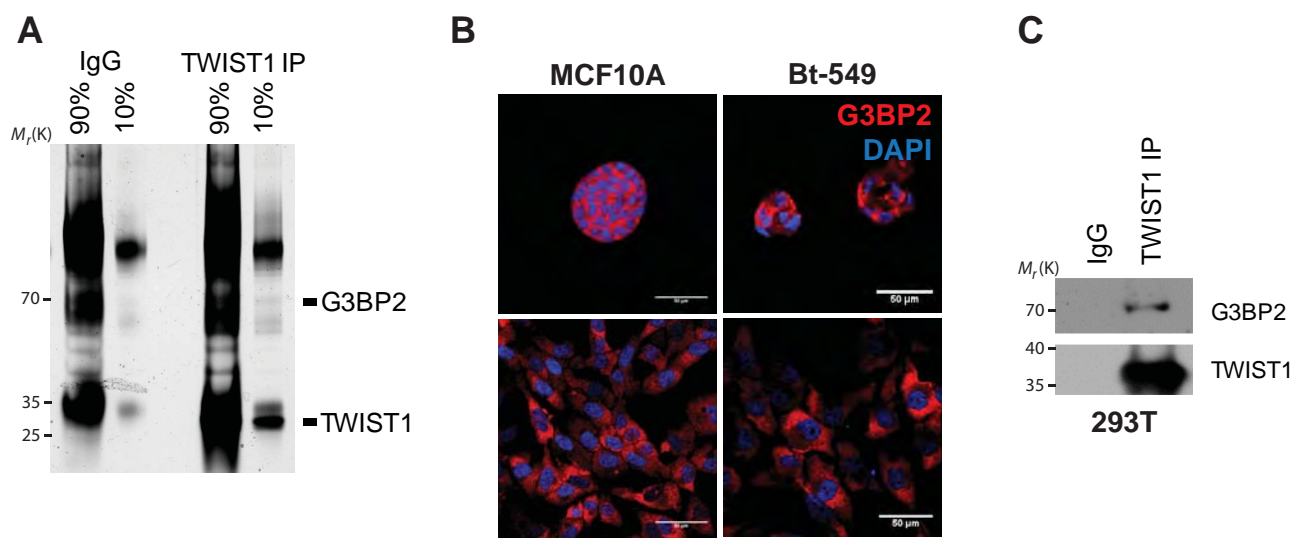
Supplementary Figure 3 G3BP2 is a TWIST1 binding protein that localizes in the cytoplasm. (**A**) Immunoprecipitation of endogenous TWIST1 from MCF10A cell lysates resolved by SDS-PAGE and silver stained. Unique bands were identified, excised, and analyzed by mass spectrometry. (**B**) Confocal images of MCF10A and Bt-549 cells grown in 3D culture stained for endogenously expressed G3BP2 (red) and DAPI (blue) (scale bar, 50 μm). (**C**) Exogenously expressed Twist1 from 293T cell lysates was immunoprecipitated and analyzed by SDS-PAGE, and probed for G3BP2 and Twist1.
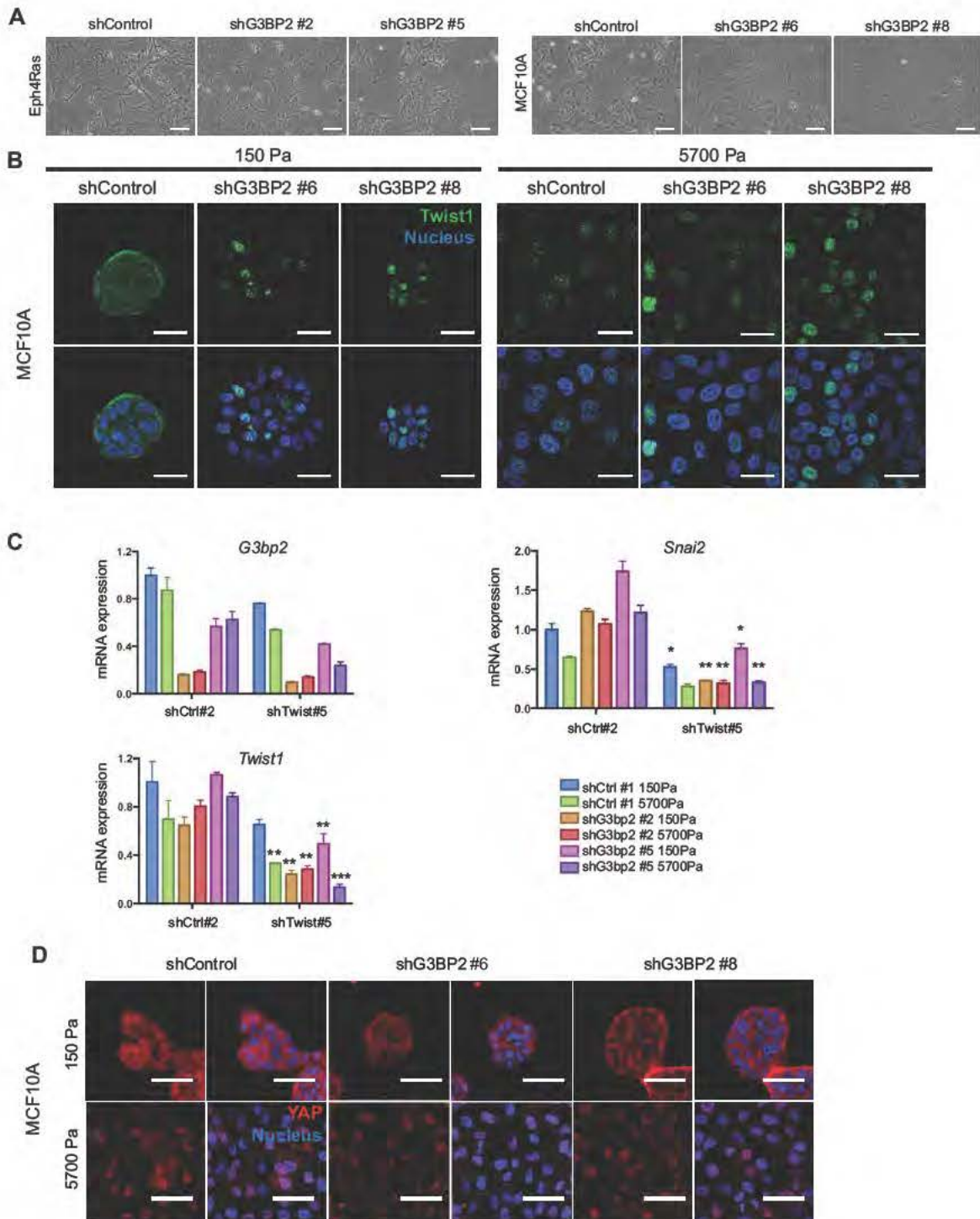
Supplementary Figure 4 G3BP2 mediates mechanoregulation of TWIST1 and EMT. (**A**) Brightfield images of Eph4Ras (left panel) and MCF10A (right panel) cells expressing control and *G3BP2* shRNAs (scale bar, 75 µm). (**B**) Confocal images of MCF10A cells expressing shRNAs against *G3BP2* grown in 3D culture for 5 days on varying matrix rigidities and stained for endogenously expressed TWIST1 (green) and DAPI (blue) (scale bar, 25 µm). (**C**) qPCR analysis of *G3bp2*, *Twist1* and *Snai2* in Eph4Ras cells expressing control (shCtrl#1) or *G3bp2* shRNAs, together with control (shCtrl#2) or

Twist1 shRNA (shTwist1#5), 3D cultured under indicated matrix rigidities for 5 days (*, P<0.05; **, P<0.01; ***, P<0.001, unpaired two-tailed T-test with Welch's correction, n=3 independent experiments, statistics source data can be found in Supplementary Table 1; double knockdown compared to the respective single knockdown, error bars represent s.d.). (**D**) Confocal images of MCF10A cells expressing shRNAs against *G3BP2* grown in 3D culture for 5 days on varying matrix rigidities and stained for YAP1 (red) and DAPI (blue) (scale bar, 50 µm).
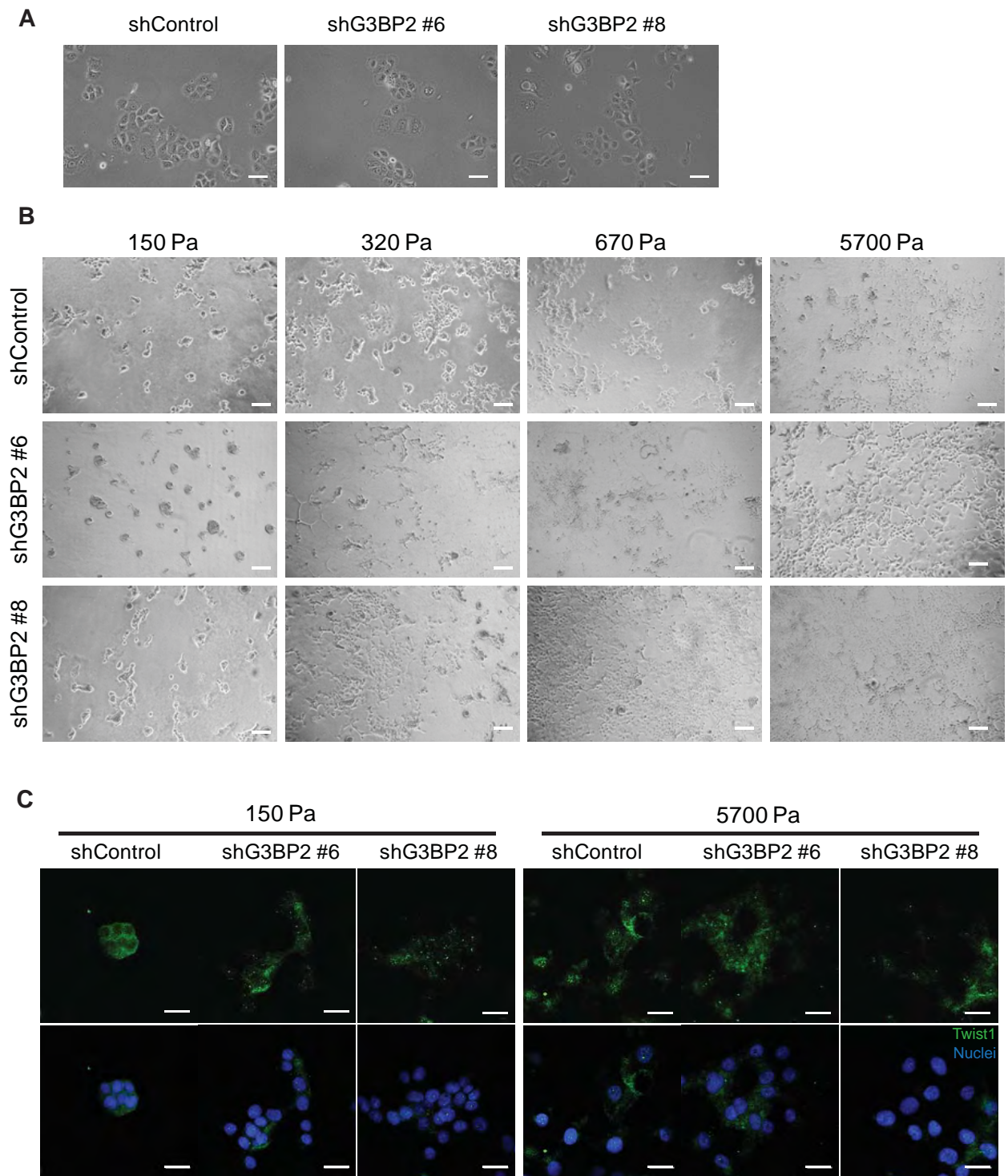
Supplementary Figure 5 G3BP2 is required for mechanosensing in MCF10DCIS cells. (**A**) Brightfield images of MCF10DCIS cells expressing control and *G3BP2* shRNAs (scale bar, 25 μm). (**B**) Brightfield images of MCF10DCIS cells expressing control and *G3BP2* shRNAs cultured in 3D at indicated matrix rigidities for 5 days (scale bar, 150 μm). (**C**) Confocal images of MCF10DCIS cells expressing shRNAs against *G3BP2* grown in 3D culture for 5 days on varying matrix rigidities and stained for endogenously expressed TWIST1 (green) and DAPI (blue) (scale bar, 25 μm).

A

B

	G3BP2 Low	G3BP2 High
Median Survival (Months)	91.99	146.50
Total Patients	291	273
Hazard ratio	0.7797	
Hazard ratio 95% CI	0.5155 to 1.181	

C

D

E

F
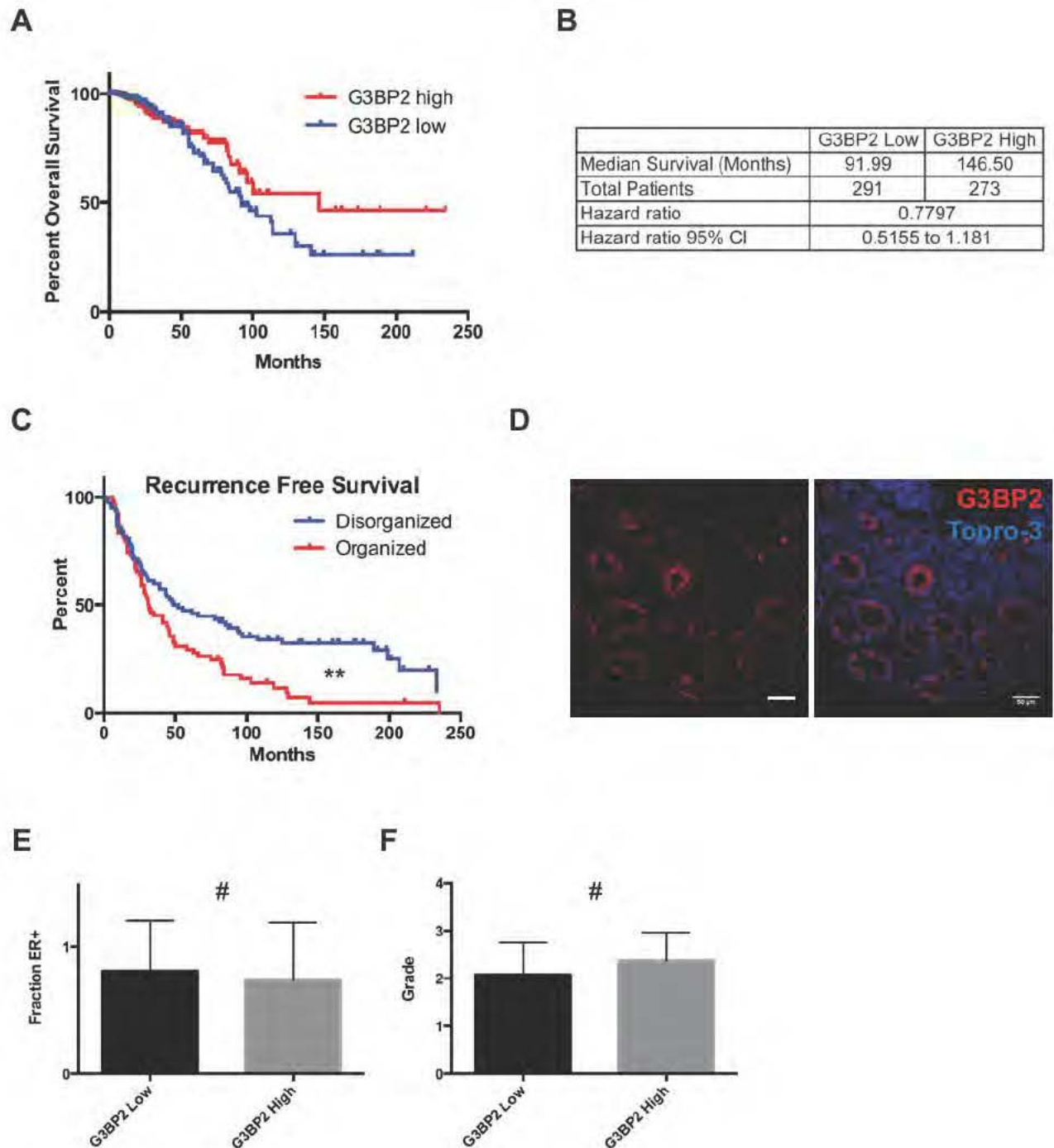
Supplementary Figure 6 G3BP2 expression profile in normal and cancer human tissues. (**A**) Kaplan-Meier survival curve of patients stratified by G3BP2 expression in the TCGA breast cancer dataset (TCGA_BRCA_G4502A_07_3) (P=0.2435, Log-Rank). (**B**) Statistics of overall survival of patients stratified by G3BP2 expression in the TCGA breast cancer dataset (TCGA_BRCA_G4502A_07_3). (**C**) Kaplan-Meier curve of recurrence free survival in stage 3 breast cancer patients based on SHG imaging (**, P=0.0047, Log-Rank, n=197 breast tumors). (**D**) Confocal microscopy of normal human colon luminal epithelial cells stained for G3BP2 (red) and nuclei (blue) (scale bar, 50 μm). (**E, F**) Correlation between G3BP2 expression and ER positivity (**E**) or tumor grade (**F**) in stage 3 breast cancer patient samples analyzed in (C) (#, not significant, Fisher's Exact, n=197 breast tumors, error bars represent s.d.).
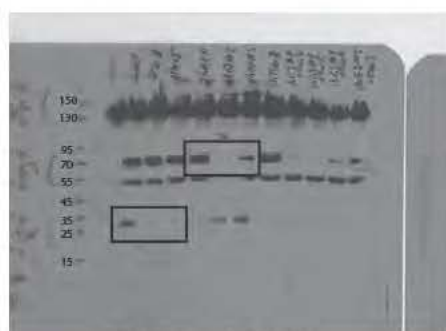
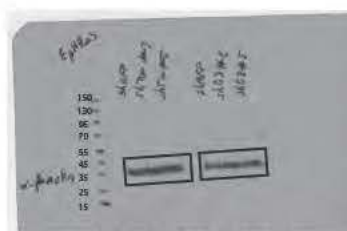Fig. 1B Twist1   Fig. 5A G3BP2

Fig. 1B bActin   Fig. 5A bActin

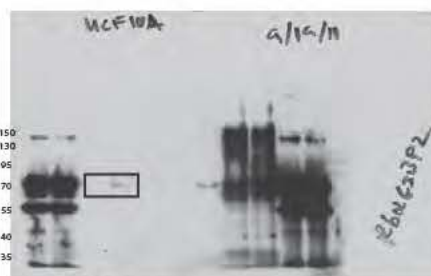Fig. 2B Twist1   Fig. 2B bActin

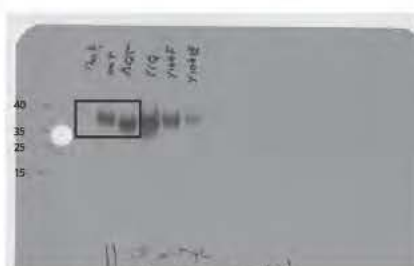Fig. 4A Twist1

Fig. 4A G3BP2

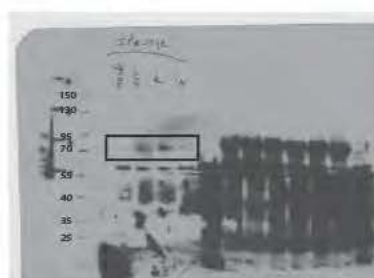Fig. 4D input G3BP2

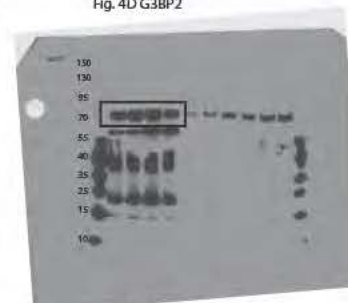Fig. 4D Myc

Fig. 4D G3BP2

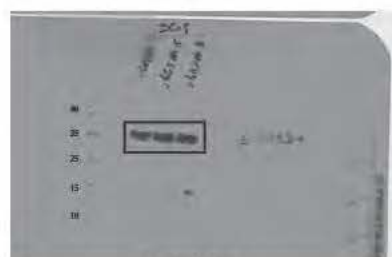Fig. 4J Myc

Fig. 4J G3BP2

Fig. 4J input G3BP2

Fig. 6A G3BP2

Fig. 6A GAPDH

Supplementary Figure 7 Uncropped Western blots images.

1 / 2 / 3 (replicate headers)

GAPDH

	Rep 1 Ct1	Rep 1 Ct2	Rep 2 Ct1	Rep 2 Ct2	Rep 3 Ct1	Rep 3 Ct2
shGFP 150	17 498	17 467	16 08	16 26	19 03	18 95
shGFP 5700	17 503	17 382	16 41	15 89	19 11	18 80
shGFP 150 TGF	17 609	17 816	17 33	17 01	19 12	19 24
shGFP 5700 TGF	17 671	17 570	17 03	16 54	19 05	19 15
sh#3 150	17 388	17 588	15 75	15 76	18 16	18 20
sh#3 5700	16 475	17 093	15 83	15 75	17 63	17 52
sh#3 150 TGF	17 329	17 512	16 23	16 66	17 62	17 50
sh#3 5700 TGF	17 120	17 036	16 64	16 94	18 06	18 26
sh#5 150	17 093	17 165	16 84	16 39	18 30	18 26
sh#5 5700	17 059	16 557	16 44	16 50	17 94	18 26
sh#5 150 TGF	17 035	17 308	17 27	17 22	18 16	17 88
sh#5 5700 TGF	17 334	17 420	16 74	16 97	18 45	18 42

Tw st1

	Rep 1 Ct1	Rep 1 Ct2	Rep 2 Ct1	Rep 2 Ct2	Rep 3 Ct1	Rep 3 Ct2
shGFP 150	22 758	23 058	22 45	22 26	24 70	24 97
shGFP 5700	23 282	23 476	22 50	22 09	25 40	24 94
shGFP 150 TGF	23 447	23 316	23 57	23 52	25 57	25 63
shGFP 5700 TGF	23 881	23 880	23 57	23 38	25 57	25 88
sh#3 150	25 463	25 374	25 21	25 01	28 40	28 28
sh#3 5700	26 001	25 449	25 30	24 86	28 42	28 61
sh#3 150 TGF	25 912	25 953	25 66	26 11	28 58	28 18
sh#3 5700 TGF	26 142	25 834	26 21	26 06	28 89	28 60
sh#5 150	24 090	24 149	24 49	24 25	27 38	27 38
sh#5 5700	24 373	24 521	24 65	24 25	27 02	26 58
sh#5 150 TGF	24 302	24 552	25 13	25 01	26 53	26 51
sh#5 5700 TGF	25 124	24 882	24 53	24 30	27 51	27 75

GAPDH

	Rep 1 Ct1	Rep 1 Ct2	Rep 2 Ct1	Rep 2 Ct2	Rep 3 Ct1	Rep 3 Ct2
shGFP 150	17 498	17 467	16 08	16 26	19 03	18 95
shGFP 5700	17 503	17 382	16 41	15 89	19 11	18 80
shGFP 150 TGF	17 609	17 816	17 33	17 01	19 12	19 24
shGFP 5700 TGF	17 671	17 570	17 03	16 54	19 05	19 15
sh#3 150	17 388	17 588	15 75	15 76	18 16	18 20
sh#3 5700	16 475	17 093	15 83	15 75	17 63	17 52
sh#3 150 TGF	17 329	17 512	16 23	16 66	17 62	17 50
sh#3 5700 TGF	17 120	17 036	16 64	16 94	18 06	18 26
sh#5 150	17 093	17 165	16 84	16 39	18 30	18 26
sh#5 5700	17 059	16 557	16 44	16 50	17 94	18 26
sh#5 150 TGF	17 035	17 308	17 27	17 22	18 16	17 88
sh#5 5700 TGF	17 334	17 420	16 74	16 97	18 45	18 42

Slug

	Rep 1 Ct1	Rep 1 Ct2	Rep 2 Ct1	Rep 2 Ct2	Rep 3 Ct1	Rep 3 Ct2	Rep 3 Ct3
shGFP 150	24 074	23 926	23 96	23 50	25 13	24 84	25 20
shGFP 5700	24 059	24 197	23 36	23 72	25 67	25 33	25 44
shGFP 150 TGF	23 985	23 925	24 52	24 54	25 37	25 29	25 21
shGFP 5700 TGF	23 955	24 210	24 23	24 43	25 33	25 23	25 24
sh#3 150	25 169	25 228	24 43	24 44	25 99	26 06	26 15
sh#3 5700	25 276	25 183	24 12	24 30	25 86	25 87	25 75
sh#3 150 TGF	24 244	24 235	24 53	24 53	25 29	25 05	25 29
sh#3 5700 TGF	24 593	24 644	24 83	24 95	26 01	25 48	25 40
sh#5 150	24 817	24 904	24 97	24 87	25 88	25 62	
sh#5 5700	24 886	24 662	24 52	24 52	25 72	26 03	26 14
sh#5 150 TGF	24 144	24 336	25 07	24 98	25 08	25 03	24 92
sh#5 5700 TGF	25 033	25 087	24 97	24 99	25 74	25 76	25 96

GAPDH

	Rep 1 Ct1	Rep 1 Ct2	Rep 2 Ct1	Rep 2 Ct2	Rep 3 Ct1	Rep 3 Ct2
shGFP 150	17 498	17 467	16 08	16 26	19 03	18 95
shGFP 5700	17 503	17 382	16 41	15 89	19 11	18 80
shGFP 150 TGF	17 609	17 816	17 33	17 01	19 12	19 24
shGFP 5700 TGF	17 671	17 570	17 03	16 54	19 05	19 15
sh#3 150	17 388	17 588	15 75	15 76	18 16	18 20
sh#3 5700	16 475	17 093	15 83	15 75	17 63	17 52
sh#3 150 TGF	17 329	17 512	16 23	16 66	17 62	17 50
sh#3 5700 TGF	17 120	17 036	16 64	16 94	18 06	18 26
sh#5 150	17 093	17 165	16 84	16 39	18 30	18 26
sh#5 5700	17 059	16 557	16 44	16 50	17 94	18 26
sh#5 150 TGF	17 035	17 308	17 27	17 22	18 16	17 88
sh#5 5700 TGF	17 334	17 420	16 74	16 97	18 45	18 42

Sna l1

	Rep 1 Ct1	Rep 1 Ct2	Rep 2 Ct1	Rep 2 Ct2	Rep 3 Ct1	Rep 3 Ct2	Rep 3 Ct3
shGFP 150	23 70	23 40	22 32	22 37	25 72	26 02	25 75
shGFP 5700	22 98	23 10	22 19	22 23	25 07	25 20	25 05
shGFP 150 TGF	20 49	20 59	20 83	20 59	22 86	22 72	22 82
shGFP 5700 TGF	20 58	20 44	20 23	20 17	22 25	22 23	22 37
sh#3 150	22 87	22 74	22 90	22 74	24 43	24 39	24 37
sh#3 5700	22 52	22 55	22 64	22 87	24 03	23 71	24 05
sh#3 150 TGF	20 27	20 40	20 58	20 89	21 42	21 42	21 54
sh#3 5700 TGF	20 09	20 35	20 85	20 80	21 81	21 55	22 00
sh#5 150	23 28	23 00	22 41	22 37	24 36	24 18	24 57
sh#5 5700	22 59	22 43	22 06	22 04	24 18	23 99	24 05
sh#5 150 TGF	20 41	20 53	20 07	20 08	21 53	21 48	21 72
sh#5 5700 TGF	20 15	20 06	20 20	19 85	21 41	21 58	21 39

GAPDH

	Rep 1 Ct1	Rep 1 Ct2	Rep 2 Ct1	Rep 2 Ct2	Rep 3 Ct1	Rep 3 Ct2
shGFP 150	17 498	17 467	16 08	16 26	19 03	18 95
shGFP 5700	17 503	17 382	16 41	15 89	19 11	18 80
shGFP 150 TGF	17 609	17 816	17 33	17 01	19 12	19 24
shGFP 5700 TGF	17 671	17 570	17 03	16 54	19 05	19 15
sh#3 150	17 388	17 588	15 75	15 76	18 16	18 20
sh#3 5700	16 475	17 093	15 83	15 75	17 63	17 52
sh#3 150 TGF	17 329	17 512	16 23	16 66	17 62	17 50
sh#3 5700 TGF	17 120	17 036	16 64	16 94	18 06	18 26
sh#5 150	17 093	17 165	16 84	16 39	18 30	18 26
sh#5 5700	17 059	16 557	16 44	16 50	17 94	18 26
sh#5 150 TGF	17 035	17 308	17 27	17 22	18 16	17 88
sh#5 5700 TGF	17 334	17 420	16 74	16 97	18 45	18 42

ZEB1

	Rep 1 Ct1	Rep 1 Ct2	Rep 2 Ct1	Rep 2 Ct2	Rep 3 Ct1	Rep 3 Ct2	Rep 3 Ct3
shGFP 150	23 59	23 70	24 82	24 63	26 44	26 56	27 15
shGFP 5700	24 18	24 21	24 30	24 33	27 51	26 93	27 33
shGFP 150 TGF	22 46	22 42	23 90	23 95	26 15	26 83	26 38
shGFP 5700 TGF	23 75	23 42	23 41	23 34	26 84	26 88	27 79
sh#3 150	24 33	24 48	25 02	25 03	28 21	28 46	27 93
sh#3 5700	24 69	24 96	24 83	24 78	28 43	28 51	28 01
sh#3 150 TGF	23 12	22 79	23 60	23 72	26 18	26 06	26 09
sh#3 5700 TGF	23 60	23 57	24 05	23 91	28 99	26 88	26 82
sh#5 150	24 97	24 78	26 52	26 57	28 19	28 51	29 36
sh#5 5700	25 39	25 41	26 20	26 27	29 51	29 72	29 94
sh#5 150 TGF	22 79	22 49	25 02	24 83	26 20	26 87	26 93
sh#5 5700 TGF	24 05	23 86	24 67	24 54	28 19	28 32	28 47

GAPDH

	Rep 1 Ct1	Rep 1 Ct2	Rep 2 Ct1	Rep 2 Ct2	Rep 3 Ct1	Rep 3 Ct2
shGFP 150	17 498	17 467	16 08	16 26	19 03	18 95
shGFP 5700	17 503	17 382	16 41	15 89	19 11	18 80
shGFP 150 TGF	17 609	17 816	17 33	17 01	19 12	19 24
shGFP 5700 TGF	17 671	17 570	17 03	16 54	19 05	19 15
sh#3 150	17 388	17 588	15 75	15 76	18 16	18 20
sh#3 5700	16 475	17 093	15 83	15 75	17 63	17 52
sh#3 150 TGF	17 329	17 512	16 23	16 66	17 62	17 50
sh#3 5700 TGF	17 120	17 036	16 64	16 94	18 06	18 26
sh#5 150	17 093	17 165	16 84	16 39	18 30	18 26
sh#5 5700	17 059	16 557	16 44	16 50	17 94	18 26
sh#5 150 TGF	17 035	17 308	17 27	17 22	18 16	17 88
sh#5 5700 TGF	17 334	17 420	16 74	16 97	18 45	18 42

ZEB2

	Rep 1 Ct1	Rep 1 Ct2	Rep 2 Ct1	Rep 2 Ct2	Rep 3 Ct1	Rep 3 Ct2	Rep 3 Ct3
shGFP 150	21 26	21 75	22 03	22 16	20 84	20 53	20 58
shGFP 5700	22 23	21 84	21 95	21 87	21 96	21 62	22 26
shGFP 150 TGF	21 17	20 84	21 48	21 37	21 36	21 26	21 22
shGFP 5700 TGF	21 63	21 53	21 19	21 07	21 69	21 31	22 07
sh#3 150	21 90	21 99	22 15	22 23	21 24	21 69	21 50
sh#3 5700	22 33	22 41	21 37	21 29	21 26	22 37	22 42
sh#3 150 TGF	20 96	20 96	21 37	21 29	20 88	20 85	20 64
sh#3 5700 TGF	21 67	21 61	21 42	21 30	21 28	20 57	20 93
sh#5 150	22 69	23 00	23 75	23 70	22 19	22 63	22 30
sh#5 5700	22 93	23 47	23 27	23 37	22 28	23 03	22 84
sh#5 150 TGF	21 21	21 43	22 24	22 20	20 83	20 28	21 07
sh#5 5700 TGF	22 32	22 30	22 11	22 12	21 55	21 41	22 28

Supplementary Table 1 Statistical source data.

Molecular Pathways: Linking Tumor Microenvironment to Epithelial–Mesenchymal Transition in Metastasis

Hae Yun Jung[1], Laurent Fattet[1], and Jing Yang[1,2]

Abstract

During tumor development, tumor cells constantly communicate with the surrounding microenvironment through both biochemical and biophysical cues. In particular, the tumor microenvironment can instruct carcinoma cells to undergo a morphogenesis program termed epithelial to mesenchymal transition (EMT) to facilitate local invasion and metastatic dissemination. Growing evidence uncovered a plethora of microenvironmental factors in promoting EMT, including proinflammatory cytokines secreted by locally activated stromal cells, hypoxia conditions, extracellular matrix components, and mechanical properties. Here, we review various biochemical and biophysical factors in the tumor microenvironment that directly impinge upon the EMT program. Specifically, cytokines such as TGFβ, TNFα, and IL6 and hypoxia are capable of inducing EMT in various tumors. Several extracellular matrix (ECM) proteins, including collagen I, fibronectin, and hyaluronan, and ECM remodeling via extracellular lysyl oxidase are also implicated in regulating EMT. In preclinical studies and ongoing clinical trials, targeting these tumor microenvironmental signals has shown promises in halting tumor progression in various human cancers. *Clin Cancer Res; 21(5); 1 7.* ©2014 AACR.

Background

During tumor metastasis, the epithelial to mesenchymal transition (EMT) program has been indicated in giving rise to the dissemination of single tumor cells from primary epithelial tumors (1). EMT refers to a global cellular and molecular transition by which polarized epithelial cells gain mesenchymal properties to migrate. During EMT, epithelial cells reorganize cytoskeleton and resolve cell cell junctions, which are accompanied with switching off the expression of epithelial markers and turning on mesenchymal genes. Although changes in epithelial and mesenchymal markers during EMT can vary significantly in different biologic contexts, a network of transcription factors, including TWIST1/2, SNAIL1/2, ZEB1/2, and FOXC2, are consistently required to orchestrate the EMT program (2). Numerous studies have shown that the expression of these transcription factors is associated with poor prognosis and distant metastasis in various human cancers (3). Besides its role in promoting tumor cell invasion, EMT is shown to confer tumor cells with resistance to apoptosis (4) and anoikis (5), thus allowing cell survival in the blood stream after intravasation. EMT could also facilitate tumor cells' escape from the senescence program, especially through TWIST1 and ZEB1 (6, 7). Furthermore, EMT has been shown to

endow cancer cells with cancer stem cell (CSC) like features, which further aid tumor dormancy and chemoresistance (8, 9).

Studies with tumor samples or experimental tumor xenograft models have provided convincing evidence for the activation of EMT in various primary epithelial tumors. Interestingly, more recent studies reveal a dynamic requirement of EMT in tumor metastasis: activation of EMT promotes local tumor invasion, intravasation, and extravasation of the systemic circulation, whereas reversion of EMT is essential to establish macrometastases in distant organs (1, 10). The "reversible" EMT model implies that EMT is unlikely to be regulated by permanent genetic and epigenetic changes in tumor cells; instead, EMT is dynamically controlled by various proinvasion signals from the tumor microenvironment (TME).

The TME is defined as the cellular and physical environment surrounding the primary tumor including endothelial, inflammatory and immune cells, fibroblasts, extracellular matrix (ECM) components, and soluble factors. In this review, we discuss the most relevant and direct connections between TME signals and the EMT inducing transcription factors in cancer. On the basis of the properties of the TME signals, we divide our discussion into four major categories: inflammatory signals, hypoxia, ECM components, and ECM mechanical properties (Fig. 1).

Inflammatory cytokines

An association between cancer development and inflammation has long been observed. During tumor progression, tumor cells recruit activated fibroblasts and immune cells that in turn secrete many cytokines to affect tumor development and metastasis (11). Interestingly, such cytokines have been shown to directly regulate the EMT program. Transforming growth factor β (TGFβ), abundantly secreted by cancer associated fibroblasts, platelets, and tumor cells, is the best characterized EMT inducer. TGFβ has been

[1]Department of Pharmacology, University of California, San Diego, La Jolla, California. [2]Department of Pediatrics, University of California, San Diego, La Jolla, California.

H. Y. Jung and L. Fattet contributed equally to this article.

Corresponding Author: Jing Yang, Moores UCSD Cancer Center, University of California, San Diego, 3855 Health Sciences Drive, MC0819, La Jolla, CA 92093. Phone: 858 534 1994; Fax: 858 534 7390; E mail: jingyang@ucsd.edu

AACR OF1
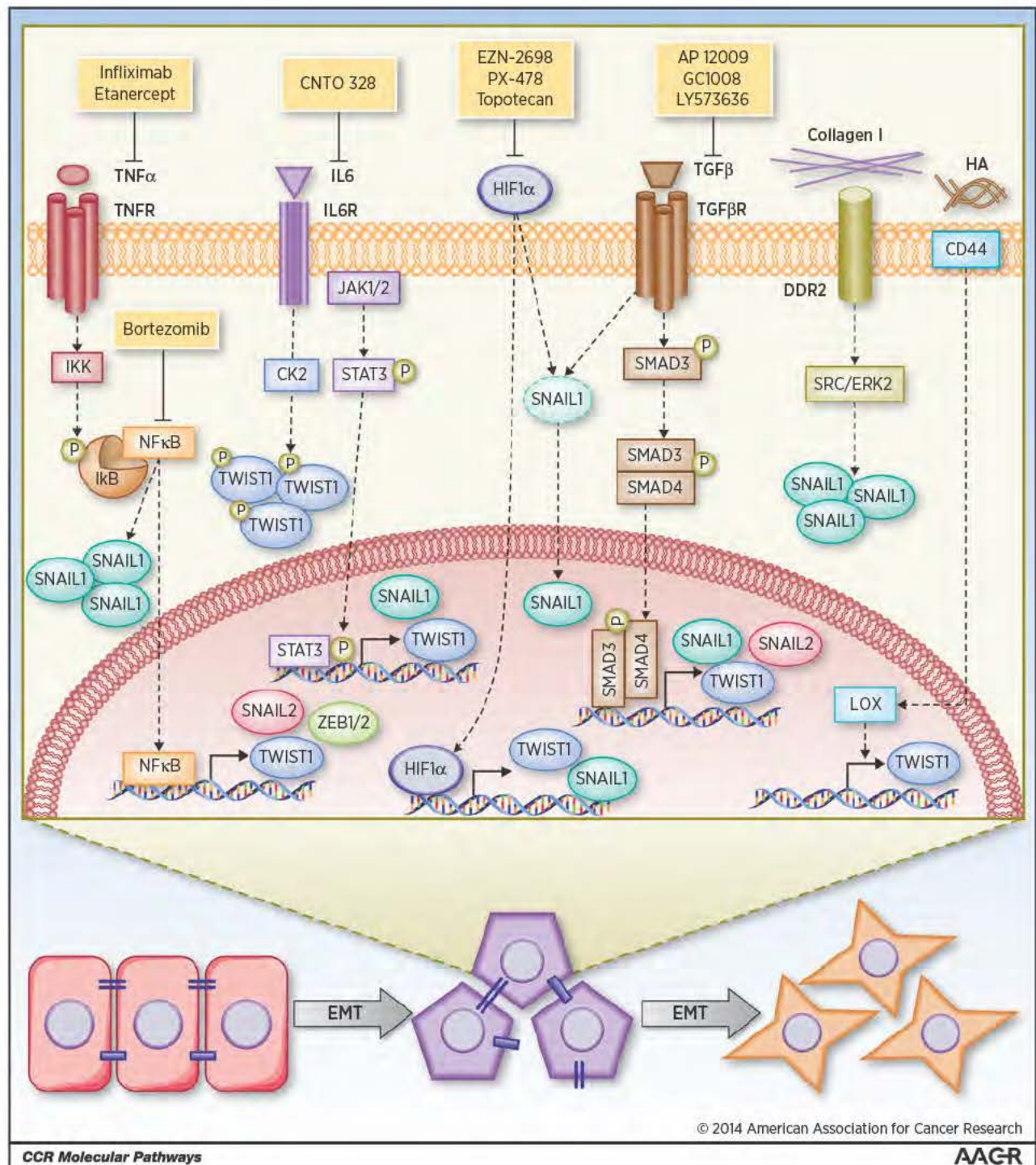
Figure 1.

Regulation of EMT transcription factors by tumor microenvironmental signals. TGFβ regulates upregulation of TWIST1, SNAIL1, and SNAIL2 via the SMAD signaling pathway. Drugs that inhibit TGFβ are AP12009, GC1008, and LY573636, which are in clinical trials for advanced solid tumors. TNFα activates NFκB to induce TWIST1, SNAIL2, and ZEB1/2 expression and TNFα/NFκB activation also increases SNAIL1 protein stability. Therapeutic approaches to inhibit TGFβ signaling include TNFα antagonist (infliximab and etanercept) and NFkB inhibitor (bortezomib), all of which have been assessed in phase II clinical trials for several cancer types. IL6 induces TWIST1 and SNAIL1 expression via JAK/STAT3 signaling and increases TWIST1 stability through CK2 dependent phosphorylation. An IL6 ligand blocking antibody, CNTO 328, has been tested in phase I/II clinical trials with metastatic renal cell carcinoma. HIF1α induces TWIST1 and SNAIL1 expression and HIF1α either alone or in cooperation with TGFβ promotes SNAIL1 nuclear localization to stabilize SNAIL. Agents to inhibit HIF1α include EZN 2698, PX 478, and topotecan. Topotecan has been tested in phase I/II clinical trials in combination with conventional chemotherapy, and EZN 2698 and PX 478 are currently being tested in phase I clinical trials. Collagen I can promote SNAIL1 stability through binding to its receptor DDR2 and activating SRC/ERK2 pathway. HA binding to CD44 induces nuclear translocation of CD44 to directly induce lysyl oxidase (LOX) expression, which in turn increases TWIST1 expression.

shown to induce TWIST1 and SNAIL2 expression in prostate and non small cell lung cancer (12, 13). TGFβ can also induce SNAIL1 and SNAIL2 via IKKα and SMAD signaling in pancreatic cancer cells (14). Furthermore, Vincent and colleagues (15) showed that SNAIL SMAD3/4 transcriptional repressor complex could pro mote TGFβ mediated EMT in breast cancer. Tumor necrosis factor α (TNFα) is a crucial activator of the NFκB signaling pathway, and activated NFκB has been shown to induce multiple EMT transcription factors expression, including TWIST1, SNAIL2, and ZEB1/2 (16 18). Furthermore, Wu and colleagues (19) found that NFκB activation could stabilize SNAIL1 to further promote cell migration and invasion. The release of interleukins by immune cells, endothelial cells, and fibroblasts can also contribute to EMT. IL6 promotes EMT in head and neck cancer cells and correlates with increased TWIST1 and SNAIL1 expres sions (20). Sullivan and colleagues (21) showed that an IL6 TWIST1 positive feedback loop induces EMT in breast cancer cells. Taken together, various inflammatory cytokines from TME can regulate the expression and/or protein stability of EMT transcrip tion factors to activate EMT and tumor invasion.

Hypoxia

Hypoxia condition has been shown to select tumor cells to become more invasive and metastatic. Specifically, hypoxia can promote EMT via hypoxia inducible factor 1α (HIF1α; ref. 22). HIF1α is found to increase SNAIL1 protein stability, leading to suppression of E cadherin in ovarian carcinoma (23). Yang and colleagues (24) found that HIF1α could induce TWIST1 expres sion by binding directly to the TWIST1 promoter. In addition, HIF1α cooperates with inflammatory cytokines to promote EMT. For example, HIF1α, together with TGFβ, promotes SNAIL1 nuclear translocation to induce EMT through the suppression of estrogen receptor β in prostate carcinoma (25). Also, HIF1α could enhance the expression of TWIST1 by upregulating TNFα, IL6, and TGFβ in prostate cancer (26). Hypoxia, together with the Wnt/β catenin signaling, can also promote SNAIL1 stability by inhibit ing GSK3β (27). Taken together, HIF1α, often in cooperation with additional TME factors, can induce EMT, suggesting a promising strategy to target hypoxic signaling for cancer therapeutics.

ECM components

ECM includes structural and nonstructural components that can activate cellular signaling through membrane bound recep tors such as integrins. The critical role of ECM in promoting EMT was already evident in the original experiments conducted by Greenburg and Hay (28). They showed that epithelial cells from embryonic and adult anterior lens cultured in three dimen sional collagen gels can elongate and migrate as individual cells. Indeed, Greenburg and Hay (28) concluded that "interactions with ECM may be a major factor in the ability of a cell to become mesenchymal."

Recently, Zhang and colleagues (29) unraveled a direct con nection between ECM structural protein collagen I and SNAIL1. They found that collagen I binds to its receptor DDR2 and activates downstream SRC/ERK2 to stabilize SNAIL1 in breast tumors cells. SNAIL1 further upregulates MT1 MMP and collagen I to promote tumor cell invasion. Another ECM structural com ponent, fibronectin, partly through binding to integrin receptors, induces SNAIL1 expression in tumor cells. This study demon strated that cooperation of fibronectin and TGFβ was required to activate the downstream SRC and ERK/MAPK kinases and induce

EMT (30). Hyaluronan (HA) is a major component of ECM and signals through its membrane receptor CD44, which is over expressed in many human cancers. HA binding to tumor cells was found to induce CD44 nuclear translocation and activate LOX expression, which in turn upregulates TWIST1 expression to promote breast cancer metastasis (31). Periostin, a nonstructural ECM component highly expressed in human tumors, could signal through integrins to increase cell survival and promote metastatic progression of colon cancer *in vivo* (32). Kim and colleagues (33) identified differential roles of periostin in EMT: it induces SNAIL1 expression in prostate cancer cells, whereas it inhibits TWIST1 expression in bladder cancer cells. These studies show that many ECM components are key regulators of EMT and tumor invasion.

ECM mechanical properties

During tumor progression, ECM is constantly remodeled by various cell types in the TME. Specifically, increasing matrix stiffness through LOX mediated collagen cross linking plays a critical role in tumor invasion and metastasis. Pioneer study by Paszek and colleagues (34) showed that increasing ECM stiffness induced a malignant phenotype, associated with activated FAK and ERK signaling. LOX mediated ECM stiffening promoted tumor progression *in vivo* partially via an activated FAK signaling (35). Conversely, treatment with a LOX inhibitor reduced focal adhesions and PI3K signaling, demonstrating that LOX modu lates tumor progression through ECM stiffening to drive focal adhesion assembly. Furthermore, ECM stiffening was required to corporate with TGFβ to induce EMT in human breast tumor cells (36), further strengthening the notion that mechanical properties of the tumor microenvironment are key factors regulating EMT and promoting tumor progression.

Clinical–Translational Advances

Accumulating evidence supports a critical role of EMT in many aspects of tumor development, including resistance to apoptosis and senescence, CSCs, and invasion and metastasis, thus suggest ing that targeting this process could be a promising therapeutic approach. However, the core EMT transcription factors remain technically challenging to target. Instead, a number of preclinical studies suggest that inhibiting EMT inducing TME signals could serve as alternative approaches to impinge upon the EMT pro gram. Here, we summarize therapeutics in preclinical and clinical studies that target TME to prevent tumor progression (Table 1).

Inflammatory cytokines

Preclinical studies support the importance of inflammatory cytokines, including TNFα and IL6, in promoting EMT and tumor invasion. Several TNFα inhibitors have been tested in clinical trial in different types of cancers. For example, infliximab, a TNFα monoclonal blocking antibody, has been tested in phase II clinical trials in renal cell carcinoma and advanced cancers (37, 38). These studies suggested that TNFα inhibitor was effective to suppress the levels of IL6 and CCL2 in patients and improved progress free survival. Two clinical studies examined the therapeutic effects of etanercept, a TNFα antagonist, in recurrent ovarian cancer and metastatic breast cancer. Etanercept is well tolerated in patients and significantly improved progress free survival with consistent decrease in CCL and IL levels (39, 40). Because NFκB is the essential downstream activator of the TNFα signaling, several clinical trials tested whether inhibition of NFκB signaling could

Table 1. Clinical studies of drugs that target tumor microenvironment

Target	Drug	Types of drug	Cancer types	Clinical studies	Response Median/mo[a]	PFS Median/mo[a]	OS Median/mo[a]	Reference
TNFα	Infliximab	Monoclonal antibody	Renal cell carcinoma	Phase	Study 1: 32% PR+SD (7.7) Study 2: 61% SD (6.2)	Study 1: 3.1 Study 2: 4.1	Study 1: 10 Study 2: 13.1	37
			Ovarian, renal, cervical cancer, endometrial stromal sarcoma, metastatic melanoma, and metastatic colon cancer	Phase	6.2% SD (3.9)			38
	Etanercept (Enbrel)	Monoclonal antibody	Metastatic breast cancer	Phase	6.25% SD (4.1)			39
			Recurrent ovarian cancer	Phase	33.3% SD (6.25)			40
NFκB	Bortezomib	Proteasome inhibitor	Unresectable/metastatic gastric and gastroesophageal junction adenocarcinoma	Phase	6.25% SD (3.3)	1.28	5.08	41
			Recurrent and/or metastatic head and neck squamous cell carcinoma	Phase	53% PR+SD (3.0)	3.0	9.4	42
IL6	Siltuximab (CNTO-328)	Monoclonal antibody	Metastatic renal cell cancer	Phase I	Part 2: 54% PR+SD (7.6)	3.4	5	43
TGFβ	AP-12009	Antisense oligonucleotide	Recurrent malignant glioma	Phase I	29.1% SD (6)		11	44
	GC-1008	Monoclonal antibody	Metastatic melanoma and renal cell carcinoma	Phase I (ongoing)				45
	LY-573636 (Tasisulam Sodium)	Small-molecule inhibitor	Unresectable/metastatic non–small cell lung cancer	Phase	43.8% SD (4.21)	2.69	8.48	46
			Unresectable/metastatic soft tissue sarcoma	Phase	46.0% PR+SD (4.44)	2.64	8.71	47
			Unresectable/metastatic melanoma	Phase	47.1% CR+PR+SD (6.6)	2.6	9.6	48
HIF1α	EZN-2698	Antisense oligonucleotide	Advanced solid tumors and metastatic renal cell carcinoma	Phase (ongoing)				49
	PX-478	Small-molecule inhibitor	Advanced metastatic cancer	Phase (ongoing)				49
	Topotecan	Small-molecule inhibitor	Advanced, refractory non–small cell lung cancer	Phase I	69.1% PR+SD (5.1)	5.2	11.5	50
Tenascin C	211At-ch81C6	Radioactive particles	GBM, anaplastic astrocytoma (AA), anaplastic oligodendroglioma (AO)	Pilot	GBM: SD (13.5) AA: SD (13) AO: SD (29)		GBM: 37.5 Non-GBM: 60	53
FAK	PF-00562271	Small-molecule inhibitor	Advanced solid tumors	Phase	34% SD (1.5) 17% SD (9)			59

Abbreviations: CR, complete response; OS, overall survival; PFS, progression-free survival; PR, partial response; SD, stable disease.
[a]Median/mo: median duration/months.

suppress tumor progression and metastasis. Bortezomib, a proteasome inhibitor that suppresses NFκB activation, was tested in phase II clinical studies with metastatic gastric adenocarcinoma, and recurrent and metastatic head and neck squamous cell carcinoma (41, 42). Although bortezomib alone showed poor response in patients, combination therapy with docetaxel or targeted inhibition of other oncogenic pathways are currently under way in solid tumors. Finally, various blocking antibodies against cytokines have been used in various clinical studies. CNTO 328, an IL6 ligand blocking antibody, was tested in phase I/II clinical trials for the treatment of metastatic renal cell carcinoma. This study showed that CNTO 328 could increase patient survival and more than 50% of progressive metastatic renal cell carcinoma patients presented stable diseases upon treatment (43). Together, these clinical trials in progress could bring a number of promising anti inflammatory cytokine agents to the forefront of antimetastasis therapeutics.

The TGFβ signaling is extensively targeted to block tumor progression and metastasis, and various approaches have been taken to inhibit the TGFβ signaling. AP 12009, an antisense oligonucleotide against TGFβII, was tested in patients with high grade glioma and significantly improved survival compared with standard chemotherapy treatment (44). Furthermore, TGFβ neutralizing antibody GC 1008 showed promises in phase I trial for metastatic melanoma and renal cell carcinoma (45). Small molecule inhibitor, LY 573636, used in phase II clinical studies in patients with metastatic NSCLC, soft tissue sarcoma, and melanoma, has also shown modest activity as a second/third line therapy (46 48). These studies showed that inhibiting TGFβ signaling pathway is safe, well tolerated in patients and could provide promising new therapeutics against tumor invasion.

Hypoxia

Several HIF1α inhibitors have also shown remarkable antitumor activities in a variety of preclinical and clinical trials. EZN 2698, an antisense oligonucleotide against of HIF1α, is being tested in a phase I clinical trial with advanced solid tumors (49). Another HIF1α inhibitor, PX 478, which inhibit HIF1α expression, is currently tested in phase I clinical trials in patients with advanced metastatic cancer (49). Several novel compounds have also been identified in a high throughput screen using a cell based reporter of HIF1α transcriptional activity. One such compound topotecan has been tested in phase I/II clinical trials with conventional chemotherapies such as cisplatin or bevacizumab in patients with advanced lung cancer. Clinical results indicate that combination treatment is well tolerated and worthy of further clinical investigation (50), thus making them promising agents against tumor metastasis.

ECM components

Disruption of tumor ECM integrity has shown promising results in halting tumor metastasis in preclinical studies. Methylumbelliferone, a HA synthesis inhibitor, was effective in preventing bone metastasis of lung cancer *in vivo* (51). Neutralizing antibody directed against periostin resulted in 40% inhibition of tumor growth ($P < 0.001$), 80% inhibition of lung metastasis ($P < 0.001$), and significant increase in survival ($P < 0.05$) using mouse breast tumor xenografts (52).

Because cells that have undergone EMT secrete many unique ECM components, these ECM molecules have also been used for targeting drug delivery to tumors. For example, a promising approach has been used in clinical trials for patients with glioblastoma multiforme (GBM), linking anti Tenascin C antibody to radioactive particles to specifically target tumor cells. Result showed minimal toxicity associated with a promising antitumor benefit and encouraging overall outcomes (53). Recently, engineered HA based conjugates have emerged as a promising strategy to efficiently target tumors with drugs exerting poor solubility and strong side effects, such as paclitaxel (54). These strategies take advantage of unique EMT associated TME components to achieve targeted delivery of traditional chemotherapeutics, thus presenting a new anticancer therapeutic strategy.

ECM mechanical properties

In patients, the presence of fibrotic foci in breast tumors is a prognostic marker of distant metastasis and correlates with poor survival (55). In addition, LOX is essential for hypoxia induced breast cancer metastasis and its expression in patients is correlated to a poor outcome (56). Finally, a recent study shows that LOX is critical to establish a permissive microenvironment within fibrotic tissues, characterized by increased EMT, to favor the colonization of metastasizing tumor cells (57). Thus, anti LOX strategies could suppress metastatic progression of the disease, not only by targeting the TME of the premetastatic niche, but also by targeting tumor cells themselves, as shown by the direct effect of LOX inhibition in attenuating FAK dependent breast cancer cell invasion in a preclinical study (58). Therapeutic inhibition of FAK, recently validated in a phase I study, may also be a promising approach to prevent the effect of TME stiffness on metastatic progression of several types of cancer. Indeed the use of pharmacologic inhibitor PF 00562271 in patients with advanced solid tumors unresponsive to existing therapies showed a significant stabilization of the disease, thus supporting FAK as a potential therapeutic target (59).

Conclusion and Discussion

As discussed, a number of inhibitors targeting TME are being tested in preclinical and clinical trials and well tolerated in patients and several showed promising results. Because these TME signals regulate various signaling pathways, the impacts of these inhibitors on tumor progression are likely beyond the EMT program. Given the critical role of EMT in multiple steps of tumor progression, targeting the EMT inducing TME signals is indeed worth pursuing to combat metastatic cancers.

However, there are also a number of issues to be resolved to better decide how to effectively affect tumor progression by targeting the EMT program. First, current clinical trials largely aim to shrink established metastases, in which the EMT program may not be involved. Instead, metastasis prevention trials in patients with cancer with high metastasis risk would be the appropriate setting to test the effect of EMT inhibition on metastasis occurrence. Second, recent studies demonstrated the dynamic involvement of EMT in tumor metastasis: activation of EMT promotes tumor dissemination and reversion of EMT is essential for outgrowth of macrometastases. Therefore, EMT inhibitor alone could be counter productive in preventing distant metastases if patients already have disseminated tumor cells in distant organs. In these cases, combining therapies targeting TME signals with traditional chemotherapy and targeted therapies to simultaneously inhibit EMT and cell proliferation could be a more powerful approach to eradicate both migrating as well as proliferating tumor cells, thus halting tumor progression.

Jung et al.

Disclosure of Potential Conflicts of Interest

No potential conflicts of interest were disclosed. .

Authors' Contributions

Conception and design: H.-Y. Jung, L. Fattet, J. Yang
Writing, review, and/or revision of the manuscript: H.-Y. Jung, L. Fattet, J. Yang

Acknowledgments

The authors apologize to the many researchers in this field whose work they were unable to cite due to space restrictions.

References

1. De Craene B, Berx G. Regulatory networks defining EMT during cancer initiation and progression. Nat Rev Cancer 2013;13: 97–110.
2. Sánchez-Tilló E, Liu Y, de Barrios O, Siles L, Fanlo L, Cuatrecasas M, et al. EMT-activating transcription factors in cancer: beyond EMT and tumor invasiveness. Cell Mol Life Sci 2012;69: 3429–56.
3. Thiery JP, Acloque H, Huang RYJ, Nieto MA. Epithelial-mesenchymal transitions in development and disease. Cell 2009;139: 871–90.
4. Valdés F, Alvarez AM, Locascio A, Vega S, Herrera B, Fernández M, et al. The epithelial mesenchymal transition confers resistance to the apoptotic effects of transforming growth factor Beta in fetal rat hepatocytes. Mol Cancer Res 2002;1: 68–78.
5. Derksen PWB, Liu X, Saridin F, van der Gulden H, Zevenhoven J, Evers B, et al. Somatic inactivation of E-cadherin and p53 in mice leads to metastatic lobular mammary carcinoma through induction of anoikis resistance and angiogenesis. Cancer Cell 2006;10: 437–49.
6. Ansieau S, Bastid J, Doreau A, Morel A-P, Bouchet BP, Thomas C, et al. Induction of EMT by TWIST proteins as a collateral effect of tumor-promoting inactivation of premature senescence. Cancer Cell 2008;14: 79–89.
7. Browne G, Sayan AE, Tulchinsky E. ZEB proteins link cell motility with cell cycle control and cell survival in cancer. Cell Cycle 2010;9: 886–91.
8. Mani SA, Guo W, Liao M-J, Eaton EN, Ayyanan A, Zhou AY, et al. The epithelial-mesenchymal transition generates cells with properties of stem cells. Cell 2008;133: 704–15.
9. Morel A-P, Lièvre M, Thomas C, Hinkal G, Ansieau S, Puisieux A. Generation of breast cancer stem cells through epithelial-mesenchymal transition. PLoS ONE 2008;3: e2888.
10. Tsai JH, Donaher JL, Murphy DA, Chau S, Yang J. Spatiotemporal regulation of epithelial-mesenchymal transition is essential for squamous cell carcinoma metastasis. Cancer Cell 2012;22: 725–36.
11. Rakoff-Nahoum S. why cancer and inflammation? Yale J Biol Med 2006;79: 123–30.
12. Shiota M, Zardan A, Takeuchi A, Kumano M, Beraldi E, Naito S, et al. Clusterin mediates TGFβ-induced epithelial-mesenchymal transition and metastasis via TWIST1 in prostate cancer cells. Cancer Res 2012;72: 5261–72.
13. Slabáková E, Pernicová Z, Slavíčková E, Stars?íchová A, Kozubík A, Soucek K. TGFβ1-induced EMT of non-transformed prostate hyperplasia cells is characterized by early induction of SNAI2/Slug. Prostate 2011;71: 1332–43.
14. Brandl M, Seidler B, Haller F, Adamski J, Schmid RM, Saur D, et al. IKKα controls canonical TGFβ-SMAD signaling to regulate genes expressing SNAIL and SLUG during EMT in panc1 cells. J Cell Sci 2010;123: 4231–9.
15. Vincent T, Neve EPA, Johnson JR, Kukalev A, Rojo F, Albanell J, et al. A SNAIL1-SMAD3/4 transcriptional repressor complex promotes TGFβ mediated epithelial-mesenchymal transition. Nat Cell Biol 2009;11: 943–50.
16. Li CW, Xia W, Huo L, Lim SO, Wu Y, Hsu JL, et al. Epithelial-mesenchymal transition induced by TNFα requires NFkB-mediated transcriptional upregulation of TWIST1. Cancer Res 2012;72: 1290–300.
17. Storci G, Sansone P, Mari S, D'Uva G, Tavolari S, Guarnieri T, et al. TNFalpha up-regulates SLUG via the NFkappaB/HIF1alpha axis, which imparts breast cancer cells with a stem cell-like phenotype. J Cell Physiol 2010;225: 682–91.
18. Chua HL, Bhat-Nakshatri P, Clare SE, Morimiya A, Badve S, Nakshatri H. NFκB represses E-cadherin expression and enhances epithelial to mesenchymal transition of mammary epithelial cells: potential involvement of ZEB-1 and ZEB-2. Oncogene 2006;26: 711–24.
19. Wu Y, Deng J, Rychahou PG, Qiu S, Evers BM, Zhou BP. Stabilization of SNAIL by NFκB is required for inflammation-induced cell migration and invasion. Cancer Cell 2009;15: 416–28.
20. Su Y-W, Xie T-X, Sano D, Myers JN. IL6 stabilizes TWIST and enhances tumor cell motility in head and neck cancer cells through activation of Casein kinase 2. PLoS ONE 2011;6: e19412.
21. Sullivan NJ, Sasser AK, Axel AE, Vesuna F, Raman V, Ramirez N, et al. Interleukin-6 induces an epithelial–mesenchymal transition phenotype in human breast cancer cells. Oncogene 2009;28: 2940–7.
22. Vooijs M, Gort E, Groot A, Wall der E, van Diest P. Hypoxic regulation of metastasis via hypoxia-inducible factors. Curr Mol Med 2008;8: 60–7.
23. Imai T, Horiuchi A, Wang C, Oka K, Ohira S, Nikaido T, et al. Hypoxia attenuates the expression of E-Cadherin via up-regulation of SNAIL in ovarian carcinoma cells. Am J Pathol 2003;163: 1437–47.
24. Yang M-H, Wu M-Z, Chiou S-H, Chen P-M, Chang S-Y, Liu C-J, et al. Direct regulation of TWIST by HIF1α promotes metastasis. Nat Cell Biol 2008;10: 295–305.
25. Mak P, Leav I, Pursell B, Bae D, Yang X, Taglienti CA, et al. ERβ impedes prostate cancer EMT by destabilizing HIF1α and inhibiting VEGF-mediated SNAIL nuclear localization: implications for Gleason grading. Cancer Cell 2010;17: 319–32.
26. Kim H-J, Park J-W, Cho Y-S, Cho C-H, Kim J-S, Shin H-W, et al. Pathogenic role of HIF1α in prostate hyperplasia in the presence of chronic inflammation. Biochim Biophys Acta 2013;1832: 183–94.
27. Cannito S, Novo E, Compagnone A, Valfre di Bonzo L, Busletta C, Zamara E, et al. Redox mechanisms switch on hypoxia-dependent epithelial-mesenchymal transition in cancer cells. Carcinogenesis 2008;29: 2267–78.
28. Greenburg G, Hay ED. Epithelia suspended in collagen gels can lose polarity and express characteristics of migrating mesenchymal cells. J Cell Biol 1982;95: 333–9.
29. Zhang K, Corsa CA, Ponik SM, Prior JL, Piwnica-Worms D, Eliceiri KW, et al. The collagen receptor discoidin domain receptor 2 stabilizes SNAIL1 to facilitate breast cancer metastasis. Nat Cell Biol 2013;15: 677–87.
30. Park JH, Schwarzbauer JE. Mammary epithelial cell interactions with fibronectin stimulate epithelial-mesenchymal transition. Oncogene 2013; 33: 1649–57.
31. El-Haibi CP, Bell GW, Zhang J, Collmann AY, Wood D, Scherber CM, et al. Critical role for lysyl oxidase in mesenchymal stem cell-driven breast cancer malignancy. Proc Natl Acad Sci U S A 2012;109: 17460–5.
32. Bao S, Ouyang G, Bai X, Huang Z, Ma C, Liu M, et al. Periostin potently promotes metastatic growth of colon cancer by augmenting cell survival via the Akt/PKB pathway. Cancer Cell 2004;5: 329–39.
33. Kim CJ, Sakamoto K, Tambe Y, Inoue H. Opposite regulation of epithelial-to-mesenchymal transition and cell invasiveness by periostin between prostate and bladder cancer cells. Int J Oncol 2011;38: 1759–66.
34. Paszek MJ, Zahir N, Johnson KR, Lakins JN, Rozenberg GI, Gefen A, et al. Tensional homeostasis and the malignant phenotype. Cancer Cell 2005;8: 241–54.
35. Levental KR, Yu H, Kass L, Lakins JN, Egeblad M, Erler JT, et al. Matrix crosslinking forces tumor progression by enhancing integrin signaling. Cell 2009;139: 891–906.
36. Leight JL, Wozniak MA, Chen S, Lynch ML, Chen CS. Matrix rigidity regulates a switch between TGFβ1-induced apoptosis and epithelial-mesenchymal transition. Mol Biol Cell 2012;23: 781–91.

37. Harrison ML, Obermueller E, Maisey NR, Hoare S, Edmonds K, Li NF, et al. Tumor Necrosis Factor α as a new target for renal cell carcinoma: two sequential phase II trials of Infliximab at standard and high dose. J Clin Oncol 2007;25: 4542–9.

38. Brown ER, Charles KA, Hoare SA, Rye RL, Jodrell DI, Aird RE, et al. A clinical study assessing the tolerability and biological effects of infliximab, a TNFα inhibitor, in patients with advanced cancer. Ann Oncol 2008;19: 1340–6.

39. Madhusudan S. A phase II study of Etanercept (Enbrel), a tumor necrosis factor α inhibitor in patients with metastatic breast cancer. Clin Cancer Res 2004;10: 6528–34.

40. Madhusudan S. Study of etanercept, a tumor necrosis factor-alpha inhibitor, in recurrent ovarian cancer. J Clin Oncol 2005;23: 5950–9.

41. Shah MA, Power DG, Kindler HL, Holen KD, Kemeny MM, Ilson DH, et al. A multicenter, phase II study of Bortezomib (PS-341) in patients with unresectable or metastatic gastric and gastroesophageal junction adenocarcinoma. Invest New Drugs 2010;29: 1475–81.

42. Chung CH, Aulino J, Muldowney NJ, Hatakeyama H, Baumann J, Burkey B, et al. Nuclear factor-kappa B pathway and response in a phase II trial of bortezomib and docetaxel in patients with recurrent and/or metastatic head and neck squamous cell carcinoma. Ann Oncol 2010;21: 864–70.

43. Rossi J-F, Négrier S, James ND, Kocak I, Hawkins R, Davis H, et al. A phase I/II study of siltuximab (CNTO 328), an anti-interleukin-6 monoclonal antibody, in metastatic renal cell cancer. Br J Cancer 2010;103: 1154–62.

44. Hau P, Jachimczak P, Schlingensiepen R, Schulmeyer F, Jauch T, Steinbrecher A, et al. Inhibition of TGFβ2 with AP 12009 in recurrent malignant gliomas: from preclinical to phase I/II studies. Oligonucleotides 2007;17: 201–12.

45. Nagaraj NS, Datta PK. Targeting the transforming growth factor-β signaling pathway in human cancer. Expert Opin Investig Drugs 2010;19: 77–91.

46. Scagliotti GV, Ilaria R Jr, Novello S, Pawel von J, Fischer JR, Ermisch S, et al. Tasisulam sodium (LY573636 Sodium) as third-line treatment in patients with unresectable, metastatic non-small-cell lung cancer. J Thorac Oncol 2012;7: 1053–7.

47. Ryan CW, Matias C, Agulnik M, Lopez-Pousa A, Williams C, Alwis DP, et al. A phase II study of tasisulam sodium (LY573636 sodium) as second-line or third-line treatment for patients with unresectable or metastatic soft tissue sarcoma. Invest New Drugs 2012;31: 145–51.

48. Kirkwood JM, Gonzalez R, Reintgen D, Clingan PR, McWilliams RR, de Alwis DP, et al. A phase 2 study of tasisulam sodium (LY573636 sodium) as second-line treatment for patients with unresectable or metastatic melanoma. Cancer 2011;117: 4732–9.

49. Onnis B, Rapisarda A, Melillo G. Development of HIF1 inhibitors for cancer therapy. J Cell Mol Med 2009;13: 2780–6.

50. Powell SF, Beitinjaneh A, Tessema M, Bliss RL, Kratzke RA, Leach J, et al. Phase II study of topotecan and bevacizumab in advanced, refractory non-small-cell lung cancer. Clin Lung Cancer 2013;14: 495–501.

51. Futamura N, Urakawa H, Arai E, Kozawa E, Ishiguro N, Nishida Y. Hyaluronan synthesis inhibitor supplements the inhibitory effects of zoledronic acid on bone metastasis of lung cancer. Clin Exp Metastasis 2013;30: 595–606.

52. Morishita R. Role of periostin in cancer progression and metastasis: inhibition of breast cancer progression and metastasis by anti-periostin antibody in a murine model. Int J Mol Med 2011;28: 181–6.

53. Zalutsky MR, Reardon DA, Akabani G, Coleman RE, Friedman AH, Friedman HS, et al. Clinical experience with α-particle emitting 211At: treatment of recurrent brain tumor patients with 211At-labeled chimeric antitenascin monoclonal antibody 81C6. J Nucl Med 2007;49: 30–8.

54. Arpicco S, Milla P, Stella B, Dosio F. Hyaluronic acid conjugates as vectors for the active targeting of drugs, genes and nanocomposites in cancer treatment. Molecules 2014;19: 3193–230.

55. Colpaert C, Vermeulen P, VanMarck E, Dirix L. The presence of a fibrotic focus is an independent predictor of early metastasis in lymph node-negative breast cancer patients. Am J Surg Pathol 2001;25: 1557.

56. Erler JT, Bennewith KL, Nicolau M, Dornhöfer N, Kong C, Le Q-T, et al. Lysyl oxidase is essential for hypoxia-induced metastasis. Nature 2006;440: 1222–6.

57. Cox TR, Bird D, Baker A-M, Barker HE, Ho MWY, Lang G, et al. LOX-mediated collagen crosslinking is responsible for fibrosis-enhanced metastasis. Cancer Res 2013;73: 1721–32.

58. Chen L-C, Tu S-H, Huang C-S, Chen C-S, Ho C-T, Lin H-W, et al. Human breast cancer cell metastasis is attenuated by lysyl oxidase inhibitors through down-regulation of focal adhesion kinase and the paxillin-signaling pathway. Breast Cancer Res Treat 2012;134: 989–1004.

59. Infante JR, Camidge DR, Mileshkin LR, Chen EX, Hicks RJ, Rischin D, et al. Safety, pharmacokinetic, and pharmacodynamic phase I dose-escalation trial of PF-00562271, an inhibitor of focal adhesion kinase, in advanced solid tumors. J Clin Oncol 2012;30: 1527–33.

Clinical Cancer Research

Molecular Pathways: Linking Tumor Microenvironment to Epithelial–Mesenchymal Transition in Metastasis

Hae-Yun Jung, Laurent Fattet and Jing Yang

Updated version	

E-mail alerts	Sign up to receive free email-alerts related to this article or journal.
Reprints and Subscriptions	To order reprints of this article or to subscribe to the journal, contact the AACR Publications Department at pubs@aacr.org.
Permissions	To request permission to re-use all or part of this article, contact the AACR Publications Department at permissions@aacr.org.